SNE SIMULATION NOTES EUROPE

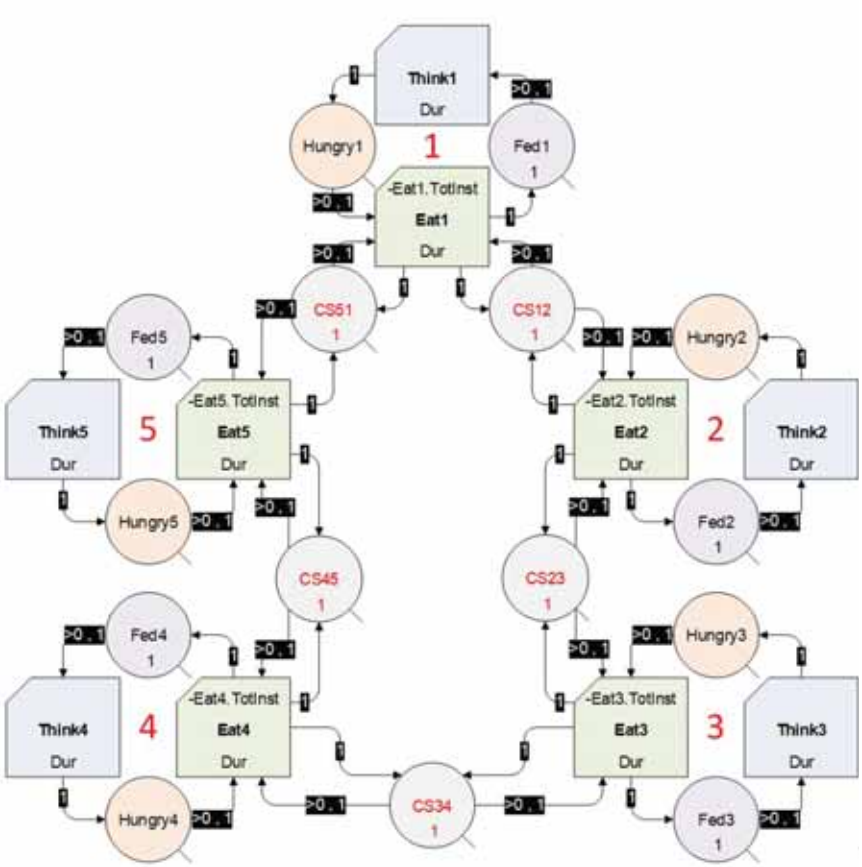

Journal on Developments and Trends in Modelling and Simulation

EUROSIM Scientific Membership Journal

Vol. 36 No.2, June 2026 ISSN Online 2306-0271 DOI 10.11128/sne.36.2.1077

ISSN Print 2305-9974

Calendar of Events

June 24 - 26, 2026, TU Wien, Austria

40th ACM SIGSIM International Conference
on Principles of Advanced Discrete Simulation

Cooperation of ASIM with ACM SIGSIM

sigsim.acm.org/conf/pads/2026/

September 16 -17, 2026, Eskilstuna, Sweden

SIMS 2026, 67th International Conference
of the Scandinavian Simulation Society

www.scansims.org

September 21 - 23, 2026, Genova, Italy

12th EUROSIM Congress

M&S & AI: Opportunities and Challenges for Present & Future
with special ASIM Track
(reduced fee for ASIM members)

www.msc-les.org/eurosim2026/

together with

I3M 2026

23rd International Multidisciplinary Modelling & Simulation Multi-Conference

www.msc-les.org/i3m2026/

December 6 - 9, 2026, Glasgow, Scotland

2026 Winter Simulation Conference

Simulation for Climate Resilience

(reduced fee for ASIM members)

meetings.informs.org/wordpress/wsc2026/

September 20 - 22, 2027, Kassel, Germany

22. ASIM Fachtagung Simulation in Produktion und Logistik

save the date

Editorial

Dear Readers, This second issue of SNE Volume 36, SNE 36(2), continues with post-conference publications from ASIM Symposium 2024 (Munich) and from ASIM's Workshop GMMS/STS 2025 at DLR (April 2025) and starts with post-conference publications from MATHMOD 2025 Vienna (February 2025). The topics of these six contributions show very broad range: system simulation with hybrid thermal storage tanks, flatness-based control of heat equation, virtual sensors for reconstruction in single resident apartments, variational multiscale models for convection-dominated problems, health self-management applications for people with rheumatoid arthritis, and terrain identification in simulation-driven terrain-aware military logistics supplier – from physics via ambient assisted living and healthcare to logistics. For a better differentiation of a post-conference publications from the conference publication we have introduced a classification: REVISED - correction of typos, improvement of text; IMPROVED - correction of typos, improvement and extension of text, a bit more figures; EXTENDED - significant improvement and extension of text, more figures, change of title and authors; and FULL PAPER - new publication based on conference abstract publication (with same title); additionally ENGLISCH VERSION – in case of non-English conference publication. And last but not least, P. G. Ioannou et al. continue ARGESIM Benchmarks solutions with STROBOSCOPE / EZStrobe, in this issue for Benchmark 'C10 Dining Philosophers II'.
*I would like to thank all authors for their contributions, and many thanks to the SNE Editorial Office for layout, typesetting, preparations for printing, electronic publishing, and much more. And have a look at the info on EUROSIM-related simulation events of this year: 12th EUROSIM Congress **EUROSIM 2026** in September 2026 in Genova (with ASIM tracks!), WinterSim Conference 2026 in December in Glasgow (this year in Europe!), and further conferences, e.g. SIMS 2026 in September in Eskilstuna, Sweden.*

Felix Breitenecker, SNE Editor-in-Chief, eic@sne-journal.org; felix.breitenecker@tuwien.ac.at

Contents SNE 36(2)

e-SNE 36(2), DOI 10.11128/sne.36.2.1077

www.sne-journal.org/sne-volumes/volume-36
SNE Basic Version with Open Access, CC BY 4.0
SNE Premium Version for Members of Publication-Active EUROSIM Societies: ASIM, CEA-SMSG, CSSS, DBSS, KA-SIM, LIOPHANT, PTSK, SIMS, SLOSIM
print-SNE for members on demand (printer INTU TU Wien)

SNE Contact & Info

SNE Online ISSN 2306-0271, SNE Print ISSN 2305-9974

→ *www.sne-journal.org*

office@sne-journal.org, eic@sne-journal.org

SNE Editorial Office
Felix Breitenecker (Organisation, Author Mentoring)
Irmgard Husinsky (Web, Electronic Publishing),
ARGESIM / Math. Modelling & Simulation Group,
Inst. of Analysis and Scientific Computing, TU Wien
Wiedner Hauptstrasse 8-10, 1040 Vienna, Austria

SNE SIMULATION NOTES EUROPE

WEB: → *www.sne-journal.org*, DOI prefix 10.11128/sne

Scope: Developments and trends in modelling and simulation in various areas and in application and theory; comparative studies and benchmarks; modelling and simulation in and for education; post-conference publication for conferences of EUROSIM societies, society information and membership information for EUROSIM members (Federation of European Simulation Societies and Groups).

Editor-in-Chief: Felix Breitenecker, TU Wien, Math. Modelling Group
Felix.Breitenecker@tuwien.ac.at, eic@sne-journal.org

Print SNE: INTU (TU Wien), Wiedner Hauptstrasse 8-10, 1040, Vienna, Austria – *www.intu.at*

ARGESIM Publisher: ARBEITSGEMEINSCHAFT SIMULATION NEWS
c/o Math. Modelling and Simulation Group, TU Wien / 101, Wiedner Hauptstrasse 8-10, 1040 Vienna, Austria;
www.argesim.org, info@argesim.org on behalf of ASIM *www.asim-gi.org* and EUROSIM → *www.eurosim.info*

SNE is a joint publication of **ARGESIM** and **ASIM.**

SNE - Aims and Scope

Simulation Notes Europe (SNE) provides an international, high-quality forum for presentation of new ideas and approaches in simulation - from modelling to experiment analysis, from implementation to verification, from validation to identification, from numerics to visualisation (www.sne-journal.org).

SNE seeks to serve scientists, researchers, developers and users of the simulation process across a variety of theoretical and applied fields in pursuit of novel ideas in simulation. **SNE** follows the recent developments and trends of modelling and simulation in new and/or joining areas, as complex systems and big data. **SNE** puts special emphasis on the overall view in simulation, and on comparative investigations, as benchmarks and comparisons in methodology and application. For this purpose, **SNE** documents the **ARGESIM Benchmarks** on *Modelling Approaches and Simulation Implementations* with publication of definitions, solutions and discussions. **SNE** welcomes also contributions in education in/for/with simulation.

SNE is the scientific membership journal of **EUROSIM**, the *Federation of European Simulation Societies and Simulation Groups* (www.eurosim.info), also providing Postconference publication for events of the member societies. **SNE**, primarily an electronic journal **e-SNE** (ISSN 2306-0271), follows an open access strategy, with free download in basic version (B/W, low resolution graphics). Members of most **EUROSIM** societies are entitled to download **e-SNE** in an elaborate full version (colour, high resolution graphics), and to access additional sources of benchmark publications, model sources, etc. (via group login of the society), **print-SNE** (ISSN 2305-9974) is available for specific groups of **EUROSIM** societies.

SNE is published by **ARGESIM** (www.argesim.org) on mandate of **EUROSIM** and **ASIM** (www.asim-gi.org), the German simulation society. **SNE** is DOI indexed with prefix 10.11128.

Author's Info. Individual submissions of scientific papers are welcome, as well as post-conference publications of contributions from conferences of **EUROSIM** societies. **SNE** welcomes special issues, either dedicated to special areas and/or new developments, or on occasion of events as conferences and workshops with special emphasis.

Authors are invited to submit contributions which have not been published and have not being considered for publication elsewhere to the **SNE** Editorial Office.

SNE distinguishes different types of contributions (*Notes*), i.e.

- **TN** Technical Note, 6–10 p.
- **SN** Short Note, max. 5 p.
- **SW** Software Note , 4–6 p.
- **BN** Benchmark Note, 2–10 p.
- **ON** Overview Note – only upon invitation, up to 14 p.
- **EN** Education Note, 6–8 p.
- **PN** Project Note 6–8 p.
- **STN** Student Note, 4-6 p., on supervisor's recommendation
- **EBN** Educational Benchmark Note, 4–10 p.

Further info and templates (doc, tex) at **SNE**'s website, or from the Editor-in-Chief

www.sne-journal.org

office@sne-journal.org, *eic@sne-journal.org*

SNE Editorial Board

Dynamic System Simulation with Hybrid Thermal Storage Tanks

Sarah Jäger*, Peter Renze

Institute for Technology and Energy Economics, University of Applied Sciences Ulm, 89075 Ulm, Germany,
*sarah.jaeger@thu.de

SNE 36(2), 2026, 65-71, DOI: 10.11128/sne.36.tn.10771
Sel. ASIM GMMS/STS 2025 Postconf. Publication: 2025-10-22
Received Extended: 2026-01-30; Accepted: 2026-02-15
SNE - Simulation Notes Europe, ARGESIM Publisher Vienna
ISSN Print 2305-9974, Online 2306-0271, www.sne-journal.org

This paper is focused on recent advancements in the integration of thermal storage systems with phase change material (PCM) packed beds for energy storage applications. A simulation environment is presented that combines detailed PCM modeling with dynamic load profiles corresponding to specific consumers and producers. By incorporating individual building and user parameters, this approach provides the foundation for simulating and analyzing application scenarios and their impact on the thermal performance of storage systems with different PCM configurations, compared to a conventional stratified water tank.

Introduction

The model is based on a one-dimensional mathematical approach that represents temperature distributions in two zones (Jäger et al. 2024). It is adaptable to arbitrary tank geometries and various PCM layer configurations and is currently being enhanced to investigate storage behavior under dynamic operating conditions.

The thermal dynamics within the water zone of the storage tank during charging or discharging processes are modeled as an open system with energy and mass exchange.

This is described through differential equations for discrete tank, accounting for heat loss to the environment, conduction between layers using an effective conductivity, mass flow during charging and discharging processes, and heat transfer between water and PCM capsules.

1 Modelling

The governing equations describe the temporal evolution of thermal energy within discretized storage layers. For a generic layer i, where $i = 1, \dots, n$, A_{ax} denotes the base area of the cylindrical control volume. The formulation for the bottom layer of the water zone is given by:

$$\begin{aligned}\rho\, c_p\, A_{ax}\, \varepsilon\, \Delta z \frac{dT_1}{dt} &= A_{Tank}\, U_{Tank}(T_{amb} - T_1) + \\ &+ \frac{\lambda_{eff}\,(A_{ax} - \varepsilon)}{\Delta z}\,(T_2 - T_1) + \\ &+ \dot{m}_{down}\, c_p\, (T_2 - T_1) + \\ &+ \dot{m}_{up}\, c_p\, (T_{dis} - T_1) + U_C\, A_C\, (T_{PCM1} - T_1)\end{aligned} \tag{1}$$

For the intermediate layers between the bottom and top of the storage tank:

$$\begin{aligned}\rho\, c_p\, A_{ax}\, \varepsilon\, \Delta z \frac{dT_i}{dt} &= A_{Tank}\, U_{Tank}\, (T_{amb} - T_i) + \\ &+ \frac{\lambda_{eff}\,(A_{ax} - \varepsilon)}{\Delta z}(T_{i-1} - 2\,T_i + T_{i+1}) + \\ &+ \dot{m}_{down}\, c_p\, (T_{i+1} - T_i) + \\ &+ \dot{m}_{up}\, c_p\, (T_{i-1} - T_i) + U_C\, A_C\, (T_{PCM\,i} - T_i)\end{aligned} \tag{2}$$

For the last layer *n* at the tank top:

$$\begin{aligned}\rho\, c_p\, A_{ax}\, \varepsilon\, \Delta z \frac{dT_n}{dt} &= A_{Tank}\, U_{Tank}\, (T_{amb} - T_n) + \\ &+ \frac{\lambda_{eff}\,(A_{ax} - \varepsilon)}{\Delta z}\,(T_{n-1} - T_n) + \\ &+ \dot{m}_{down}\, c_p\, (T_{ch} - T_n) + \\ &+ \dot{m}_{up}\, c_p\, (T_{n\text{-}1} - T_n) + U_C\, A_C\, (T_{PCM\,n} - T_n)\end{aligned} \tag{3}$$

Heat exchange with the environment is represented by a wall heat transfer term, whose coefficient U_{Tank} depends on internal and external flow conditions as well as on the thermal properties of the tank wall and insulation and may vary along the tank height.

For the bottom and top layers, the effective tank area additionally includes the corresponding end surfaces, which generally leads to increased thermal interaction compared to intermediate layers. Axial heat transport between adjacent layers is represented by an effective thermal conductivity that accounts for heat conduction through both the water domain and the tank wall, thereby capturing the additional vertical heat flux induced by the high thermal conductivity of the metallic storage wall and its influence on thermal mixing (Untrau et al. 2022).

The PCM domain is modelled by a separate energy balance (4), assuming heat exchange exclusively with the surrounding water and no interaction with adjacent layers. Heat transfer between the water and the PCM capsules, as well as heat conduction within the capsules, is represented by a temperature-dependent overall heat transfer coefficient U_C, while phase change is modeled using an enthalpy-based approach.

$$\rho\, c_p\, A_{ax}\,(1-\varepsilon)\,\Delta z \frac{dT_i}{dt} = U_C\, A_C\,(T_i - T_{PCM\,i}) \qquad (4)$$

Zones within the tank are determined based on PCM placement and inlet and outlet locations, and if no PCM is present, the corresponding heat transfer term is omitted. As the PCM capsules form a packed-bed configuration within the storage tank, only a portion of the total tank volume is available for the water phase.

This portion is described by the porosity ε, which is defined as the ratio of the void volume to the overall tank volume. The void volume is obtained by subtracting the total volume of the PCM capsules from the tank volume, yielding

$$\varepsilon = \frac{V_T - V_{PCM}}{V_T} \qquad (5)$$

A schematic representation visualizing the described model is provided in Figure 1.

2 Experiments and Results

Developed in MATLAB, the model was validated using experimental data from a hardware in the loop test facility, successfully simulating continuous charging scenarios. This integration of simulation and experimental validation enables a comprehensive evaluation of storage system performance under realistic conditions.

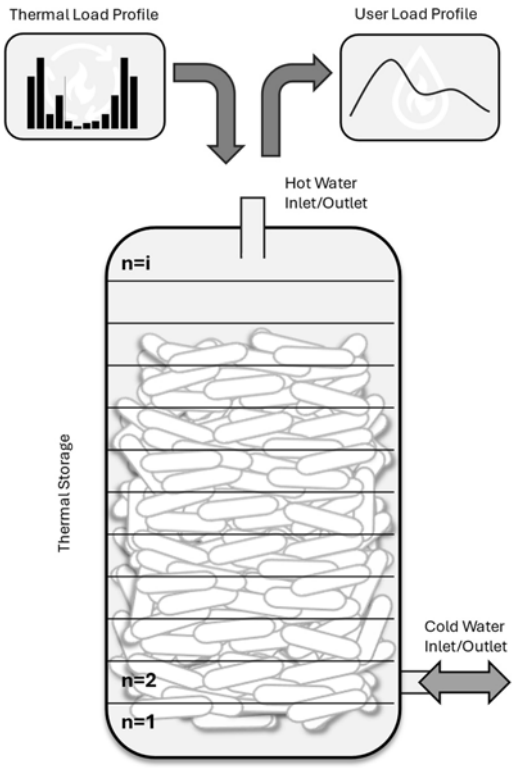

Figure 1: Schematic representation of the hybrid thermal storage model, illustrating the surrounding system modeled as load profiles.

The recent modifications enabling predefined charging and discharging profiles to be implemented by converting hourly energy demands of both consumers and heat generators, defined at specified hot water temperature levels, into corresponding volume flow rates entering or leaving the tank, thus directly affecting the energy balance calculations of the discretized tank layers.

A domestic hot water tank with $V = 2$ m³ was top loaded at $\vartheta = 60$ °C and discharged following a standard family load profile (Bundesverband Wärmepumpe (BWP) e.V. 2023).

The study compared three tank configurations without losses: an ideal stratified tank, a tank filled with PCM capsules with a melting point of 58 °C, and one with capsules at 37 °C.

A 24-hour segment of a simulation cycle is presented in Figure 2. The first column illustrates the hourly temperature distribution along the tank height, while the second column depicts the stored heat distributions at each 2 cm layer of height. The PCM58 capsules did not fully melt in this scenario.

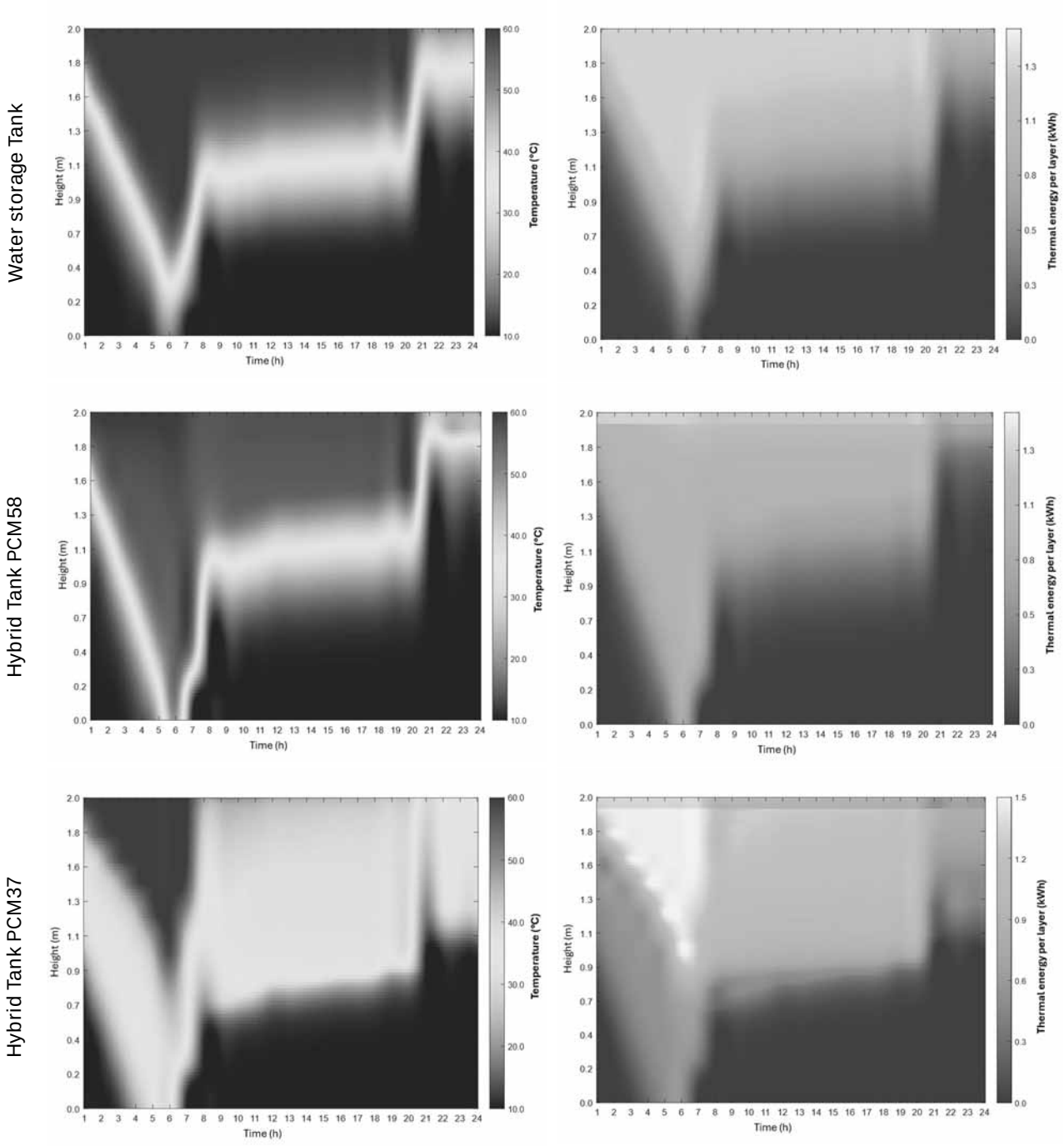

Figure 2: Temperature Distribution and Stored Heat for each of 100 Layers across a 24-Hour Segment of a Simulation

In contrast, the PCM37 configuration demonstrated a higher energy density spreading downward until hour 6, indicating significant latent heat absorption.

Despite storing 109 kWh (PCM37) at its peak or immediately after the last charging hour, compared to 83.5 kWh (PCM58), the temperature in the upper_section of the PCM37 tank decreased more rapidly during discharge, reaching 38 °C by hour 21.

At the same time, the PCM58 tank retained 52 °C, while the stratified tank provided 57 °C. After discharge (after hour 22), both PCM tanks exhibited slight reheating, stabilizing near the melting temperature of the respective PCM.

For this scenario, the stratified tank maintained a stable hot water temperature over a longer time period, proving to be the better option when a minimum temperature of 55 °C is required.

For this scenario, the stratified tank maintained a stable hot water temperature for a longer period when a minimum temperature of 55 °C is required.

To place this observation into a broader context, the following section examines the applied control strategy and the temporal availability of energy above the usable temperature level. Comparable boundary conditions are ensured through a temperature-based control approach. The system temperature is limited to a usable level of 55 °C, which corresponds to the required supply temperature of the building.

Charging of the storage tank is controlled by a simple temperature based controller that stops charging once an upper temperature limit is reached in defined storage regions. This prevents the storage tank from being fully heated, particularly in the lower section. After a defined hysteresis, charging is enabled again. During discharge, heat supply to the consumer is stopped if the temperature falls below 55°C.

For comparison, the storage systems are simulated over extended periods under identical conditions with respect to storage volume, control strategy, charging logic, load profile and temperature requirements on the consumer side. The weekday load profile differs slightly from the weekend profile, with higher domestic hot water demand occurring later in the day on weekends. Differences between the systems therefore result only from the use of PCM capsules and the associated increase in energy density at the melting temperature.

Figure 3 illustrates the evaluation approach, showing the total stored energy relative to a reference temperature of 10 °C as a solid gray line, while the fraction of energy above the usable temperature level of 55 °C is indicated by a dashed gray line.

For the water storage, charging and discharging occur without restrictions on the usable temperature range. During charging, the temperature in the lower storage region increases gradually until charging is interrupted by the controller.

As a result, the water storage is able to supply the consumer continuously over the entire simulation period.

The hybrid storage using PCM with a melting temperature around 58 °C can store more energy at the desired temperature level, although this energy cannot always be delivered immediately. At high discharge rates, temporary temperature drops occur, followed by a temperature recovery. These effects are observed around 22 h on a daily basis. This behavior is caused by the delayed phase change process.

The available sensible heat in the water is utilized. Cool water enters the region of freezing PCM capsules and absorbs latent heat, reheating the water to a slightly higher temperature.

Consistent with this effect, the gray dashed line shows that part of the stored energy remains available at the desired temperature level at the end of the day.

In contrast, the storage system with PCM 37 cannot provide the required supply temperature, even though the total stored energy is higher, since the control strategy allows charging to continue to lower temperature levels before charging is stopped. Toward the end of each day, the temperature drops well below the minimum required level. Although some energy above 55 °C is available at the beginning of each cycle, it is almost completely depleted during the first heat extraction. The PCM latent energy does not contribute, since phase change occurs below the usable temperature level.

Under the investigated boundary conditions, no direct benefit for the consumer is observed from PCM integration compared to an ideal stratified water storage. Although the hybrid tank with PCM and a melting temperature of 58 °C maintains a slightly larger amount of energy at the required temperature level, this additional energy is not accessed in the considered scenario.

This outcome highlights that a higher overall storage capacity alone does not lead to improved consumer level performance and motivates the analysis of alternative load profiles. Advantages arise when the limited discharge power of the PCM capsules is explicitly taken into account. If the maximum discharge power is reduced while the daily energy demand is increased, the PCM storage with a melting temperature of 58 °C provides benefits compared to the water storage.

Under a modified load profile with reduced peak discharge rates within one hour and a higher daily total heat demand, the PCM storage is able to fully cover the demand, as shown in Figure 4.

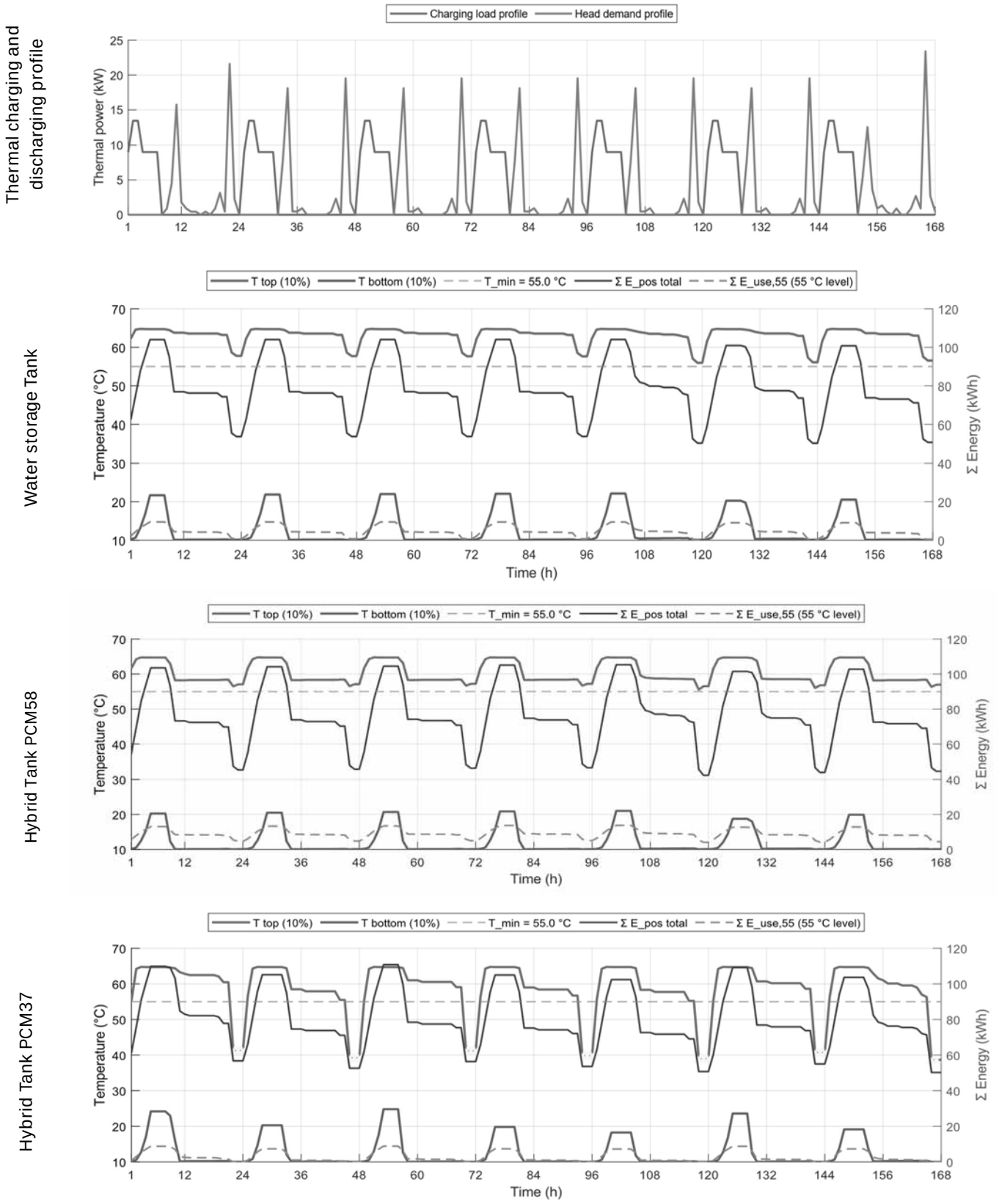

Figure 3: Storage temperatures at the top and bottom and energy level over time under the weekly load profile, including the fraction of energy available above 55 °C.

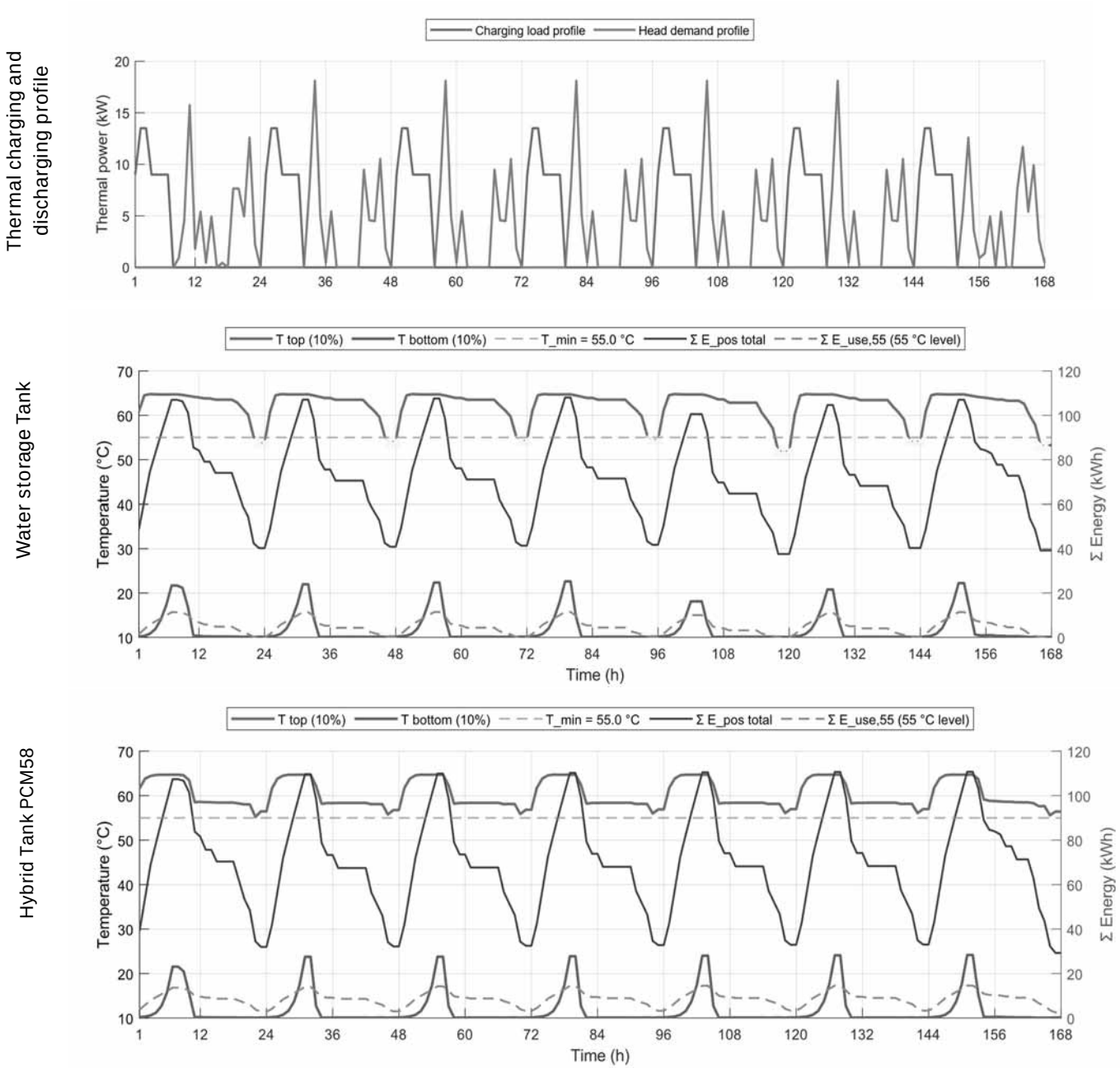

Figure 4: Storage temperatures at the top and bottom and energy level over time under the modified weekly load profile, including the fraction of energy available above 55 °C.

Under the same conditions, the stratified water storage reaches a coverage of 87 percent, leaving 948 hours uncovered out of a total of 7776 hours with heat demand. These results demonstrate that PCM based storage systems can provide benefits under specific operating conditions. In this case, for load profiles with lower peak demands, PCM enables a higher amount of energy to be available at the required temperature level than water storage, while the discharge power remains constrained by the PCM properties and its interaction with the surrounding water.

Further evaluation is required for storage systems with indirect heat transfer and for concepts with multiple charging sources operating at different temperature levels. On the system level, temperature dependent effects must also be taken into account, since both the efficiency of heat generators such as heat pumps and the requirements of consumers strongly depend on the operating temperature level and influence overall system performance.

In addition, long term thermal storage concepts that operate beyond hourly fluctuations should be analyzed to assess their impact on overall system efficiency. Within this context, the presented approach provides a practical tool for evaluating PCM integrated storage systems under dynamic operating conditions.

Nomenclature

Latin Symbols		
Symbol	**Unit**	**Quantity**
A	m^2	Area
c_p	$J/(kg\,K)$	specific heat capacity at constant pressure
T	K	temperature
t	s	time
U	$W/(m^2\,K)$	overall heat transfer coefficient
V	m^3	volume
Greek Symbols		
Symbol	**Unit**	**Quantity**
ε	-	porosity
λ	$W/(mK)$	thermal conductivity
ρ	kg/m^3	density

References

[1] Jäger, Sarah; Pabst, Valerie; Renze, Peter (2024): Multizone Modeling for Hybrid Thermal Energy Storage. In: *Energies* 17 (12), S. 2854. DOI: 10.3390/en17122854

[2] Untrau, Alix; Sochard, Sabine; Marias, Frédéric; Reneaume, Jean-Michel; Le Roux, Galo A. C.; Serra, Sylvain (2023): *A fast and accurate 1-dimensional model for dynamic simulation and optimization of a stratified thermal energy storage*. In: *Applied Energy* 333, DOI: 10.1016/j.apenergy.2022.120614

[3] Bundesverband Wärmepumpe (BWP) e.V. (2023): Leitfaden Trinkwassererwärmung. Hg. v. BWP. Online verfügbar unter https://www.waermepumpe.de/verband/publikationen/fachpublikationen/, zuletzt geprüft am 29.01.2025

Publication Remark

This contribution is the significantly extended version of the Workshop proceedings version for

ASIM Workshop GMMS/ STS 2025 - Munich/Oberpfaffenhofen 2025,

published in

ASIM Workshop GMMS/STS 2025 Tagungsband ARGESIM Report 48, e-ISBN 978-3-903347-66-3, Volume DOI 10.11128/arep.48, p 61-63.

EZStrobe Model for ARGESIM Benchmark C10 'Dining Philosophers Problem II'

Photios G. Ioannou[1*], Marios C. Papaefthymiou[2], Constantine A. Ioannou[2]

[1]Dept. of Civil and Environmental Engineering, University of Michigan, Ann Arbor, MI, USA, *photios@umich.edu
[2]School of Information and Computer Sciences, University of California, Irvine, CA, USA

SNE 36(2), 2026, 73-76, DOI: 10.11128/sne.36.bn10.10772
Submitted: 2025-12-21
Received: 2026-01-30; Accepted: 2026-02-10
SNE - Simulation Notes Europe, ARGESIM Publisher Vienna
ISSN Print 2305-9974, Online 2306-0271, www.sne-journal.org

Abstract. The EZStrobe add-on for the STROBOSCOPE simulation system is used to model the classic "Dining Philosophers" problem, where five philosophers sit around a table in front of five plates of food and alternate between thinking and eating. There are only 5 chopsticks available, and because philosophers need two chopsticks to eat, at most two can be eating at the same time. Thus, activities compete for limited resources. The EZStrobe simulation model is presented, and the reasons for the differences in its results from previous solutions are examined.

Introduction

The *ARGESIM Benchmark C10* [1] depicts five philosophers seated around a table, each with a plate of food in front of them. The philosophers alternate between thinking and eating, which requires the use of two chopsticks. Only five chopsticks are available, positioned between the five plates. Thus, only two philosophers could be eating at the same time. The durations of the thinking and eating activities are such that, although random, they could result in more than one philosopher wanting to start eating at exactly the same simulation time and thus competing for the available chopsticks.

1 EZStrobe - STROBOSCOPE

EZStrobe is an add-on for the STROBOSCOPE discrete-event simulation system [2] that provides a graphical drag-and-drop modelling user interface (GUI) that runs within Microsoft Visio using VBA (Figure 1).

Both EZStrobe and STROBOSCOPE are based on three-phase activity scanning, which is especially suited for cyclic operations, such as those in *ARGESIM Benchmark C10*.

EZStrobe models are simpler and utilize only one predefined type of generic resource named EZs. Simulation models are networks of nodes where resources spend time (such as activities and queues), connected by links that control both when activities can start and the flow of resources (from preceding to succeeding nodes).

An important objective of EZStrobe is that it does not require the user to be proficient in the STROBOSCOPE modelling language. Additionally, the EZStrobe GUI is designed to communicate graphically nearly all the key details of a simulation model network, such as the duration and priority of activities, the initial contents of queues at the start of simulation, the *enough* attributes and *draw amounts* of *drawing* links, and the *release amount* of *releasing* links. Only the global simulation controls, such as the initial seed, the simulation stopping conditions, and the number of replications, are hidden from view. They are accessed in a dialog box that appears when the user right-clicks the Visio model page.

2 EZStrobe Simulation Model

The EZStrobe simulation model network is shown in Figure 1. The rectangles with clipped corners are the conditional activities (*combis*) "Think*k*" (blue) and "Eat*k*" (green) for each philosopher *k*.

A key modelling concept in EZStrobe (and STROBOSCOPE) is that a combi activity can only be preceded by queues, and queues can only precede combi activities. Each combi activity cannot start and create an instance unless it has the required resources, which are provided by the directly preceding queues.

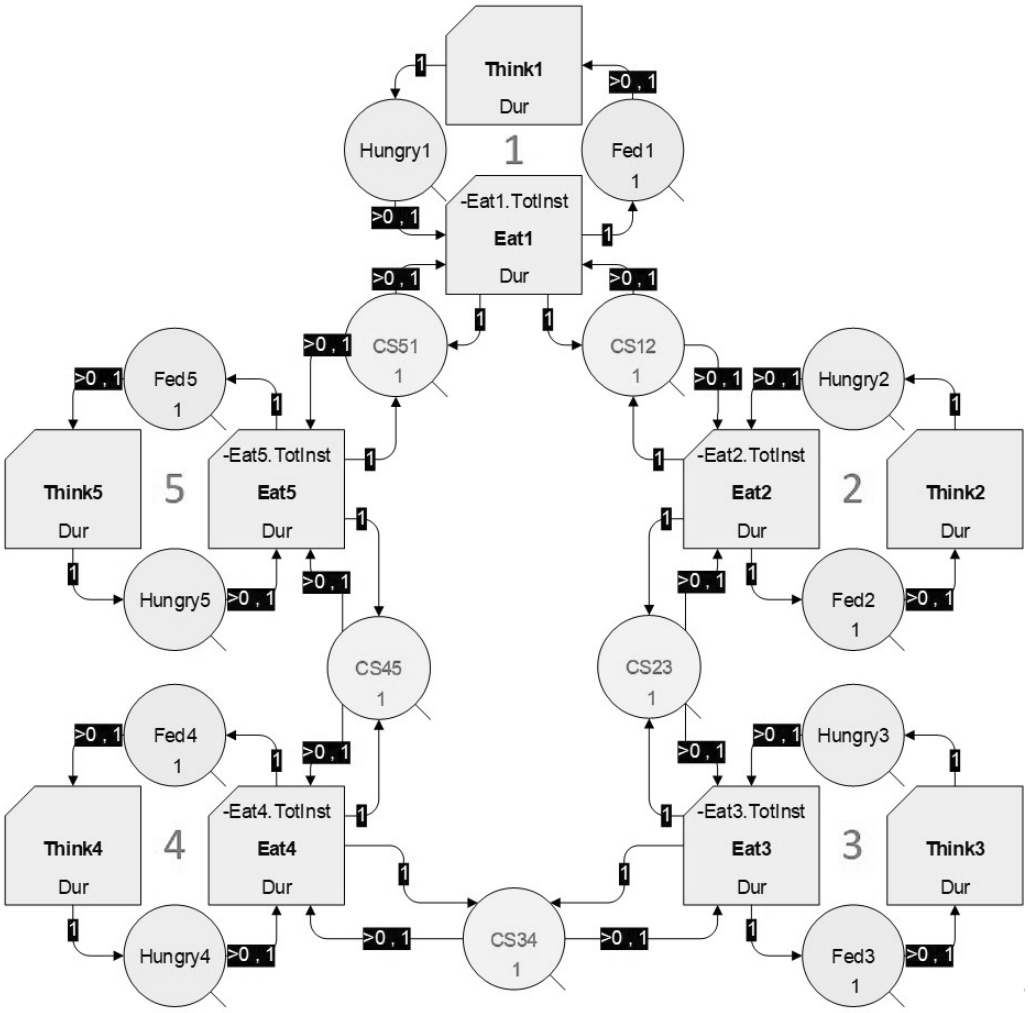

Figure 1: EZStrobe Simulation Model Network for ARGESIM Benchmark C10 'Dining Philosophers'.

The startup of each combi activity is managed by its *drawing links*, which are the links from each preceding queue to the combi, and through which a new combi instance draws resources when it starts. To ensure that *all* preceding queues will have *enough* resources to support a new combi activity instance, each *drawing link* has two attributes (defined below): the '*enough*' and the '*draw amount*', which are displayed in white letters inside a black box on top of each drawing link.

The *enough* attribute is a logical condition about the contents of the preceding queue. The default *enough* expression is ">0", which checks that the contents of the queue are greater than zero.

This means that the preceding queue has enough resources to support the start of a new instance of the succeeding combi activity when the queue is not empty.

A combi activity can start a new instance and draw resources *only* when the *enough* attributes for *all* its incoming drawing links return the logical value *true*.

The *draw amount* is the number of resources moved from the queue to the combi each time the combi starts and creates an instance. The default draw amount is 1.

Similarly, each *releasing link* from a combi to a queue displays its *release amount* with white letters in a black box.

The *release amount* is the number of resources released to the succeeding queue each time a combi instance finishes. The default *release amount* is 1.

Each of the five "Fed*k*" queues represents a philosopher who has just eaten and is ready to start thinking. At the start of the simulation, they are initialized with one resource, as shown at the bottom of each queue.

Each of the five "CS*ij*" queues represents the chopstick between philosophers *i* and *j*. They are also initialized with one resource each.

In this model, the *enough* attributes for all drawing links are the default ">0". Thus, at time zero, all five "Think*k*" can start because their preceding queues "Fed*k*" are not empty (they are initialized with 1 resource). Later, a combi "Eat*k*" will only be able to start when *all three* of its preceding queues "Hungry*k*", "CS*jk*", and "CS*kl*" are not empty.

Each time the simulation clock advances, *all* combi activities are first *sorted* according to their *priority* attribute and then examined one by one to determine if they can start, in that order. If all the *enough* attributes of all drawing links for the examined combi return the value *true*, then the activity creates an instance and removes *draw amount*, i.e., "1" resource from each preceding queue as shown on the drawing link.

Thus, in an EZStrobe simulation model with the default *enough* link attributes, each combi activity "Eat*k*" first checks that both chopsticks it needs are available, and then creates an instance and draws both chopsticks, one after the other. Thus, it is impossible for only one chopstick to be drawn and for deadlock to occur, unless the model is specifically contrived (which serves no practical purpose).

This model sets the priorities of the "Eat*k*" activities by the dynamic expression "-Eat*k*.TotInst" (shown at the top of the "Eat*k*" combi activity nodes in Figure 1). Larger values of the activity priority attribute result in higher priority. Thus, top priority is given to the combi activity "Eat*k*" that has had the *least total instances* up to now (to make eating equitable). (Priorities could also reflect the philosophers' current waiting-to-eat time.)

The durations of activities "Think*k*" and "Eat*k*" follow discrete uniform distributions in the interval [1, 10] that were implemented by the variable *Dur*, defined by the expression: 'Int[Uniform[0,10]] + 1'.

This ensured that more than one "Eat*k*" activity would want to start at exactly the same simulation time and thus compete for the adjacent chopsticks.

In this model, whenever adjacent "Eat*k*" activities could start at the same simulation time, the one with the fewest number of instances up to now will be the one examined first and be able to start a new instance and take both adjacent chopsticks.

3 Results

The model shown in Figure 1 was run for 100,000 time units (this run took 0.3 seconds). A subset of the default statistics reported by STROBOSCOPE is shown in Tables 1 and 2.

As expected, the statistics for "Thinking" and "Eating" are close to the moments $m = 5.5$ and $\sigma = 2.87$ for the discrete uniform distribution in the interval [1, 10].

However, the Avg=4.19 and StDev=4.39 for the times when the philosophers are "Waiting" to eat are less than half of those in [3] and [4], which report values closer to Avg=11.5 and StDev=8.

State	P1	P2	P3	P4	P5	All
Thinking	5.53	5.51	5.41	5.51	5.54	5.50
	2.87	2.88	2.84	2.86	2.84	2.86
Waiting	4.13	4.19	4.27	4.18	4.17	4.19
	4.32	4.45	4.54	4.28	4.37	4.39
Eating	5.50	5.46	5.48	5.46	5.46	5.47
	2.90	2.87	2.87	2.88	2.86	2.88

Table 1: Philosophers' times in respective states (average and standard deviation).

State	CS1	CS2	CS3	CS4	CS5	All
Waiting	2.10	2.11	2.11	2.12	2.10	2.11
	2.57	2.58	2.57	2.60	2.56	2.58
Utilization	72%	72%	72%	72%	72%	72%

Table 2: Chopstick times in respective states (average and standard deviation) and utilization.

The chopstick "Utilization" of 72% in Table 2 is also less than the 92% reported in [3] and [4]. (Previous solutions do not report the "Waiting" times for chopsticks.)

A possible explanation for the differences in the reported statistics is that the default *enough* attribute of links in EZStrobe does *not allow* a hungry philosopher to draw just the chopstick on his left without also drawing the one on his right and start eating. Drawing just the chopstick on the left would also block the philosopher on their left from eating and increase their waiting time, too, as they would have to wait for the philosopher on the right to start and finish eating. It might also cause a deadlock when all five philosophers are hungry and have all drawn the chopsticks on their left.

By design, the *enough* link attributes in EZStrobe and STROBOSCOPE do not allow deadlock to occur by *ensuring first* that an activity can draw *all the resources it needs, before* allowing the activity to start a new instance and draw *any* resources. Clearly, this is the preferred strategy since it reduces the time philosophers wait before they can eat to less than half (from 11.5 to 4.19).

To investigate the system's behaviour, this model was also run with a different priority rule for the "Eat*k*" activities. Specifically, higher priority was given to the "Eat*k*" activity for the philosopher who had currently been waiting the longest time to eat. The resulting statistics were indistinguishable from those in Tables 1 and 2.

4 Conclusion

The simulation model presented here is particularly suitable for educational purposes, as it can be easily developed in EZStrobe using drag-and-drop graphics.

All the modelling elements (i.e., activities, queues, and links) shown in Figure 1 are instances of predefined intelligent EZStrobe shapes in Visio that were dragged, positioned, and connected on the model page.
The only additional requirement was to double-click these shapes and define the initial contents of queues, as well as the expressions for the duration and priority of activities in the custom dialogs that would appear.

To define the time at which the simulation should stop, the user right-clicks the model page, which opens the appropriate dialog. To run the simulation, the user right-clicks the model page and selects the option "Run simulation" from the menu that appears.

This instructs EZStrobe to construct the appropriate simulation model using the STROBOSCOPE language and send it to STROBOSCOPE for processing (all of which are hidden from the user). STROBOSCOPE then performs the simulation and presents the results in its own window.

References

[1] Breitenecker F, Schmidt B. Comparison 10: Dining Philosophers II. Definition of ARGESIM Benchmark C10. Simulation Notes Europe SNE. 1996; 06(18): 32-33.

[2] STROBOSCOPE Simulation System Software. Retrieved from www.stroboscope.org. Sept. 20, 2025.

[3] Legourski V, Huang Y, Cevan O, Breitenecker F. Statechart Modelling for ARGESIM Benchmark C10 'Dining Philosophers Problem II' using Simulink/Stateflow. Simulation Notes Europe SNE. 2008; 18(1): 39-40.

[4] Löscher T, Breitenecker F. A Petri Net-based solution to ARGESIM Comparison C10 'Dining Philosophers II' using MATLAB and PetriSim. Simulation Notes Europe SNE. 2005; 15(43): 29.

Benchmarking of Flatness-based Control of the Heat Equation

Stephan Scholz[1*], Lothar Berger[2], Dirk Lebiedz[3]

[1]Independent Researcher [*]*stephan.scholz@alumni.uni-ulm.de*
[2]Control and Process Engineering, University of Applied Sciences Ravensburg-Weingarten, Weingarten, Germany
[3]Institute of Numerical Mathematics, Ulm University, Ulm, Germany

SNE 36(2), 2026, 77-86, DOI: 10.11128/sne.36.tn.10773
Selected ASIM SST 2024 Postconf. Publication: 2025-06-10
Received Revised Extended: 2026-02-13; Accepted: 2026-03-15
SNE - Simulation Notes Europe, ARGESIM Publisher Vienna
ISSN Print 2305-9974, Online 2306-0271, www.sne-journal.org

Abstract. Flatness-based control design is a well established method to generate open-loop control signals. Several articles discuss the application of flatness-based control design for (reaction-) diffusion problems in various scenarios. Beside the pure analytical derivation also the numerical computation of the input signal is crucial to yield a reliable trajectory planning. Therefore, we derive the input signal step-by-step and describe the influence of system and controller parameters on the computation of the input signal. In particular, we benchmark the control design of the one-dimensional heat equation with Neumann-type boundary actuation for pure aluminum and steel 38Si7, and discuss the applicability of the found input signals for realistic scenarios.

1 Introduction

The flatness-based control method is an open-loop technique to steer the system output along a reference trajectory [1]. In case of finite-dimensional linear and nonlinear systems the input signal $u(t)$ is found by a finite number of derivatives of a (differentially flat) output which equals the reference signal. This approach is extended to infinite-dimensional and distributed parameter systems where theoretically an infinite number of derivatives of output signal $y(t)$ is necessary to compute the input signal $u(t)$, see [2, 3, 4].

However, for practical reasons we can only consider a finite number of derivatives of the output signal. Thus, we need to show that the computation of input signal $u(t)$ converges for a certain number of derivatives of $y(t)$.

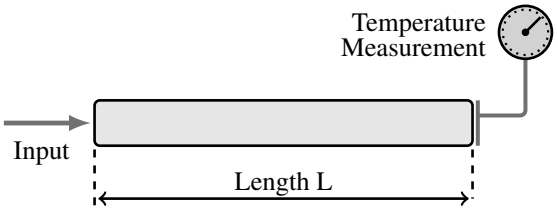

Figure 1: Scheme of one-dim. heat conduction with heat supply at $x = 0$ and temperature measurement at $x = L$.

In general, this estimation of convergence is not trivial because the computation of $u(t)$ depends on system and control parameters. A related approach about the controllability of the heat equation with a finite number of derivatives of y is discussed in [4].

In this contribution, we assume a one-dimensional linear heat equation with Neumann boundary actuation as depicted in Fig. 1 to discuss the impact of system and control parameters on the computation of input signal $u(t)$. For this purpose, we compare pure aluminum and steel 38Si7 to exemplify our findings. They differ in their material properties: thermal conductivity λ, specific heat capacity c and density ρ. Regarding the control parameters, we design the reference trajectory as a smooth step, which is configured by the transition time and the steepness [5]. In each step of the analysis, we evaluate numerically the significance of the system and control parameters on the final control signal. Hence, we show the transition from a pure analytical towards a simulation-based control design and this enables us to distinguish whether or not a control signal is indeed applicable for a system.

In Section 2, we introduce the flatness-based modeling for the one-dim. heat equation and we derive an input signal $u(t)$. The influence of the system parameters are analyzed in Section 3.

The trajectory planning problem and the subsequent discussion of the control parameters are described in Section 4 and 5, respectively. Finally, we present the simulation results of the open-loop system and review the applicability for realistic scenarios in Section 6.

2 Flatness-based Control

We assume a one-dim. heat conduction model as portrayed in Fig. 1 with a rod of length $L > 0$, final time $T > 0$, temperature $\vartheta : [0,L] \times [0,T] \to \mathbb{R}_{\geq 0}$ and diffusivity $\alpha = \frac{\lambda}{c\,\rho}$, where λ, c, $\rho > 0$. We describe the thermal dynamics inside the rod as

$$\dot{\vartheta}(t,x) = \alpha \frac{\partial^2}{\partial x^2} \vartheta(t,x) \tag{1}$$

for $(t,x) \in (0,T) \times (0,L)$ and we model the dynamics on the boundary sides $x \in \{0\} \cup \{L\}$ with Neumann boundary conditions. On the left side we have actuation

$$u(t) = \lambda \frac{\partial}{\partial x} \vartheta(t,x) \cdot \vec{n}_0 \Big|_{x=0}, \tag{2}$$

and on the right side we note thermal insulation as

$$0 = \lambda \frac{\partial}{\partial x} \vartheta(t,x) \cdot \vec{n}_L \Big|_{x=L} \tag{3}$$

with the outer normal vectors $\vec{n}_0 = -1$ and $\vec{n}_L = 1$.

This heat conduction model is strongly simplified because in real world scenarios, often we have to consider two- or three-dimensional heat conduction with temperature-dependent material properties and probably thermal emissions consisting of linear heat transfer and nonlinear heat radiation towards the environment, see also [6, 7, 8].

However, such realistic heat conduction scenarios lead to a much more complex mathematical discussion which is out of scope of this contribution, and the presented control method and its numerical analysis might not be applicable anymore. We have the constant uniform initial temperature data

$$\vartheta(0,x) = \vartheta_0 > 0$$

for $x \in [0,L]$ and the temperature is measured on the right boundary as

$$y(t) = \vartheta(t,L). \tag{4}$$

As known from the literature [2, 3, 4] the heat equation can be represented by a power series approach. So, we define power series

$$w(t,x) := \sum_{i=0}^{\infty} w_i(t) \frac{(L-x)^i}{i!}$$

and find its derivatives with respect to position x as

$$\begin{aligned} \frac{\partial}{\partial x} w(t,x) &= -\sum_{i=0}^{\infty} w_{i+1}(t) \frac{(L-x)^i}{i!} \quad \text{and} \\ \frac{\partial^2}{\partial x^2} w(t,x) &= \sum_{i=0}^{\infty} w_{i+2}(t) \frac{(L-x)^i}{i!}. \end{aligned} \tag{5}$$

We model heat equation (1) in terms of

$$\dot{w}(t,x) = \alpha \frac{\partial^2}{\partial x^2} w(t,x),$$

identify both sides by its power series expressions as

$$\sum_{i=0}^{\infty} \dot{w}_i(t) \frac{(L-x)^i}{i!} = \alpha \sum_{i=0}^{\infty} w_{i+2}(t) \frac{(L-x)^i}{i!}$$

and yield identity

$$\dot{w}_i(t) = \alpha\, w_{i+2}(t). \tag{6}$$

Next, we apply the information of both boundary sides on identity (6) to derive the input signal.

Firstly, we consider the output signal (4) as

$$y(t) = w(t,L) = \sum_{i=0}^{\infty} w_i(t) \frac{0^i}{i!} = w_0(t)$$

which implies $\frac{d^i}{dt^i} y(t) = \frac{d^i}{dt^i} w_0(t) = \alpha^i w_{2i}$ with identity (6) above.

Secondly, the boundary condition on the right side (3) is formulated as

$$\lambda \frac{\partial}{\partial x} w(t,L) = -\lambda \sum_{i=0}^{\infty} w_{i+1}(t) \frac{0^i}{i!} = -\lambda w_1(t) = 0$$

and we find $\frac{d^i}{dt^i} w_1(t) = \alpha^i w_{2i+1} \equiv 0$.

Thus, identity (6) is described by the sequences

$$w_{2i}(t) = \alpha^{-i} y^{(i)}(t) \quad \text{and} \quad w_{2i+1}(t) = 0 \tag{7}$$

for all $n \in \{0, 1, \ldots, \infty\}$.

In the definition of boundary actuation (2) we insert Equation (5) to derive the input signal $u(t)$ as

$$u(t) = -\lambda \frac{\partial}{\partial x} w(t,0) = \lambda \sum_{i=0}^{\infty} w_{i+1}(t) \frac{L^i}{i!}$$

and further with $i \to 2i+1$ and Equation (7) as

$$u(t) = \lambda \sum_{i=0}^{\infty} \frac{L^{2i+1}}{\alpha^{i+1}} \frac{1}{(2i+1)!} y^{(i+1)}(t). \tag{8}$$

3 Influence of System Parameters

We are interested in the sequence values of series (8) because for implementation reasons we need to how much memory has to be reserved for the computation of u and at which iteration i the summation can be stopped. The power series to compute input signal $u(t)$ can be separated in sequence

$$\eta_i = \frac{L^{2i+1}}{\alpha^{i+1}} \frac{1}{(2i+1)!}. \tag{9}$$

and the derivatives of the (desired) output signal $y^{(i+1)}(t)$. In this section, we discuss the influence of the physical properties length L and diffusivity α on sequence η_i, and in section 5 we analyze the parameters of (target) output $y(t)$ and its derivatives.

Sequence η_i is positive for all $i \in \{0,1,\ldots,\infty\}$ as we assume $L > 0$, $\alpha > 0$, and has a crucial influence on the computation of the input function u because it scales the derivatives $y^{(i+1)}$. Thus, we need to know the approximate values of η_i. We use a rescaled version of sequence (9) as

$$\tilde{\eta}_i := \left(\frac{L^2}{\alpha}\right)^{i+1} \frac{1}{(2i+1)!} = \frac{\gamma^{i+1}}{(2i+1)!} = L\,\eta_i$$

where $\gamma := \frac{L^2}{\alpha}$ to show that η_i and $\tilde{\eta}_i$ increase up to some index i and decrease afterwards to zero. Increasing iterator i by one we yield

$$\begin{aligned}\tilde{\eta}_{i+1} &= \frac{\gamma^{[i+1]+1}}{(2[i+1]+1)!} \\ &= \frac{\gamma^{i+1}}{(2i+1)!} \frac{\gamma}{(2i+2)(2i+3)} = \tilde{\eta}_i\,\beta_i\end{aligned}$$

where $\beta_i = \frac{\gamma}{(2i+2)(2i+3)}$ and we notice

$$\frac{\tilde{\eta}_{i+1}}{\tilde{\eta}_i} > 1 \quad \Leftrightarrow \quad \beta_i > 1$$

and

$$\frac{\tilde{\eta}_{i+1}}{\tilde{\eta}_i} < 1 \quad \Leftrightarrow \quad \beta_i < 1.$$

Due to the definition of $\tilde{\eta}$ this concept holds also for the original sequence (9) as $\eta_{i+1} = \beta_i\,\eta_i$. So, the maximum value of $\tilde{\eta}_i$ and η_i and its corresponding iterations i_{max} depend only on γ.

For example, if we assume $\gamma = 100$ then $\gamma < (2i+2)(2i+3)$ holds for $i \in \{1,2,3\}$ and we find the maximum value $\tilde{\eta}_4 = \frac{100^5}{9!} \approx 27557$.

Example: Comparison Aluminum and Steel

For our numerical evaluations we consider a rod of length $L = 0.2$ for two case scenarios: a rod made of pure aluminum [9] and a rod made of steel 38Si7 [10]. The physical properties of both materials are listed in Table 1. For aluminum we have $\gamma_{al} \approx 410$ and for steel 38Si7 we have $\gamma_{st} \approx 3588$.

The sequences $\eta_{al,i}$ and $\eta_{st,i}$ and their ratios $\frac{\eta_{al,i+1}}{\eta_{al,i}}$ and $\frac{\eta_{st,i+1}}{\eta_{st,i}}$ are portrayed in Fig. 2 in semi-logarithmic scaling.

These ratios $\frac{\eta_{al,i+1}}{\eta_{al,i}}$ and $\frac{\eta_{st,i+1}}{\eta_{st,i}}$ describe an evolution of the sequences by iteration and we find that inequality $\frac{\eta_{i+1}}{\eta_i} > 1$ or equally $\log_{10}\left(\frac{\eta_{i+1}}{\eta_i}\right) > 0$ holds in case of aluminum for $i \in \{1,\ldots,8\}$ and in case of steel $i \in \{1,\ldots,28\}$. Thus, the maximum values of η_i for aluminum and steel are calculated by

$$\eta_{al,9} = \frac{L^{19}}{\alpha_{al}^{10}\ 19!} \approx 5.53 \cdot 10^9$$

and

$$\eta_{st,29} = \frac{L^{59}}{\alpha_{st}^{30}\ 59!} \approx 1.59 \cdot 10^{27}.$$

Table 1: Physical Properties

	λ	ρ	c	$\alpha = \frac{\lambda}{\rho c}$
Aluminum	237	2700	900	$9.75 \cdot 10^{-5}$
Steel 38Si7	40	7800	460	$1.11 \cdot 10^{-5}$

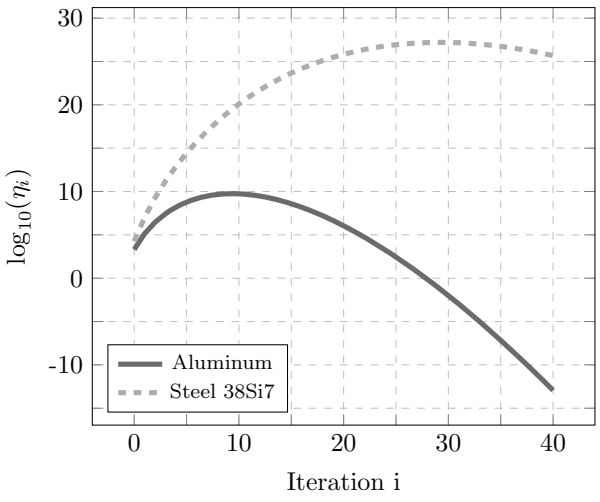

(a) Sequence η_i

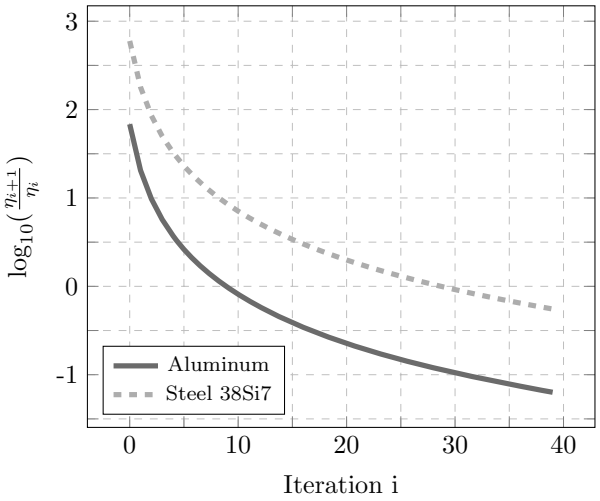

(b) Ratio η_{i+1}/η_i

Figure 2: Sequence η_i (top) and ratio $\frac{\eta_{i+1}}{\eta_i}$ (bottom) for aluminum and steel 38Si7.

As both sequences $\eta_{al,i}$ and $\eta_{st,i}$ reach such enormous maximum values, computational issues related to big numbers and data types have to be considered in the implementation process.

Moreover, sequence $\log_{10}(\eta_{al,i})$ drops below zero for $i > 27$: $\eta_{al,28} \approx 0.73$, $\log_{10}(\eta_{al,28}) \approx -0.13$; and $\log_{10}(\eta_{st,i})$ drops below zero for $i > 82$: $\eta_{st,83} \approx 0.13$, $\log_{10}(\eta_{st,83}) \approx -0.87$ (not displayed in Fig. 2).

4 Trajectory Planning

According to [3, 5] we consider a transition from one fixed operating point to the next one as

$$y(t) = y_0 + \Delta y \, \Phi_{\omega,T}(t) \tag{10}$$

where $\Delta y = y_f - y_0$.

The transition is defined by

$$\Phi_{\omega,T}(t) = \begin{cases} 0 & t \le 0, \\ 1 & t \ge T, \\ \frac{\int_0^t \Omega_{\omega,T}(\tau)\,\mathrm{d}\,\tau}{\int_0^T \Omega_{\omega,T}(\tau)\,\mathrm{d}\,\tau} & t \in (0,T) \end{cases}$$

with the integral of the bump function

$$\Omega_{\omega,T}(t) = \begin{cases} 0 & t \notin [0,T], \\ \exp\left(-1/\left([1-\frac{t}{T}]\frac{t}{T}\right)^{\omega}\right) & t \in (0,T). \end{cases}$$

Parameter ω steers the steepness of transition $\Phi_{\omega,T}$ and is chosen such that the Gevrey order $go = 1 + \frac{1}{\omega} < 2$ or equally $\omega > 1$.
A small value of ω, e.g. $\omega = 1.1$ means a rather flat transition, whereas a large value, e.g. $\omega = 3.0$ means a quite steep transition, as depicted in Fig. 3.
To compute the input signal $u(t)$ in Equation (8) we only need to find the derivatives

$$\frac{d^i}{dt^i} y(t) = \Delta y \, \Phi^{(i)}_{\omega,T}(t) \tag{11}$$

where the derivatives of transition $\Phi_{\omega,T}$ are calculated as

$$\Phi^{(i)}_{\omega,T}(t) = \frac{\Omega^{(i-1)}_{\omega,T}(t)}{\hat{\Omega}_{\omega,T}} \quad \text{for} \quad t \in (0,T) \tag{12}$$

and $\Phi^{(i)}_{\omega,T}(t) = 0$ for $t \notin (0,1)$, using integral

$$\hat{\Omega}_{\omega,T} := \int_0^T \Omega_{\omega,T}(\tau)\,\mathrm{d}\,\tau. \tag{13}$$

In Fig. 3 trajectory $\Phi_{\omega,T}(t)$ and its first derivative are portrayed for varying $\omega \in \{1.1, 1.5, 2.0, 2.5, 3.0\}$. The derivatives $\Phi^{(i)}_{\omega,T}(t)$ can be computed symbolically using for example computer-algebra systems, see for example the MATLAB implementation [11].

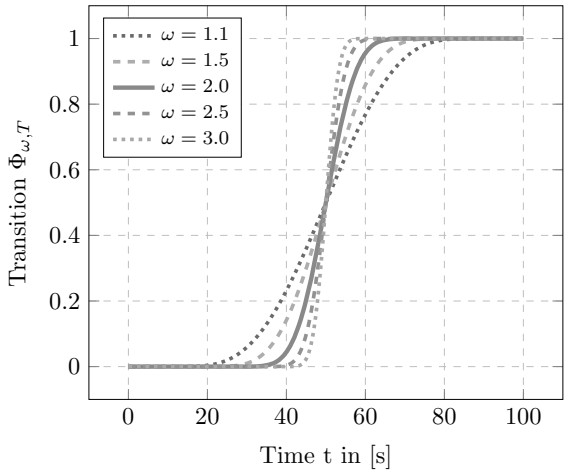

(a) Trajectory

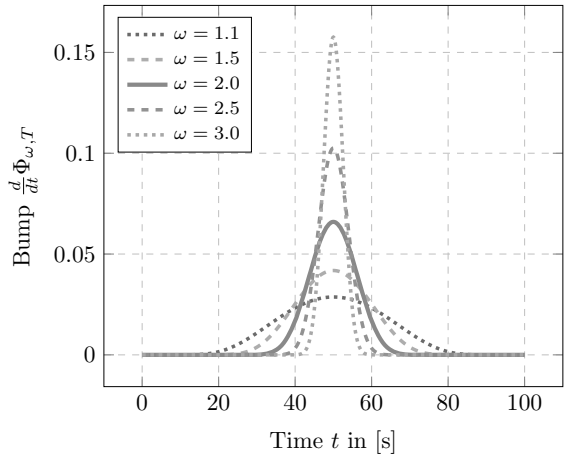

(b) First derivative

Figure 3: Trajectory $\Phi_{\omega,T}$(top) and its first derivative (bottom) with $T = 100$ seconds and varying steepness ω.

In this contribution, we compute the derivatives $\Omega^{(i)}_{\omega,T}$ with the JULIA library *BellBruno.jl* [12, 13].

We note without a proof that an increasing order of differentiation of $\Omega^{(i)}_{\omega,T}$ leads to stronger oscillations because bump function $\Omega_{\omega,T}$ is a function composition and smooth as $\Omega_{\omega,T} \in \mathscr{C}^{\infty}((0,T))$, see also [2, 13].

5 Influence of Control Parameters

The configuration of transition $\Phi_{\omega,T}$ and its derivatives are mainly driven by two parameters: final time T and exponent ω.

In this section, we apply the L^2 norm

$$\|f\|_{L^2} = \sqrt{\int_0^T |f(t)|^2 dt}$$

on $\frac{d^i}{dt^i}\Omega_{\omega,T}(t)$ to unveil the influence of final time T and exponent ω on the computation of input signal (8).

Noting the input signal with sequence η_n as

$$u(t) = \lambda \sum_{i=0}^{\infty} \eta_i \, y^{(i+1)}(t) \;=\; \frac{\lambda\ \Delta y}{\hat{\Omega}_{\omega,T}} \sum_{i=0}^{\infty} \eta_i \, \Omega^{(i)}_{\omega,T}(t)$$

and applying the identities (11, 12, 13), we find the L^2 norm of $u(t)$ as

$$\begin{aligned} \|u(t)\|_{L^2} &= \left\| \frac{\lambda\ \Delta y}{\hat{\Omega}_{\omega,T}} \sum_{i=0}^{\infty} \eta_i \, \Omega^{(i)}_{\omega,T}(t) \right\| \\ &\leq |\Delta y| \ \frac{\lambda}{\hat{\Omega}_{\omega,T}} \sum_{i=0}^{\infty} \eta_i \ \left\| \Omega^{(i)}_{\omega,T}(t) \right\| \end{aligned}$$

where we assume $\lambda, \hat{\Omega}_{\omega,T}, \eta_i > 0$.

We see that the power series is mainly driven by η_i (as discussed before) and derivatives $\Omega^{(i)}_{\omega,T}(t)$. Therefore, we are able to describe the quantitative behavior of the input signal by evaluating sequence

$$\mu_i := \frac{\lambda |\Delta y|}{\hat{\Omega}_{\omega,T}} \ \eta_i \ \left\| \Omega^{(i)}_{\omega,T}(t) \right\|_{L^2}. \tag{14}$$

The scaled norm $\| \frac{d^i}{dt^i}\Omega_{\omega,T}(t) \|_{L^2} / \hat{\Omega}_{\omega,T}$ is portrayed in Fig. 4 in logarithmic scaling for two scenarios: fixed $\omega = 2$ and varying $T \in \{10, 100, 1000\}$; and fixed $T = 1000$ and varying $\omega \in \{1.1, 1.5, 2.0, 2.5, 3.0\}$. One notes that an increasing value only of final time T leads to a reduction of $\|\Omega^{(i)}_{\omega,T}(t)\| / \hat{\Omega}_{\omega,T}$, the influence of steepness ω may not be so clear here.

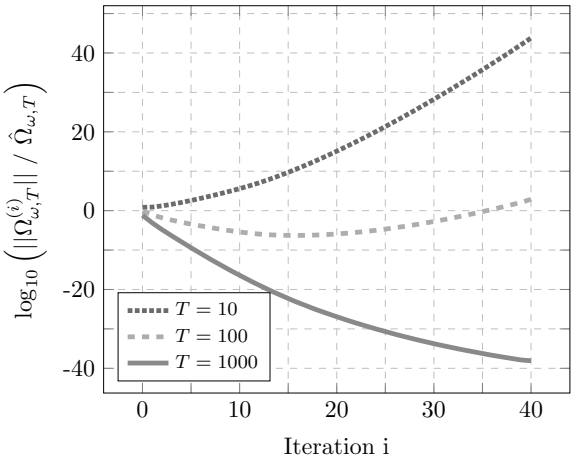

(a) Fixed $\omega = 2.0$, varying T

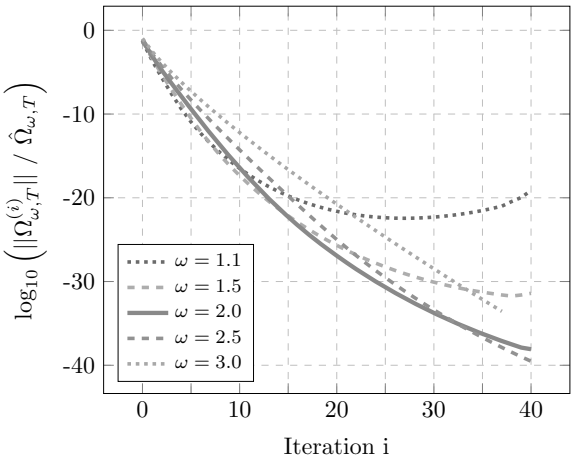

(b) Fixed $T = 1000$, varying ω

Figure 4: Norm of $\Omega^{(i)}_{\omega,T}$ with fixed $\omega = 2.0$ (top), and fixed $T = 1000$ (bottom).

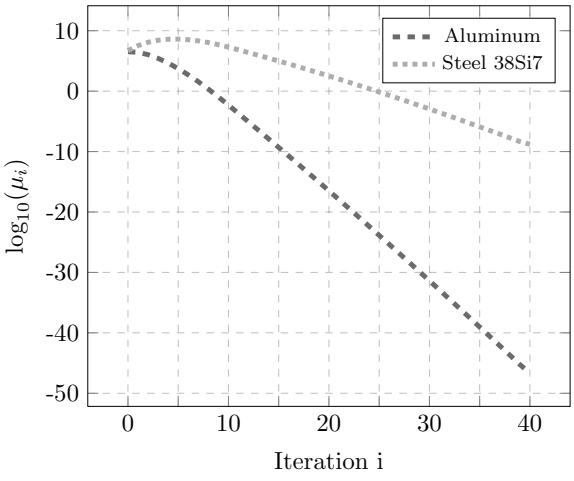

(a) Sequence μ_i as in (14)

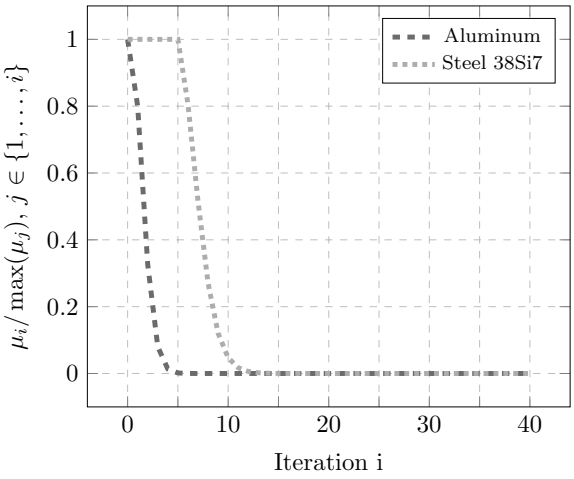

(b) $\mu_i / \max\limits_{j\in\{1,\ldots,i\}} \mu_j$

Figure 5: Sequence μ_i (top) and ratio $\frac{\mu_i}{\max\limits_{j\in\{1,\ldots,i\}} \mu_j}$ (bottom) for $\omega = 2.0$ and $T = 1000$.

Furthermore, we take advantage of sequence μ_i to find a suitable maximum iteration number i_{max} to terminate the power series of $u(t)$ in Equation (8).

Sequence μ_i consists of η_i as defined in Equation (9) and so we distinguish aluminum and steel 38Si7 as noted in Table 1).
The different values of η_i for aluminum and steel 38Si7 as in Fig. 2 lead to different values of μ_i: sequence μ_i approaching zero *faster* in case of aluminum than steel 38Si7 as depicted in Fig. 5 (a).

Introducing the ratio $\frac{\mu_i}{\max\limits_{j\in\{1,\ldots,i\}} \mu_j}$, we find that the sequence elements μ_i vanish in case of aluminum for iterations approximately above $i = 5$ whereas in case of steel 38Si7 it takes at least $i = 12$ iterations - as portrayed in Fig. 5 (b).

The evaluation of μ_i and ratio $\frac{\mu_i}{\max\limits_{j\in\{1,\ldots,i\}} \mu_j}$ unveils two facts about the generation of input signal $u(t)$.

Comparing the results for aluminum and steel 38Si7, we find in case of aluminum that only the very first derivatives of $\Phi_{\omega,T}$ are weighted by η_i and higher order derivatives have almost no influence on the computation of $u(t)$.

In case of steel 38Si7, the weights of derivatives increase up to the fifth derivative and this means that higher order derivatives (which tend to oscillatory behavior) influence the found input signal, too.

We find an approximation of the signal input

$$u(t) \approx \frac{\lambda\ \Delta y}{\hat{\Omega}_{\omega,T}} \sum_{i=0}^{N} \eta_i\ \Omega_{\omega,T}^{(i)}(t) =: u_N(t) \qquad (15)$$

where $N \in \mathbb{N}_{\geq 0}$ denotes the upper limit of iterations.

Following the previous ideas, in case of aluminum a small value of N, e.g. $N = 7$, suffices to generate a good approximation. However, for steel 38Si7 we need a higher number of iterations, e.g. $N = 15$.

The progress of input signals for aluminum with $N \in \{1,3,7\}$ and steel 38Si7 with $N \in \{5,10,15\}$ are presented in Fig. 6.
These results confirm our previous analysis that the input signal needs more series elements for steel 38Si7 than for aluminum, and this leads the stronger oscillations in Fig. 6 (b) because higher derivatives of trajectory $\Phi_{\omega,T}^{(i)}(t)$ are necessary.

In a nutshell, we find four important parameters to compute the input signal: length of rod L and diffusivity α, which define sequence η_n, and final time T and steepness ω, which adjust the derivatives of trajectory $\Phi_{\omega,T}$.

6 Simulation Results

In this section, we compare the computed input signals and the resulting heat conduction simulation for aluminum and steel 38Si7.

As above, we assume the physical properties for both materials as listed in Table 1 and two trajectories with simulation time $T = 1000$ seconds and steepness parameters $\omega \in \{1.5, 2.0\}$.

Further, we have an initial temperature $\vartheta_0 = 300$ Kelvin, which shall be increased by $\Delta y = 100$ Kelvin; and we take a maximum iteration number of $N = 40$ to approximate the input signal (15) for both materials and both trajectories.

As explained in Section 5 lower values than $N = 40$ are also sufficient sbut it may rather imitate a summation until $N = \infty$. Heat equation (1) is discretized in space using finite differences with 101 grid points and is simulated using a Runge-Kutta numerical integration method for stiff systems, see [14].

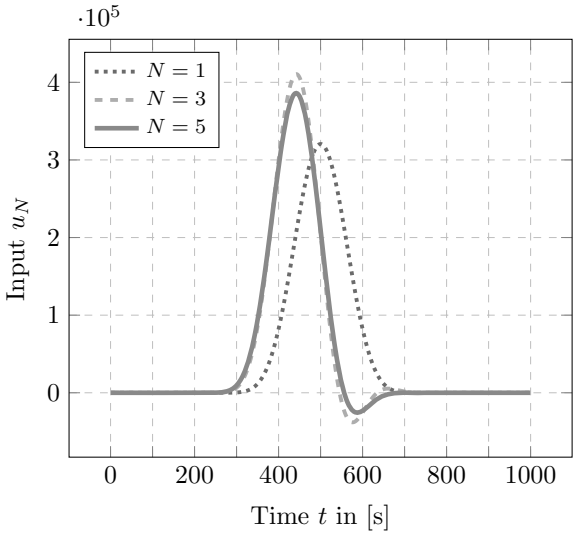

(a) Aluminum

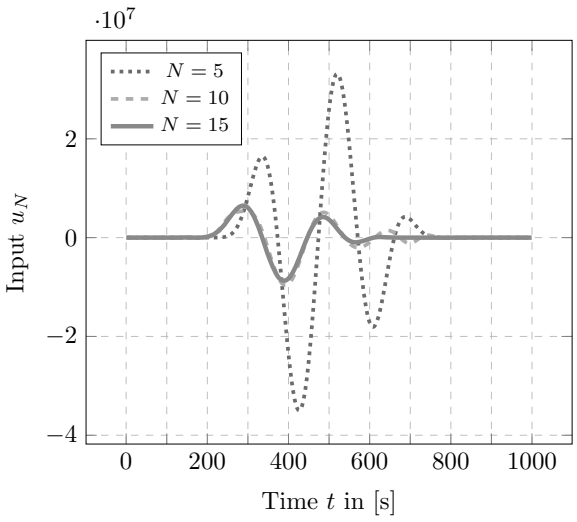

(b) Steel 38Si7

Figure 6: Progress of approximated input signals u_N for aluminum (top) and steel 38Si7 (bottom) with $T = 1000$ and $\omega = 2$.

The input signals and the resulting temperatures are illustrated in Fig. 7: the input signals for both trajectories are drawn in the first row for aluminum in (a) and for steel 38Si7 in (b); the resulting thermal dynamics for the less steep trajectory ($\omega = 1.5$) is visualized in the second row (c,d) and for the steep case ($\omega = 2.0$) in the third row (e,f).

In all cases the output, meaning the temperature at $x = L = 0.2$ meter, follows the reference and reaches 400 Kelvin; and we notice that a steeper trajectory ($\omega = 2.0$) causes higher temperatures in the rod, $x < L$. So, from a pure *mathematical* point of view the input signals are computed correctly for all scenarios.

However, from a *physical* point of view we need to discuss the input signals and the resulting temperatures rather critically. Beside the fact that it may not be possible to apply negative input signals, e.g. if the actuator offers only heating and not cooling, it is in fact not possible to reach temperatures below zero Kelvin as portrayed for steel reference in Fig. 7 (f).

We highlight that the strong oscillations of the input signal for steel 38Si7 in Fig. 7 (b) lead to the unrealistic temperature evolution in Fig. 7 (f). Therefore, the control parameters final time T and steepness ω have to be readjusted to decrease the necessary number of series elements, to yield a input signal with weaker or eliminated oscillations and hence a realizable temperature evolution.

7 Conclusion & Discussion

In this article we presented the computation of input signals for trajectory planning of a one-dim. heat equation using flatness-based control design.

We found in our analysis of the influence of system and control parameters on the computation of the input signal that different material properties (aluminum, steel 38Si7) result in completely different input signals and open-loop dynamics - even if all other parameters (length of rod, final time, steepness of transition) are the same.

We demonstrate that strictly following the flatness-based control design may not lead to an physically realizable input signal even if the series in Eq. (8) converges.

Thus, we recommend to simulate the heat equation with input signal to gain trustworthy arguments for the applicability of the computed flatness-based input signal.

We motivate further research on the proposed approach for realistic scenarios in two and three dimensions including thermal convection and radiation.

Source Code

The source code is developed in JULIA programming language [15] and is available on *GitHub* and *Zenodo*: [16]. We used the JULIA libraries *OrdinaryDiffEq.jl* [17] for the numerical integration in time of the spatially approximated heat equation and *BellBruno.jl* [12] to compute the derivatives $\Omega^{(i)}_{\omega,T}$. The figures are created with *TikZ* and *pgfplots*.

Acknowledgements

S. Scholz conducted the majority of the work for this article during his professional position at the University of Applied Sciences Ravensburg-Weingarten and his doctoral studies at Ulm University.

Publication Remark

This contribution is the revised extended version of the conference version for

ASIM SST 2024
27th Symposium Simulation Technique
Munich September 2024,

published in

ASIM 2024 Tagungsband Langbeiträge
ARGESIM Report 47, e-ISBN 978-3-903347-65-6,
Volume DOI 10.11128/arep.47
Article DOI: 10.11128/arep.47.a4703, p 103-111.

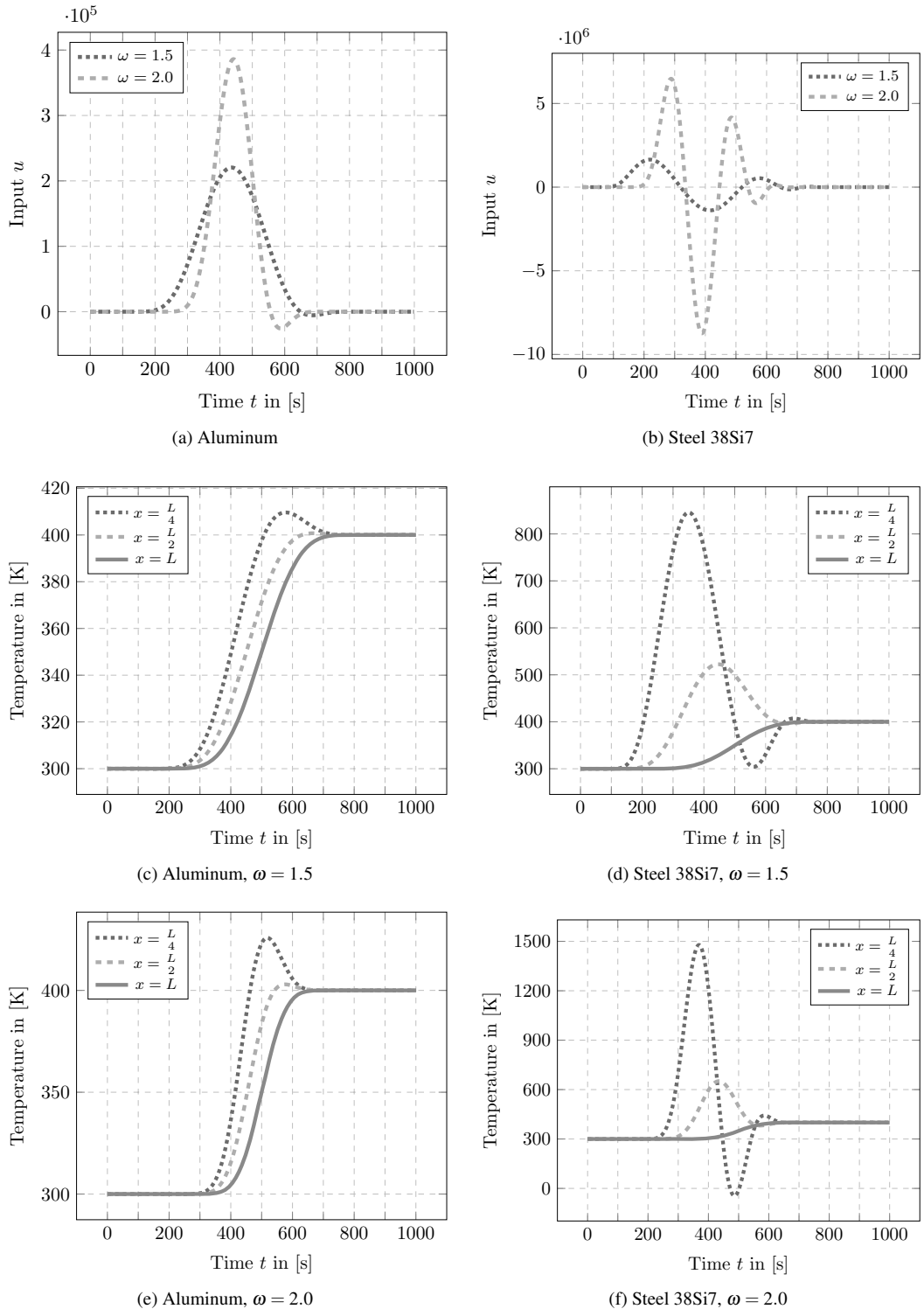

(a) Aluminum

(b) Steel 38Si7

(c) Aluminum, $\omega = 1.5$

(d) Steel 38Si7, $\omega = 1.5$

(e) Aluminum, $\omega = 2.0$

(f) Steel 38Si7, $\omega = 2.0$

Figure 7: Input signals for transitions with steepness parameter $\omega \in \{1.5, 2.0\}$ and the resulting temperatures at position $x \in \{0.05, 0.1, 0.2\}$.

References

[1] Fliess M, Lévine J, Martin P, Rouchon P. Flatness and defect of non-linear systems: introductory theory and examples. International Journal of Control. 1995; 61(6) (1995): 1327–1361.

[2] Laroche B, Martin P, Rouchon P. Motion planning for the heat equation. International Journal of Robust and Nonlinear Control: IFAC-Affiliated Journal. 2000; 10(8): 629–643.

[3] Rudolph J, Winkler J, Woittennek F. Flatness Based Control of Distributed Parameter Systems: Examples and Computer Exercises from Various Technological Domains. Shaker. 2003.

[4] Martin P, Rosier L, Rouchon P. Null controllability of the 1D heat equation using flatness. IFAC Proceedings Volumes. 2013; 46(26): 7–12.

[5] Utz T, Graichen K, Kugi A. Trajectory planning and receding horizon tracking control of a quasilinear diffusion-convection-reaction system. IFAC Proceedings Volumes. 2010; 43(14): 587–592.

[6] Scholz S, Berger L. Modeling of a multiple source heating plate. arXiv preprint. arXiv:2011.14939 (2020).

[7] Scholz S, Berger L. Hestia.jl: A Julia library for heat conduction modeling with boundary actuation. Simulation Notes Europe SNE. 2023; 33(1): 27–30.

[8] S. Scholz, "Scientific computing for multidimensional nonlinear heat conduction and control of multiple heat sources," Doctoral thesis, Universität Ulm, Ulm, 2025.

[9] Connor N. Aluminium - Periodic Table. [Online]. Available:https://www.periodic-table.org/Aluminium-periodic-table/. [Accessed: Mar. 28, 2024].

[10] Ovako AB. 38Si7. [Online]. Available: https://steelnavigator.ovako.com/steel-grades/38si7/. [Accessed: Mar. 28, 2024].

[11] Fischer F, Gabriel J, Kerschbaum S. coni-a Matlab toolbox facilitating the solution of control problems. Zenodo. 2022. Available: https://zenodo.org/record/6420876.

[12] Scholz S. BellBruno.jl. Zenodo. 2023. Available: https://doi.org/10.5281/zenodo.7685927

[13] S. Scholz and L. Berger, "Fast computation of function composition derivatives for flatness-based control of diffusion problems," Journal of Mathematics in Industry, vol. 14, no. 1, p. 15, 2024.

[14] Kennedy CA, Carpenter MH. Additive Runge-Kutta schemes for convection-diffusion-reaction equations. Applied numerical mathematics. 2003; 44(1-2): 139–181.

[15] Bezanson J, Edelman A, Karpinski S, Shah VB. Julia: A fresh approach to numerical computing. SIAM review. 2017; 59(1):65–98.

[16] Scholz S. BenchmarkFlatnessbasedControl.jl. Zenodo. 2026. Available: https://doi.org/10.5281/zenodo.18499122

[17] Rackauckas C, contributors. SciML/DifferentialEquations.jl. Zenodo. 2022. Available: https://doi.org/10.5281/zenodo.7239171

Generalized Virtual Stochastic Sensors - Training and Reconstruction in Various Single Resident Apartments

Claudia Krull*, Vishwajeet Karumuri

Fakultät für Informatik, Otto-von-Guericke-Universität, Postfach 4120, 39016 Magdeburg, Germany
*claudia.krull@ovgu.de

SNE 36(2), 2026, 87-94, DOI: 10.11128/sne.36.tn.10774
Selected ASIM GMMS/STS 2025 Postconf. Publ.: 2025-10-22
Rec. Full English: 2026-03-30; Accepted: 2026-05-10
SNE - Simulation Notes Europe, ARGESIM Publisher Vienna
ISSN Print 2305-9974, Online 2306-0271, www.sne-journal.org

Abstract. The advancements in Ambient Assisted Living (AAL) have been prompted by the growing population of elderly individuals facing diagnoses such as Dementia or Alzheimer's, aiming to enhance their overall quality of life. To provide support it is important to know their daily activities and aid them when needed. A large portion of research in the field of Human Activity Recognition uses black box learning approaches such as deep learning, but there are cases where model based methods, such as Virtual Stochastic Sensors (VSSs) are competitive. This is possible because the model based methods can include system structure in the modeling process if it is known. VSS's are derived from Hidden Markov Models (HMM) and applied to single resident datasets, which are collected in apartments fitted with different types of ambient sensors. For future applications a generalization of behavior, sensors or models is necessary so that models are not just trained and used for one specific apartment and setup. In this paper we test different model and activity setups while training and testing on different apartments. The results show that a model trained on a set of similar apartments can be used for behavior reconstruction on an apartment outside of that training set.

Introduction

Advancements in the medical field led to long and healthier lives, roughly around 20% of the world population will be aged above 60 by 2050 [1], seeking to explore effective solutions that empower elderly individuals to maintain independent living.

Studies of Counsel and Care in UK showed that elderly people have a preference to stay in their apartments rather than nursing homes [2]. Researchers have shown that having clinical therapy at home has no negative effect on the process [3]. There are multiple ways to make this happen, one way is Ambient Assisted Living, where some ambient sensors are installed, e.g. motion sensors, to monitor the behavior of elderly residents, a model is used to guess the behavior using the sensor readings, then, this is used to identify if everything aligns with the usual behavior, and if not, assistance can be provided. This ensures a safer living space without unduly intruding on the privacy of the residents.

For replicating human behavior [4], [5] and [6] successfully implemented machine and deep learning algorithms for this task. In [7] Virtual Stochastic Sensors (VSSs) are used, which are designed to facilitate the reconstruction of partially observable stochastic systems and enable solving backward problems in the realm of stochastic modeling and simulation. The model is based on the ideas of Hidden Markovian Models (HMM) but extends these by arbitrary non-Markovian distribution functions for multiple concurrent processes and symbol outputs at arbitrary points in time [8]. VSS discretize the time domain and use a simple iterative algorithm to discover the reachable state space of a model, therefore being very flexible. However, they cannot be applied in real-world scenarios on a large scale yet, because model parametrization is not automated, and the model needs to be trained for a specific system to be used for reconstruction. The application of pre-trained models is tested in this paper for the first time, where previously the training and testing data were taken from the same apartment.

This research aims to test different model setups and activity granularities for the task of using a pre-trained model on the behavior reconstruction for a different apartment, comparing different performance measures.

The datasets contain activities performed by the residents and the corresponding active sensors for the activities performed. The rest of the paper is structured as follows, Section 1 contains the details of related research, Section 2 underlines the details of the datasets, Section 3 explains the conceptual model and the algorithm design, Section 4 shows the outcome of the research.

1 Related Work

This section explores different approaches for reconstructing human behavior in the field of ambient assisted living that are similar in approach or goal to this research. Additionally, it presents relevant information for Virtual Stochastic Sensors (VSSs).

[9] has mainly emphasized the duration of the activity to find the abnormality in human behavior using Explicit State Duration Hidden Markov Model (ESD-HMM). They checked the deformity of current activity which might be shorter or longer than the usual routine, the dataset used for this research was limited to the kitchen.

[10] introduced a new observation probabilistic model to recognize daily activities, incorporating temporal data which had information regarding 77 sensors.

[4] tried to identify the critical features from the sensor data, these features are used to classify overlapped activities. Unsupervised K nearest neighbor (KNN) was applied to day-to-day activities but with a small set of activities.

[5] implemented long short-term memory (LSTM) recurrent neural network (RNN) to perform activity recognition from wearable sensors, this implementation was not tested for activities of daily living.

[11] suggested another approach using RNN on three different datasets, this approach outperformed similar approaches concerning accuracy and speed, but the dataset is not publicly available.

[6] proposed an unobtrusive activity recognition classifier using deep convolutional neural network (DCNN) and publicly available CASAS Aruba dataset.

[12] used a knowledge-driven approach, including a Partially Observable Markov Decision Process (POMDP) and exploited the task information, while the location is combined with the sensor events in the smart home, but the series of conditions are used to classify activity.

This shows that AAL is a current research field with several approaches all with their individual features.

1.1 Virtual Stochastic Sensors

Virtual Stochastic Sensors represent a framework for analyzing partially observable stochastic systems, including different modeling paradigms and solution methods [13]. VSS can compete with some black box models when the hidden system structure information is available [7], and can incorporate such information to accurately represent dynamic system behavior and its relationship with the observable output. VSS use augmented stochastic Petri nets (ASPN) as user models that contain multiple concurrent non-Markovian transitions [14]. ASPNs generate observable output by the firing of transitions depending on the discrete system state, the discrete system output is collected in a protocol with associated time stamps, since in contrast to the Hidden Markovian Model (HMM), the model is defined in continuous time and can produce output at arbitrary points in time [7].

[7] has applied VSS on CASAS Aruba 2010 dataset and produced a very promising result, based on this VSS is considered to be a viable option for activity classification. However, the previous implementations were all trained and tested on the same use case, which is not a feasible approach for broad scale applicability. Therefore we are examining different methods of generalization to eventually enable generalized models to be applied on systems not used for the training.

2 CASAS Dataset and VSS Model

In this paper we are using data from the CASAS Research Project of Washington State University [15]. There are different types of datasets, one contains the daily activities of 20 participants, few other datasets include pets for single or multiple residents, and finally, HH datasets are mostly single residents but a small portion of them are two-resident apartments. In this research, the HH101 to HH105 single resident apartment datasets are considered because they are multivariate, sequential, and time series. The data is collected using different kinds of sensors, like motion, door/temperature, and light switch sensors placed throughout the apartment, while the residents perform their normal routines. The dataset format is Date, Time, Sensor, Room, Furniture, Activity, and Sensor Type (Table 1). In this research we will concentrate on the motion sensors, omitting all other sensor types.

The time frame of the datasets is for all roughly two summer months in the years 2011 and 2012.

Date	Time	Sensor	Room	Furniture	Activity	Type
08/01/2012	00:00:06	M008	LivingRoom	Chair	Watch_TV	Control4Motion
08/01/2012	00:00:07	M008	LivingRoom	Chair	Watch_TV	Control4Motion
08/01/2012	00:00:09	M008	LivingRoom	Chair	Watch_TV	Control4Motion
		.....				
08/01/2012	01:12:51	M012	Bedroom	Bed	Sleep	Control4Motion
08/01/2012	01:12:54	M012	Bedroom	Bed	Sleep	Control4Motion
08/01/2012	01:12:55	M012	Bedroom	Bed	Sleep	Control4Motion
		.....				

Table 1: Sample extract from single resident HH101 dataset.

To ensure balance, one full month is selected from each dataset, for details check [16]. The remainder of the section will outline the generalization steps that were performed on the sensors and the activities, in preparation for the experiments.

2.1 Generalization of Sensors

Different types of sensors are installed across the apartments to record the resident's behavior, such as motion sensors for specific locations or broader areas. Based on these sensor readings the activity that the person is performing is recorded.

There are three levels of sensor descriptions in the datasets, one field (*Sensor*) contains the actual sensor ID that is active. The second one (*Room*) contains room-level reading, specifying on which room the sensor is located.

The third (*Furniture*) contains a specification of the place or area the sensor is monitoring, which can be a specific piece of furniture (e.g. *Chair* or *Bed*), or the room which the area sensor is monitoring.

Where the sensor ID is unique to a particular apartments sensor setup, both the room level and furniture level sensor descriptions are shared across apartments. The superset of rooms contains six rooms: *Bathroom*, *Bedroom*, *Kitchen*, *Livingroom*, wich are present in all five apartments and *Diningroom* and *Work_area*, which are present in three out of five apartments each.
Similarly, some furniture is present in all apartments (e.g. *Bed*, *Chair*) while others is only shared in some (e.g. *Desk*).

These three different levels of sensor descriptions already provide two levels of generalization, where in the current research we will use the room level sensors and the furniture level sensor descriptions, as only these allow a generalization across apartments.

2.2 Generalization of Activities

Each of the five datasets contains around 30 labeled activities that were recorded, describing the daily routine of a person living in this residence. Before grouping similar activities, some were removed from the datasets, specifically activities with very short durations or very rare occurrences. Very short activities (e.g. Step_Out) are hard to detect using the given sensor setups. Modeling infrequent activities, such as *Work_At_Table*, do not have enough data to model properly, and are also not relevant for regular behavioral patterns.

In the first step, a combined set of activities for all five apartments is created. Some activities like e.g. *Go_To_Sleep* or *Wake_Up* also have very low occurrence, but can be combined with *Sleep*, and will therefore not be omitted. Furthermore, functionally similar activities, such as *Cook_Breakfast*, *Cook_Lunch*, *Cook_Dinner*, and *Cook* are grouped to *Cook*, even though these activities occur during different times of the day. Similar to cook, we can combine all eat, wash dishes and sleep activities into *Eat*, *Wash_Dishes* and *Sleep* respectively. The resulting combined set of activities is depicted in Table 2, with the activities present in all five highlighted in bold.

To obtain the first level of generalization, the five activities with the lowest duration overall were omitted, as they do not contribute significantly to the overall behavior. For the second level of generalization, meal related activities were grouped together, as well as leisure related activities and personal hygiene, resulting in six very general activity categories. Table 3 shows the two groupings.

2.3 Data preparation

After cleaning the data, the next step is to modify the data into distributions and probabilities so that it can be used as input in the model.

Activity	Percentage %
Sleep	47.2%
Watch_TV	14.4%
Relax	13.9%
Work	4.6%
Eat	4.1%
Cook	3.5%
Personal_Hygiene	3.2%
Read	3.2%
Toilet	1.7%
Dress	1.4%
Wash_Dishes	1.2%
Entertain_Guests	0.7%
Phone	0.6%
Medicine	0.2%
Drink	0.2%
Step_Out	0.1%

Table 2: All 16 activities from the combined set and their total share in occurence time the five CASAS HH datasets, activities common to all datasets in bold

All Activities	11 Activities	6 Activities
Sleep	Sleep	Sleep
Watch_TV	Watch_TV	Personal_Activity
Relax	Relax	
Read	Read	
Eat	Eat	Meal
Cook	Cook	
Wash_Dishes	Wash_Dishes	
Personal_Hygiene	Personal_Hygiene	Personal_Hygiene
Toilet	Toilet	
Work	Work	Work
Dress	Dress	Dress
Entertain_Guests		
Phone		
Medicine		
Drink		
Step_Out		

Table 3: Activity grouping, separated by dashed lines.

Each activity has breaks, which can be characterized as short breaks or long breaks.

Distributions for all the breaks and activities are based on their duration in minutes. Distributions are estimated with the help of the MATLAB distribution fitter app. Probabilities for an activity to go to breaks are needed to be calculated.

If a break is less than or equal to 60 minutes it is considered a short break and anything longer is a long break. Depending on this probability for an activity to go to short or long break is obtained.

Once all the distributions and state transition probabilities are determined, probabilities for output symbols are calculated.

This is the final input required to run the model, and this is achieved with Equation (1).

$$P(S_i|A_i) = \frac{(\Delta t|\forall S = S_i \cap A = A_i)}{(\Delta t|\forall A = A_i)} \tag{1}$$

- S_i the sensor
- A_i the activity
- $P(S_i|A_i)$ is the probability of sensor given activity

The distributions and sensor descriptions can now be used to create ASPN for the VSS reconstruction task, which will be discribed in the next section.

3 Conceptual Model and Algorithm Design

3.1 Conceptual Model

There are different ways to model the daily activities of a resident. In this research, we compared two different model designs. The first design was also used in previous research [17], where each activity has is represented as an individual Augmented Stochastic Petri net (ASPN) with places representing three tangible system states, *Activity* where the person is currently engaged in said activity, *Short_Break* and *Long_Break*, which represent the period in between different instances of the same activity. (see Figure 1) As most activities show a distinct differentiation of the time between activity instances, two timed transitions represent the duration of long breaks and short breaks. Each ASPN is independent of the other activities ASPNs.

The second model design contains one ASPN per room. Here the places represent the tangible system states of performing a certain activity (e.g. *Work* or *Eat*) or of not performing an activity in the room *Break*, which can either mean being in between tagged activities, or performing an activity in another room of the apartment. Figure 2 shows the SPN, without the augmented symbol emissions, for better readability.

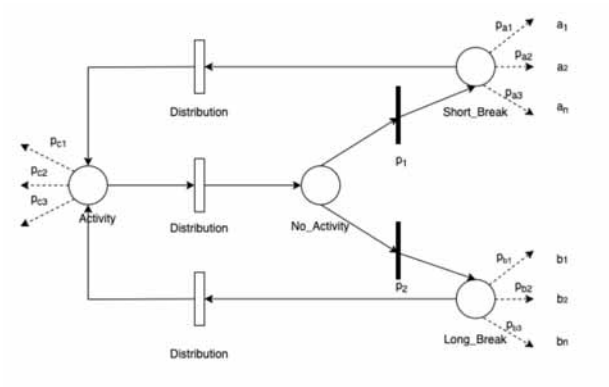

Figure 1: Augmented stochastic Petri net for one activity.

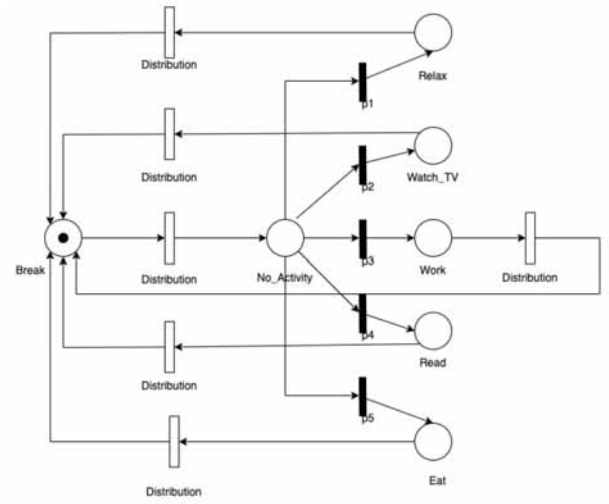

Figure 2: Stochastic Petri net for a room.

Once the structure of the Petri net is finalized, the output symbol emissions for the behavior reconstruction algorithm are added. These output symbols are linked with the Petri net places [8], as they occur, when an activity is being performed rather then when a state change occurs. From Figure 1 and 2 the output symbols are connected to all places except *No_Activity*. The p_k denote transition probabilities of the immediate transitions, p_{ak} denotes the output probability of symbol a_k.

The two different model designs will be augmented with the two different sensor level descriptions. The activity-based model can be augmented with both room level sensors as well as furniture level sensors. The room-based model is only augmented with the furniture level sensors, as the room level sensors would not enable differentiation between different activities within the room.

This results in three distinct model layouts: room-based model with furniture level sensors, activity-based model with furniture level sensors and activity-based model with room level sensors.

3.2 Algorithm Design

To reconstruct the unobserved system behavior, here the residents activities, the Proxel algorithm is used. The Proxel algorithm determines possible development paths of the system and their probability [18, 19, 8]. A Proxel is a 5-tuple, which represents one point in the expanded system state space, this tuple consists of the state of a system, age intensity, current point in simulation time, route through the state space and probability. All individual models are executed independently and determine output paths for all activities. This output path contains the probability of an activity occurring at a certain point in time.

The final reconstruction step has a different structure for the two model layouts. For the activity model, first the probabilities for each activity ASPN are computed and then the activities need to be classified. For classification a simple decision system is incorporated. This system outputs the activity which has the highest probability for all individual models for their activity state at that point in time. For every timestep of the protocol, this decision system results an activity. This type of system works because all the activities have individual ASPNs independent of each other. If for a particular timestep the probability of all activities is zero then the model returns *Other_Activity*.

For the second model setup with one model per room, the actual Proxel simulation is followed up by a reconstruction step, where the most likely path for each room is determined. Then these paths are combined over the different rooms and the most likely sequence of activities is the reconstruction result. Details of both the solution and post-processing methods can be found in [16]. The results obtained using the activity models and the room models are presented and reviewed in the following section.

4 Experiments and Results

In this section, the performance of the three different models on the three different generalization levels of activities is evaluated. These results are classified correctly if at a given time the reconstructed activity corresponds to the trace's ground truth.

The metrics precision, recall and F1 score are calculated for individual activities, and then they are averaged in two different ways one by averaging for all the activities (*Average*) and the other by adding weights depending on the overall activity duration (*Weighted Average*). The average recall is also often used as an overall accuracy measure. The above-discussed metrics are evaluated for weekdays and weekends separately, to account for differing behavioral patterns.

In a baseline experiment, the three models are applied to the reconstruction of the full set of 16 activities for model HH101. In k-fold cross validation, three weeks are used for training and one week for testing each. For all other experiments the k-fold cross validation is used for the five different datasets, training with four and testing on the fifth for each in turn.

4.1 Baseline Experiment

The results of the baseline experiments are shown in Table 4, the three different model designs are room-based model with furniture level sensors (*RoomM/-FurnS*), the activity-based model with room level sensors (*ActM/RoomS*) and the activity based model with furniture level sensors (*ActM/FurnS*). This experiment shows, that the accuracy per activity is less than the time weighted accuracy, as longer activities are detected more reliably. For the time weighted F1 score and accuracy, the room based model with furniture level sensors performed best.

4.2 Generalization Experiment

In the main experiment, we tested all three model setups and three different activity granularities, when using four apartments for training the model and the fifth as test set. This is a more realistic use case than using training and testing data from the same apartment. Having a small set of fully annotated apartments for training can be the basis of reconstruction models for apartments with a similar sensor setup, but without annotated training data.

Table 5 shows the full set of relevant performance measures, again separated by weekends and weekdays. Combining the data by averaging weekends and weekdays for the accuracy by activity results in the data shown in Figure 3. Similarly Figure 4 shows the weighted accuracy for all three models.

Compared to the basline data, the accuracy by activity seems to be improved for both models with furniture level sensors, whereas the activity-based model with room level sensors shows better performance only with the 11 activity set. This improvement in the per activity accuracy is most likely due to an increase in training data when using 4 apartments instead of just one. The improvement in performance for the furniture level sensors with more generalized activities is due to a grouping of activities with similar semantics, and therefore similar sensor activations.

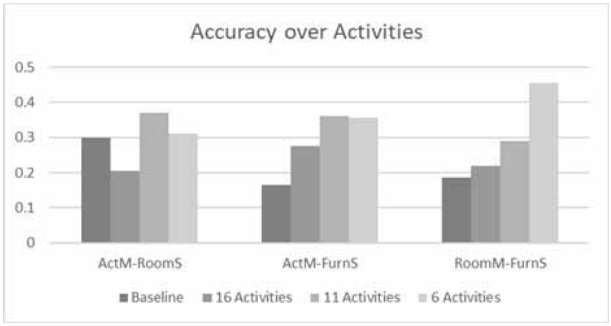

Figure 3: Accuracy per activity for all three models comparing baseline with different activity granularities.

The weighted accuracy performs better than in the baseline for the two activity based models, where in the room-based model, the baseline performance is better. The improvement in the activity based models is most likely due also to an increase in training data.

The decrease in performance for the room based model can be due to the larger differences between the apartments in the locations where activities are performed, and therefore more overlap in the models for the different rooms, which in turn results in worse reconstruction results.

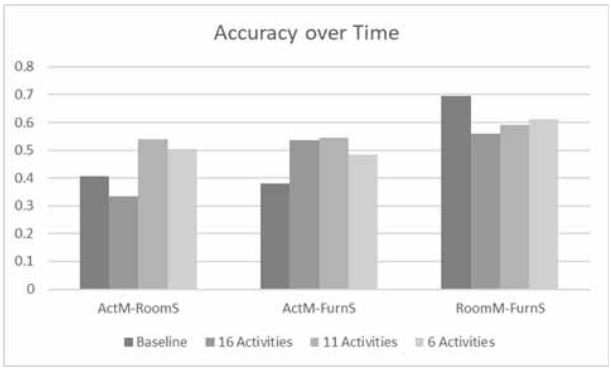

Figure 4: Time-weighted accuracy per activity for all three models comparing baseline with different activity granularities.

	RoomM/FurnS		ActM/RoomS		ActM/FurnS	
Evaluation Metric	**Weekday**	**Weekend**	**Weekday**	**Weekend**	**Weekday**	**Weekend**
Average_Recall	0.18	0.19	0.27	0.33	0.16	0.17
Weighted_Average_Recall	0.68	0.71	0.35	0.46	0.45	0.31
Average_F1	0.66	0.64	0.36	0.62	0.55	0.38
Weighted_Average_F1	0.53	0.55	0.32	0.50	0.35	0.29

Table 4: Baseline experiment performance of different models.

	RoomM/FurnS		ActM/RoomS		ActM/FurnS	
Evaluation Metric	**Weekday**	**Weekend**	**Weekday**	**Weekend**	**Weekday**	**Weekend**
Average_Recall	0.20	0.24	0.22	0.19	0.25	0.30
Weighted_Average_Recall	0.58	0.54	0.36	0.31	0.56	0.51
Average_F1	0.56	0.52	0.33	0.27	0.46	0.45
Weighted_Average_F1	0.54	0.48	0.34	0.28	0.54	0.47
Average_Recall	0.30	0.28	0.35	0.39	0.38	0.34
Weighted_Average_Recall	0.62	0.56	0.53	0.55	0.58	0.51
Average_F1	0.53	0.49	0.46	0.47	0.58	0.54
Weighted_Average_F1	0.54	0.51	0.49	0.49	0.51	0.47
Average_Recall	0.49	0.42	0.32	0.30	0.37	0.34
Weighted_Average_Recall	0.60	0.62	0.50	0.51	0.51	0.46
Average_F1	0.49	0.49	0.49	0.48	0.48	0.45
Weighted_Average_F1	0.56	0.55	0.46	0.46	0.51	0.45

Table 5: Experiment performance of different models for full activity set (top), 11 activites set (middle), and 6 activites set (bottom).

4.3 Experiment Discussion

Overall the experiment shows that models trained on a set of apartments can be used for behavior reconstruction on a different apartment with similar sensor setup and resident behavior. Sometimes the performance even improves due to a larger amount of available training data when using multiple apartments for training, also avoiding overfitting. However, the selection of a fitting activity granularity and good model setup is crucial. The combination performing best overall and at the same time yielding still useful results in this experiment was the activity-based models and the furniture level sensors.

A semantic grouping of activities by similar time of day and living area, which corresponds to a similar sensor footprint, leads to an improvement in accuracy. However, the information content of the reconstruction is considerably less, when more activities are combined under the same label.

It has to be investigated with the help of domain experts at which point the generalized set of activities with better performance measures still holds enough information to assess the residents status.

Ultimately the goal is to use this ambient sensor observation to decide, whether the residents behavior is still within normal bounds, or whether outside assistance or intervention is necessary.

5 Conclusion

This research used the CASAS datasets for several single-resident apartments. Three different model setups and three different activity granularities are tested on the behavior reconstruction of the residents when the apartment reconstructed was not part of the training set. Virtual Stochastic Sensors (VSS) are used to reconstruct resident activities. Using activity-based models and furniture level sensors resulted in the overall best performance.

5.1 Future Work

The analysis presented in this paper is only part of the research aiming at providing generalized models to be pre-trained and then applied for the reconstruction of previously unknown apartments, or systems in general.

In order to validate the results, the experiments need to be conducted on larger datasets and discussed with domain experts.

The paper shows that the approach is feasible in general, but also needs some more automation steps. An automatic adaption of the trained model to an apartment not in the trainings set can also be of interest, as well as the transfer of the idea to different domains such as non-intrusive appliance load monitoring.

Publication Remark. This contribution is the English full version of the German abstract version published in ASIM Workshop GMMS/STS 2025 Tagungsband ARGESIM Report 48, e-ISBN 978-3-903347-66-3, Volume DOI 10.11128/arep.48, p 77.

References

[1] Rashidi P, Mihailidis A. A survey on ambient-assisted living tools for older adults. *IEEE journal of biomedical and health informatics*. 2012;17(3):579–590.

[2] Sun H, Florio VD, Gui N, Blondia C. Promises and Challenges of Ambient Assisted Living Systems. In: *2009 Sixth International Conference on Information Technology: New Generations*. 2009; pp. 1201–1207. URL `https://ieeexplore.ieee.org/abstract/document/5070788`

[3] Deutsch JE, Lewis JA, Burdea G. Technical and patient performance using a virtual reality-integrated telerehabilitation system: preliminary finding. *IEEE Transactions on Neural Systems and Rehabilitation Engineering*. 2007;15(1):30–35.

[4] Fahad LG, Tahir SF, Rajarajan M. Feature selection and data balancing for activity recognition in smart homes. In: *2015 IEEE International Conference on Communications (ICC)*. IEEE. 2015; pp. 512–517.

[5] Ordóñez FJ, Roggen D. Deep convolutional and lstm recurrent neural networks for multimodal wearable activity recognition. *Sensors*. 2016;16(1):115.

[6] Gochoo M, Tan TH, Liu SH, Jean FR, Alnajjar FS, Huang SC. Unobtrusive activity recognition of elderly people living alone using anonymous binary sensors and DCNN. *IEEE journal of biomedical and health informatics*. 2018;23(2):693–702.

[7] Mueller LF. Feasibility and Applicability of Virtual Stochastic Sensors for Human Activity Recognition in the Context of Ambient Assisted Living. Master's thesis, Otto-von-Guericke-University Magdeburg. 2021.

[8] Krull C. Virtual Stochastic Sensors: Formal Background and Example Applications Reconstructing the Behavior of Partially Observable Discrete and Hybrid Stochastic Systems. Habilitation thesis, Otto-von-Guericke-University Magdeburg. 2021.

[9] Lühr S, Venkatesh S, West G, Bui HH. Explicit state duration HMM for abnormality detection in sequences of human activity. In: *PRICAI 2004: Trends in Artificial Intelligence: 8th Pacific Rim International Conference on Artificial Intelligence, Auckland, New Zealand, August 9-13, 2004. Proceedings 8*. Springer. 2004; pp. 983–984.

[10] van Kasteren T, Kroese B. Bayesian Activity Recognition in Residence for Elders. In: *3rd IET International Conference on Intelligent Environments*. 2007; pp. 209–212.

[11] Singh D, Merdivan E, Psychoula I, Kropf J, Hanke S, Geist M, Holzinger A. Human activity recognition using recurrent neural networks. In: *Machine Learning and Knowledge Extraction: First IFIP TC 5, WG 8.4, 8.9, 12.9 International Cross-Domain Conference, CD-MAKE 2017, Reggio, Italy, August 29–September 1, 2017, Proceedings 1*. Springer. 2017; pp. 267–274.

[12] Chen L, Nugent CD, Wang H. A knowledge-driven approach to activity recognition in smart homes. *IEEE Transactions on Knowledge and Data Engineering*. 2011;24(6):961–974.

[13] Krull C, Horton G. Hidden Non-Markovian Models: Formalization and Solution Approaches. In: *Proceedings of 6th Vienna Conference on Mathematical Modelling, Vienna, Austria*. 2009; pp. 682–693.

[14] Krull C. A Hybrid User Model for Virtual Stochastic Sensors. *Simulation Notes Europe SNE33*. 2023; 33(1):35–43.

[15] Cook DJ, Crandall AS, Thomas BL, Krishnan NC. CASAS: A smart home in a box. *IEEE Computer*. 2013;46(6):26–33.

[16] Karumuri V. Generalization of Virtual StochasticSensors in the Field of AmbientAssisted Living for MultipleSingle-Resident Apartments. Master's thesis.

[17] Karumuri V, Krull C. Virtual Stochastic Sensors for Ambient Assisted Living - Analyzing the Effect of Generalized Resident Behavior. In: *Tagungsband Langbeitraege ASIM SST 2024*. 2024; .

[18] Horton G. A New Paradigm for the Numerical Simulation of Stochastic Petri Nets with General Firing Times. In: *Proceedings of the European Simulation Symposium 2002*. SCS European Publishing House. 2002; pp. 129–136.

[19] Lazarova-Molnar S. The Proxel-Based Method: Formalisation, Analysis and Applications. Ph.D. thesis, Otto-von-Guericke-University Magdeburg. 2005.

Residual Data Driven Variational Multiscale Reduced Order Models for Convection-Dominated Problems in the Predictive Regime

Birgul Koc[1*], Samuele Rubino[2], Traian Iliescu[3], Tomás Chacón[2]

[1]Dpto. EDAN, Universidad de Sevilla, C/Tarfia, s/n. 41012 Sevilla, Spain; *bkoc@us.es

[2]Dpto. EDAN & IMUS, Universidad de Sevilla, C/Tarfia, s/n. 41012 Sevilla, Spain

[3]Virginia Tech, Blacksburg, VA 24061, United States

SNE 36(2), 2026, 95-98, DOI: 10.11128/sne.36.sn.10775
Selected MATHMOD 2025 Postconf. Publication: 2025-02-26
Rec. Revised Extended: 2026-05-13; Accepted: 2026-05-20
SNE - Simulation Notes Europe, ARGESIM Publisher Vienna
ISSN Print 2305-9974, Online 2306-0271, www.sne-journal.org

Abstract. In this work, we propose a novel residual based data driven closure strategy for reduced-order models (ROMs) of under-resolved, convection-dominated flows. The proposed closure model is developed within a variational multiscale (VMS) framework, leveraging available full order model (FOM) data and an ansatz that explicitly depends on the ROM residual. We emphasize that this approach is fundamentally different from existing data driven ROM closure models, which typically rely on the ROM coefficients as inputs. In contrast, the proposed residual based method utilizes the ROM residual to account for the effects of unresolved scales. We assess the performance of the proposed residual-based data-driven VMS-ROM in the numerical simulation of two-dimensional flow past a cylinder at Reynolds number Re $= 1000$. The results demonstrate that the proposed method yields significantly improved accuracy compared to standard coefficient based data driven VMS-ROM approaches.

Introduction

We consider the Navier-Stokes equations (NSE) (1)-(2) as the mathematical model:

$$\frac{\partial u}{\partial t} - Re^{-1}\Delta u + u\cdot\nabla u + \nabla p = 0, \tag{1}$$

$$\nabla\cdot u = 0, \tag{2}$$

where u denotes the velocity field, p the pressure, and Re the Reynolds number. Homogeneous Dirichlet boundary conditions are imposed.

To construct reduced order models (ROMs), we use the proper orthogonal decomposition (POD) to generate the ROM basis functions and associated operators. Owing to the orthogonality of the POD modes, the ROM space can be decomposed into large-scale and sub-scale components:

$$X^d = X^L \oplus X^S, \tag{3}$$

where

$$X^d := \text{span}\{\varphi_1,\ldots,\varphi_d\},$$
$$X^L := \text{span}\{\varphi_1,\ldots,\varphi_L\},$$
$$X^S := \text{span}\{\varphi_{L+1},\ldots,\varphi_d\}.$$

Using all d modes, the ROM approximation

$$u_d = \sum_{j=1}^{d} (a_d)_j \varphi_j \tag{4}$$

provides the most accurate representation of the full order model (FOM) solution in the POD sense.

For laminar flows, a low dimensional approximation u_L, with $L \ll d$, is typically sufficient to accurately represent the FOM solution. In this regime, the standard Galerkin ROM (G-ROM) is given by

$$\dot{a}_L = A_{LL}\, a_L + a_L^\top B_{LLL}\, a_L, \tag{5}$$

where $(A_{LL})_{ij} = -\nu(\nabla\varphi_i, \nabla\varphi_j)$, $(B_{LLL})_{ijk} = -(\varphi_i, \varphi_j \cdot \nabla\varphi_k)$, for all $i,j,k = 1,\ldots,L$.

The G-ROM system (5) is derived by substituting u_L into the NSE (1)-(2) and projecting the resulting equations onto the large-scale ROM space X^L.

However, for turbulent flows, the low dimensional G-ROM solution u_L is generally insufficient to accurately approximate the FOM solution. To alleviate this inaccurate behavior, standard ROMs are typically augmented with numerical stabilization techniques or ROM closure models, which aim to account for the effects of unresolved scales [2, 3, 4, 5, 6].

1 ROM Closure Models

ROM closure modeling aims to approximate the closure term arising in a variational multiscale (VMS) framework [2, 3]. To construct this closure term, we first decompose the most accurate ROM solution u_d into large and sub-scale components:

$$u_L := \sum_{j=1}^{L} (a_L)_j \varphi_j, \qquad u_S := \sum_{j=L+1}^{d} (a_S)_j \varphi_j. \tag{6}$$

Next, we derive the governing equations for the large and sub-scales. To this end, we substitute $u = u_d = u_L + u_S$ into (1)–(2) and project the resulting system onto the ROM spaces X^L and X^S, respectively. This yields the following coupled system:

$$\begin{aligned} \dot{a}_L &= A_{LL}a_L + A_{LS}a_S + a_L^\top B_{LLL}a_L + a_L^\top B_{LLS}a_S \\ &\quad + a_S^\top B_{LSL}a_L + a_S^\top B_{LSS}a_S, \qquad (7a) \\ \dot{a}_S &= A_{SS}a_S + A_{SL}a_L + a_S^\top B_{SSS}a_S + a_S^\top B_{SSL}a_L \\ &\quad + a_L^\top B_{SLS}a_S + a_L^\top B_{SLL}a_L. \qquad (7b) \end{aligned}$$

Here, the matrices A_{IJ} and tensors B_{IJK}, with indices $I,J,K \in \{L,S\}$, are defined by

$$\begin{aligned} (A_{IJ})_{ij} &:= -Re^{-1}(\nabla\varphi_i^I, \nabla\varphi_j^J), \\ (B_{IJK})_{ijk} &:= -(\varphi_i^I, \varphi_j^J \cdot \nabla\varphi_k^K), \end{aligned}$$

where $\varphi^L := \{\varphi_1, \ldots, \varphi_L\}$ and $\varphi^S := \{\varphi_{L+1}, \ldots, \varphi_d\}$ denote the large-scale and sub-scale ROM basis functions, respectively. The subscript indices I,J,K indicate which ROM subspace each basis function belongs to, making the coupling structure between large and sub-scales explicit.

In this work, we consider two distinct ROM closure strategies, leading to two different models: the *coefficient based data driven variational multiscale* ROM (C-ROM) and the *residual based data driven variational multiscale* ROM (R-ROM).

2 Basis of ROM Closure Models

2.1 Coefficient based ROM (C-ROM)

The coefficient-based ROM, C-ROM, [2, 3] is derived from the large-scale equation (7a) by introducing a closure model and a corresponding ansatz. Since the **closure** term is not available in closed form, we approximate it using a quadratic, coefficient-based **ansatz** that depends on the large-scale coefficients a_L:

$$\begin{aligned} \textbf{closure} &= A_{LS}a_S + a_L^\top B_{LLS}a_S + a_S^\top B_{LSL}a_L + a_S^\top B_{LSS}a_S, \\ \textbf{ansatz} &= \widetilde{A}_{LL}\,a_L + a_L^\top \widetilde{B}_{LLL}\,a_L. \end{aligned} \tag{8}$$

2.2 Residual based ROM (R-ROM)

In the proposed residual-based ROM, R-ROM, the closure modeling is constructed using information from the sub-scale equation (7b). In this case, the **closure** term and the corresponding residual-based **ansatz** are defined as:

$$\begin{aligned} \textbf{closure} &= a_S, \\ \textbf{ansatz} &= \widetilde{A}_{SS}\,\textbf{Res}_S(a_L) + \textbf{Res}_S(a_L)^\top \widetilde{B}_{SSS}\,\textbf{Res}_S(a_L), \end{aligned} \tag{9}$$

where the sub-scale residual is given by

$$\textbf{Res}_S(a_L) := A_{SL}a_L + a_L^\top B_{SLL}a_L. \tag{10}$$

2.3 Minimization Problem: Optimal Data Driven Operators

To identify the unknown operators $\widetilde{A}_{LL}$, $\widetilde{A}_{SS}$, $\widetilde{B}_{LLL}$, and $\widetilde{B}_{SSS}$, we employ a *data-driven* (D2) approach [2, 3]. These operators are obtained by solving the following least-squares minimization problem:

$$\min_{\text{D2 operators}} \quad \sum_{j=1}^{M} \left\| \textbf{closure}(a_j^{\text{FOM}}) - \textbf{ansatz}(a_j^{\text{FOM}}) \right\|_{L^2}^2. \tag{11}$$

Using the respective closure terms and ansatz for the C-ROM and R-ROM, we solve (11) to obtain the corresponding D2 operators. Substituting the resulting ansatz into the large-scale equation (7a), the C-ROM reads

$$\dot{a}_L = \left(A_{LL} + \widetilde{A}_{LL}\right) a_L + a_L^\top \left(B_{LLL} + \widetilde{B}_{LLL}\right) a_L, \tag{12}$$

while the R-ROM is given by

$$\dot{a}_L = A_{LL}a_L + a_L^\top B_{LLL}a_L + A_{LS}\widetilde{a}_S + a_L^\top B_{LLS}\widetilde{a}_S + \widetilde{a}_S^\top B_{LSL}a_L + \widetilde{a}_S^\top B_{LSS}\widetilde{a}_S, \quad (13)$$

where the approximated sub-scale coefficients are computed as

$$\widetilde{a}_S := \widetilde{A}_{SS}\mathbf{Res}_S(a_L) + \mathbf{Res}_S(a_L)^\top \widetilde{B}_{SSS}\mathbf{Res}_S(a_L). \quad (14)$$

3 Numerical Results

We investigate the numerical accuracy of the G-ROM, C-ROM, and R-ROM for 2D channel flow past a circular cylinder at $\mathrm{Re} = 1000$ in the **predictive regime**: the ROM basis and operators are built from FOM snapshots over $t \in [13, 16]$, the data-driven operators are trained over $t \in [13, 13.134]$, and all ROMs are tested over $t \in [16, 23]$, with $d = 22$.

In addition to the ROM accuracy, we investigate the consistency between the closure term and the ansatz for both the C-ROM and R-ROM. To assess ROM performance, we examine the average L^2 projection errors, the evolution of the kinetic energy, the average L^2 kinetic energy errors, Pareto plots, and the vortex shedding frequency.

3.1 Consistency and ROM Projection Errors

We define the following metrics:

$$\mathscr{E}_{\mathrm{cons}} := \frac{1}{M}\sum_{k=1}^{M}\left\|\mathbf{closure}(a_{L,S}^{\mathrm{FOM},k}) - \mathbf{ansatz}(a_L^{\mathrm{FOM},k})\right\|_{L^2}, \quad (15)$$

$$\mathscr{E}_{\mathrm{proj}} := \frac{1}{M}\sum_{k=1}^{M}\left\|u_L(t_k) - \sum_{i=1}^{L}\left(u^{\mathrm{FOM}}(t_k), \varphi_i\right)_{L^2}\varphi_i\right\|_{L^2}, \quad (16)$$

where $\mathscr{E}_{\mathrm{cons}}$ measures the discrepancy between the closure term and its approximation, and $\mathscr{E}_{\mathrm{proj}}$ denotes the ROM projection error.

In Table 1, we list the average L^2 consistency error (15). The R-ROM consistently yields lower consistency errors than C-ROM, with an overall decaying trend despite non-monotone behavior due to the sensitivity of (11). In Table 2, we list the average L^2 ROM projection errors. Both C-ROM and R-ROM significantly outperform G-ROM, with R-ROM consistently achieving better accuracy overall.

L	C-ROM	R-ROM
2	2.28e-01	2.59e-02
5	1.49e+00	1.72e-02
8	4.01e-01	1.22e-04
11	1.35e+00	1.27e-08
14	2.46e-01	1.29e-02
20	1.43e-01	2.34e-03
22	0	0

Table 1: Average L^2 FOM consistency error (15) for C-ROM and R-ROM across different values of L.

L	G-ROM	C-ROM	R-ROM
2	1.15e+00	4.11e-01	3.59e-01
3	9.22e-01	5.51e-01	6.16e-02
4	7.21e-01	1.98e-01	1.18e-01
5	7.28e-01	5.81e-01	3.11e-01
6	3.54e-01	1.48e-01	4.36e-02
7	3.02e-01	2.81e-01	5.29e-02
8	1.59e-01	9.44e-02	2.53e-02

Table 2: Average L^2 ROM projection errors (16) for different values of L.

In Figure 1, we present a Pareto plot comparing C-ROM and R-ROM in terms of average L^2 error and offline ansatz computational cost, averaged over low-dimensional ($L = 2, 3, 4, 5$) and higher-dimensional ($L = 6, 7, 8$) ROMs.

For low-dimensional ROMs, R-ROM yields higher accuracy than C-ROM at a higher computational cost. For higher-dimensional ROMs, R-ROM is both more accurate and more efficient than C-ROM.

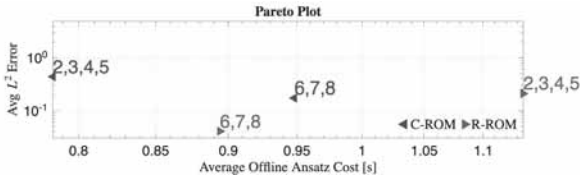

Figure 1: Pareto plot of average L^2 error of C-ROM and R-ROM.

3.2 Kinetic Energy

In this section, we use the kinetic energy (KE) criterion to compare the numerical accuracy of G-ROM, C-ROM, and R-ROM, where the KE is defined as follows:

$$E_{kin} := \frac{1}{2}\|u\|_{L^2}^2 = \frac{1}{2}\int_\Omega |u|^2 \, d\Omega. \tag{17}$$

In Figure 2, we compare the KE evolution of C-ROM and R-ROM for $L = 6$. R-ROM is significantly more accurate than C-ROM.

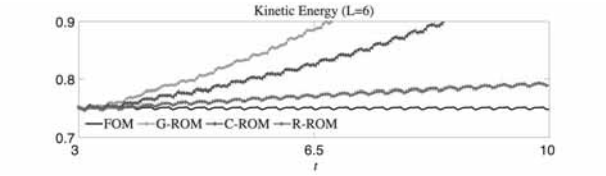

Figure 2: Time evolution of the kinetic energy for ROMs.

3.3 Vortex Shedding Frequency

In this section, we compute the average vortex shedding frequency f_s of C-ROM, R-ROM, and FOM based on the vortex shedding period $\mathscr{T}_s$, which is defined as follows:

$$\mathscr{T}_s = \frac{1}{N_s}\sum_{k=1}^{N_s}(t_s(k+1) - t_s(k)), \tag{18}$$

where $t_s(k)$ denotes successive KE peaks within $t \in [18, 23]$. In Figure 3, R-ROM more accurately recovers the FOM vortex shedding periods than C-ROM, and the KE peak amplitudes in C-ROM are noticeably higher than in R-ROM.

We observe that R-ROM more accurately recovers the vortex shedding periods of the FOM than C-ROM. Furthermore, the amplitudes of the KE peaks in C-ROM are noticeably higher than those in R-ROM.

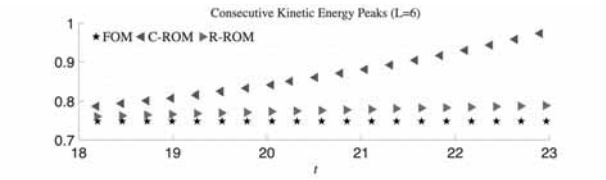

Figure 3: Comparison of vortex shedding frequency for FOM, C-ROM, and R-ROM.

Acknowledgement

The first and second authors are partially supported by Project PID2021-123153OB-C21 funded by MCIN / AEI / 10.13039 / 501100011033 / FEDER, UE, the third author is partially supported by Junta de Andalucía - Spanish Government - European Union grant SOL2024-31708, and the fourth author is partially supported by National Science Foundation grant DMS-2012253.

References

[1] Koc B, Rubino S, Chacón T, Iliescu T. Residual Data-Driven Variational Multiscale Reduced Order Models for Convection-Dominated Problems. In A. Körner & al. *MATHMOD 2025 Short Contribution Volume*, reposiTUm TU Wien, p. 11-12 DOI 10.34726/9005.

[2] Koc B, Rubino S, Chacón Rebollo T, Iliescu, T. Residual-based data-driven variational multiscale reduced order models for parameter-dependent problems. *Computational and Applied Mathematics*, 2025, 44(6), 308.

[3] Mou C, Koc B, San O, Rebholz LG, Iliescu T. Data-driven variational multiscale reduced order models. *Computer Methods in Applied Mechanics and Engineering*, 2021, 373, 113470.

[4] Azaïez M, Rebollo TC, Rubino S. A cure for instabilities due to advection-dominance in POD solution to advection-diffusion-reaction equations. *Journal of Computational Physics*, 2021, 425, 109916.

[5] Rebollo TC, Rubino S, Oulghelou M, Allery C. Error analysis of a residual-based stabilization-motivated POD-ROM for incompressible flows. *Computer Methods in Applied Mechanics and Engineering*, 2022, 401, 115627.

[6] Reyes R, Codina R. Projection-based reduced order models for flow problems: A variational multiscale approach. *Computer Methods in Applied Mechanics and Engineering*, 2020, 363, 112844.

Publication Remark. This work is an improved version of our MATHMOD 2025 conference contribution [1], closely related to [2]. Compared to [1], we include three additional results: (i) a consistency analysis of the ansatz operators; (ii) a Pareto plot comparing accuracy and computational cost; and (iii) a vortex shedding frequency analysis. Note that, unlike [2], absolute errors are reported throughout. For a comprehensive treatment including the R2-ROM variant and additional test cases, we refeer to [2].

Recommendation Modeling for Health Self-Management Applications for People with Rheumatoid Arthritis

Nadine Schwab[1*,2], Günther Zauner[1], Christoph Urach[1], Paul Studenic[3,4], Helga Radner[3], Nasim Nakhost-Lotfi[3], Tanja Stamm[5], Thomas Hammer-Jakobsen[6], Andreas Dam[6,7], Niki Popper[1,2,8]

[1]dwh simulation services & technical solutions, dwh GmbH, Neustiftgasse 57-59, 1070 Vienna, Austria
[*]*nadine.schwab@dwh.at*
[2]Institute for Information Systems Engineering, TU Wien, Favoritenstraße 9-11, 1040, Vienna, Austria
[3]Division of Rheumatology, Department of Internal Medicine III Medical University of Vienna, Vienna, Austria
[4]Division of Rheumatology, Department of Medicine (Solna), Karolinska Institutet, Stockholm, SWEDEN
[5]Center for Medical Statistics, Informatics, and Intelligent Systems, Medical University of Vienna, Vienna, Austria
[6]HealthBuddy, Vesterbrogade 149, 1620 Copenhagen, Denmark
[7]Daman, Vesterbrogade 149, 1620 Copenhagen, Denmark
[8]Inst.of Statistics and Math. Methods in Economics, TU Wien, Wiedner Hauptstraße 8, 1040, Vienna, Austria

SNE 36(2), 2026, 99-106, DOI: 10.11128/sne.36.tn.10776
Selected ASIM SST 2024 Postconf. Publ.: 2025-06-10
Received Revised: 2025-12-15; Accepted: 2025-12-20
SNE - Simulation Notes Europe, ARGESIM Publisher Vienna
ISSN Print 2305-9974, Online 2306-0271, www.sne-journal.org

Abstract. For the containment of chronic diseases, mHealth tools, for example mobile apps, provide great opportunities to track the disease progression and to give useful recommendations. In this project, possible data-driven enhancements for an already existing mobile app for patients with Rheumatoid Arthritis are discussed, developed and implemented. This happens in an ongoing feedback-cycle, including app developers, medical experts, patients and data scientists. The new features improve the app experience and are currently being evaluated in an observational study.

Introduction

Rheumatoid Arthritis (RA) is a chronic autoimmune disease, which affects over 3 Million people in Europe. People dealing with RA usually suffer from painful and tender joints. This and the whole plethora of also more subtle symptoms like fatigue strongly impacts their every day life [1], [2]. There is no cure for RA, but the symptoms and the progress of the disease can nowadays be halted effectively and improved by targeted pharmacological and non-pharmacological interventions. mHealth tools provide opportunities for the tracking and self-management of symptoms on a patient-individual basis [3].

RheumaBuddy is such an app that serves as an electronic diary for RA-specific symptoms: Users can track their symptoms, such as Mood, Pain, Fatigue and Stiffness, as well as activities such as walking or sleeping, on a daily basis. This helps keeping track of their disease progression, in general or for the next doctor appointment.

Throughout the project RheumaBuddy4.0 (RB4.0), it is the aim to improve this app. In order to achieve this, firstly, an extensive data analysis has been performed to figure out which additional features are possible and make sense in the current app. Next, these data-driven recommendations are implemented in the app and tested by the users. The whole process takes place in a permanent feedback loop including the Danish app developers DAMAN, medical experts from the Medical University of Vienna (MUV), data scientists from dwh GmbH, and RA patients who use and test the app. Fig.1 shows a schematic depiction of the workflow in the project.

1 App Status at Begin of Project

At the beginning of the project, RheumaBuddy is already available as a mobile app in multiple language with German, English, and Danish being the most popular ones. Users have the possibility to enter RA-related symptoms, such as Mood, Pain, Fatigue and Stiffness as well as self-reported symptoms, where they could track whatever they are interested in.

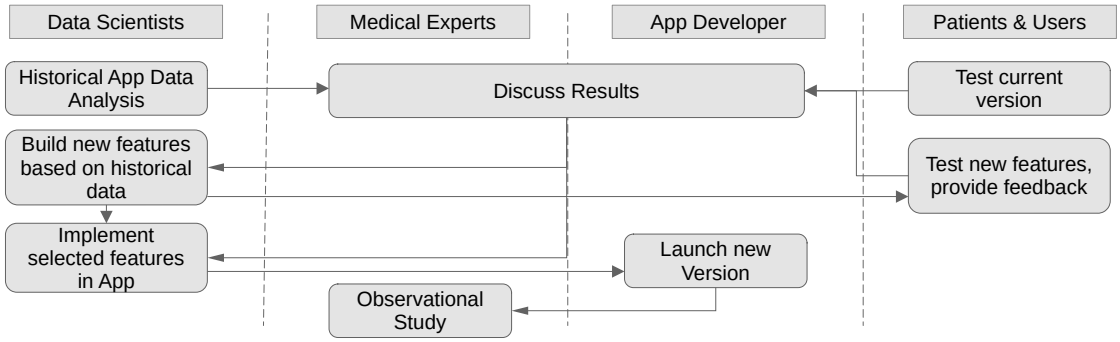

Figure 1: A schematic depiction of the general workflow of the project. The development of new features and the discussion with the experts is often repeated multiple times.

Every symptom can be scored on a smiley scale indicating the extent of the respective symp-tomatology. These smileys rank from very happy to very unhappy in five steps. Users can also enter acti-vities, such as walking or sleeping, and how long these activities took on that day. Furthermore, they can document their joint pains on a body map. And finally, they can write free-text in a diary, as well as use the community to ask or to answer to questions.

The community is also available in different languages. The user's status and progression can always be seen on the Status page, where line graphs visualize the development of all the values tracked by the user.

The goal of the project is to implement a virtual coach within the app. This coach should provide users entering sufficient data into the app with personal recommendations based on their individual entries. This goal comes with the following challenges:

- **Amount of regular data:** In order to provide useful, data-based information, a sufficient amount of data per user is required, i.e. the users must enter data on a regular (ideally daily) basis over a few weeks, at the very least. Usually, it is difficult to motivate app users to provide this amount of input.
- **Subjectivity of app entries:** The app entries are subjective for every user, and it is not trivial to compare them. E.g., for one user, "good mood" means they actually had an amazing day, while for another user, it only means that everything is alright.
- **Not measurable disease parameters:** There are hardly any RA-specific parameters that can be measured objectively on a remote basis, i.e. without a medical expert. As opposed to e.g. Diabetes, where blood sugar can be objectively measured and provides a good indicator for the current disease activity, rheumatologists can only evaluate a patient's disease status by assessing the swollen, hurting and tender joints of a patient besides deviations in inflammatory parameters, blood levels, or changes in bone and joint structure with imaging modalities.

2 Data Analysis

An extensive data analysis was conducted in order to determine which app enhancements are possible with the available data, and how the results look like. The results were frequently discussed with the app developers and medical experts. Furthermore, feedback was constantly obtained from app users. Based on these feedback loops, possible app features are discussed and designed.

The data analysis with its results is presented in this chapter. The next chapter describes a new app feature, which evolved from this analysis.

2.1 User Behavior

First we analyzed, how extensively the app is used by the users. We analyzed the development of the number of unique users per day (which means they entered at least one value into the app on that day) and which entry types are the most popular.

The development of the users can be seen in Figure 2. A peak is visible in October 2020 as a result of a big marketing campaign. The number of users didn't stay that high, but remained significantly higher than before.

The most popular entry types can be seen in Figure 3. The most popular ones are the four main symptoms Mood, Pain, Fatigue and Stiffness, followed by the Pain Map. The diary and activity tracking is far less popular, as well as the self-reported symptoms. The latter shows that the four main symptoms seem to be sufficient for most app users. The least popular is writing and reading in the community.

Possible reasons for this heterogeneous behaviour were discussed with the consortium, especially with some app users. The users claimed that for those entries that are used the most often, it is much easier and faster to enter values than for the others. It goes without saying that writing into the diary or community is more time-consuming than choosing a smiley value for a symptom. The activity values, on the other hand, are not trivial to measure. Users claimed that it is hard to remember in the middle of the day, how long exactly they slept. Considering "Motion", it was not clear to them, what accounts to this, e.g. whether a walk counts already, or only exhausting physical activities, which is why they soon stopped entering values there.

2.2 Numeric Correlations

We investigated the correlations between the entries of the users. The entries are obtained directly from the app: As mentioned in section 1, a user can enter their symptoms via a smiley, which ranks from happy to unhappy in five steps. These steps are denoted in the back-end with the integer values 1 to 5 (1 being the most unhappy one), which are used to compute correlations. Considering activity values (Sleep, Motion, Working hours), the actual time spans in seconds are used. These correlations are displayed in Figure 4. Strong corre-lations can be seen between the four main symptoms, but not between the rest of the entry types. However, no correlations between symptoms and activities might also be because the users had problems entering reasonable values for these fields, as discussed in Subsection 2.1.

2.3 Free-Text Analysis

Although these types of entries are less popular, we also analyzed the free-text entries, i.e. diary, community, and self-reported symptoms. We wanted to grasp what the users are writing about (besides the pre-defined entries), and whether some information that is relevant for all users can be extracted from the entries. To achieve this, we firstly translated all self-reported symptoms, diary and community entries to English language (using the Python Library Deep Translator), removed fill- and stop-words (using [7]) and counted which words appeared the most often in the entries. This is visualized in Figure 5.

As it can be seen immediately in the Subfigures 5b and 5a, the most important topics in the diary and in the community are RA-related symptoms or medication. Considering the self-reported symptoms in Subfigure 5c, interestingly, four of the five most frequent ones are exactly the four main symptoms that are provided in the app anyway, i.e. Mood, Pain, Fatigue and Stiffness. We assume, the users entered their data in the self-reported symptoms due to a misunderstanding - however, this indicates again that these symptoms seem to be of utmost importance. However, as the remaining symptoms (resp. the self-reported symptoms in general) are used by very few users, no further analysis was conducted in this area.

2.4 Community Crawling

The community is open for every RheumaBuddy-user, but as it was shown in Figure 3, there are only few users that use the community - even just for reading. Figure 5b indicates that many community posts and comments deal with RA-related symptoms and medication. As the community is built in a question-and-answer-style, i.e. a user can ask a question and any other user can answer to them, we assume that there are many recommendations hidden in the community. These recommendations would be of great value for many RheumaBuddy users, not only those who read and write in the community.

Therefore, we wanted to systematically collect helpful recommendations from the community. Depending on the information that could be gained, these could be forwarded to all users, or only to specific ones where it might fit (depending on the entries the users make). We collected recommendations using the following, semi-automated approach:

1. Filter the community posts by posts which ask for advice on something, using regular expressions.
2. Retrieve all answers to this post and remove all answers from the user who asked the question.
3. Read the answers in combination with the question and decide whether to keep or to discard it.

A fully-automated approach was not developed within the scope of this project, as the Community Crawling was only experimental, and the amount of data available in the community is too small to justify much research in the field of automated text mining. Nevertheless, this semi-automated approach gravely reduced the manual work and enabled to quickly obtain a document with possible recommendations collected from the community.

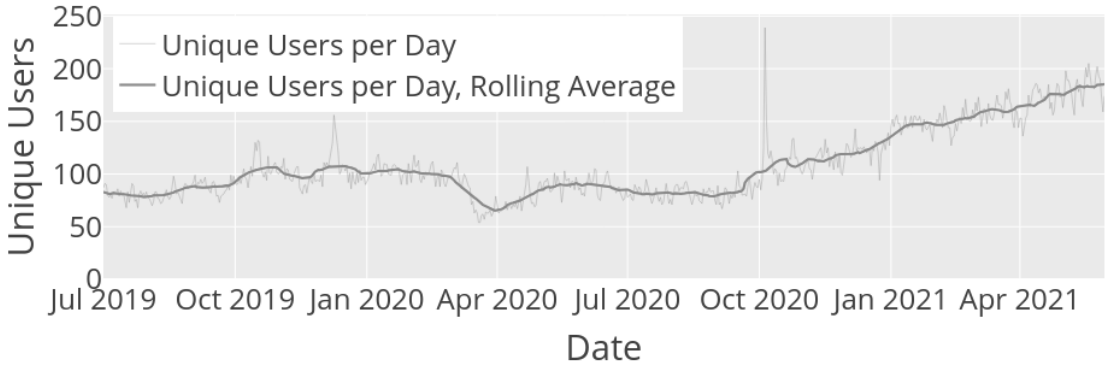

Figure 2: Plot of the development of the number of users per day. The thick line depicts a seven-day rolling average, the thin line the actual values. A peak can be seen as the result of a big marketing campaign, which led to a general increase of users per day.

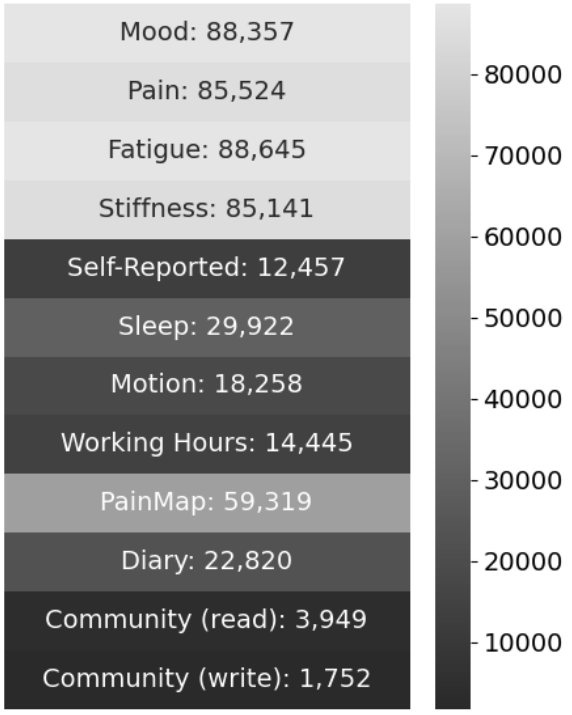

Figure 3: Depiction of the total count of entries for each entry type. The fast-to-enter symptoms as well as the pain map are the most popular entry types.

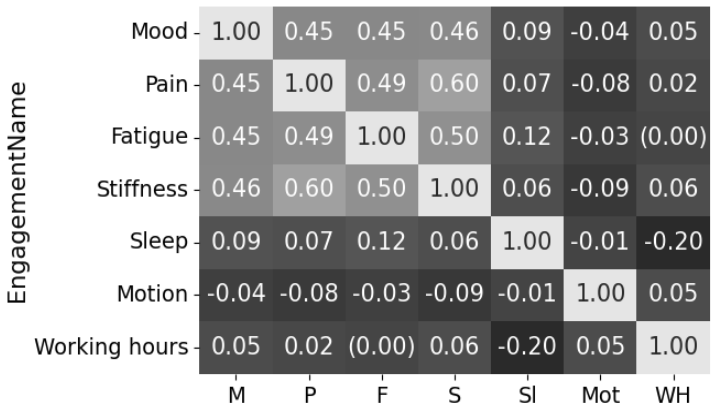

Figure 4: Linear, numeric correlations between the entry types based on 456,998 observations. Correlations between the four main symptoms are present, symptoms and activities seem to be uncorrelated.

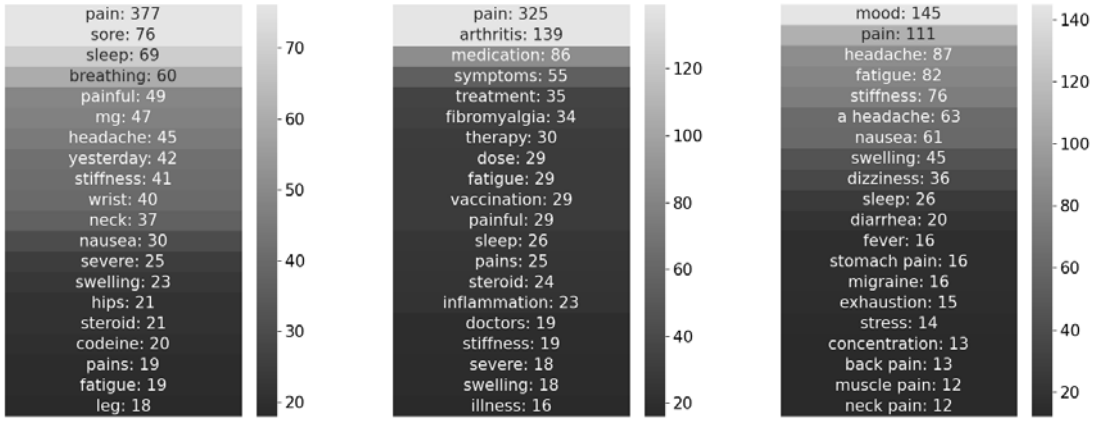

(a) Most frequent words in the diary. (b) Most frequent words in the community. (c) Most frequent Self-Reported Symptoms.

Figure 5: Heatmaps for the most often used words in all kinds of free texts. The main topics for all sources are disease-related, i.e. symptoms and medication are the most popular.

However, the obtained recommendations cannot be used as they are as app recommendations. These recommendations are mainly tips from the users who usually do not have any medical background. Sharing what might help one user does not necessarily help another user, but could in the worst case actually harm them. And while it is fair to have recommendations in the community that might not be suitable for all users, app-provided recommendations must in any case be medically solid and do no harm to the users. Therefore, the recommendations obtained via community crawling cannot automatically be used in the app.

Still, the recommendations can be collected and further used. For example, they can be shared with medical experts which can assess on a patient-individual basis whether some of the recommendations could be helpful for some of their patients. Or specific medical studies could be started, proving (or disproving) some of the interesting recommendations. And finally, the developed method can be used in different contexts, where obtaining unsuitable recommendations is not that problematic.

2.5 User Clustering

Another idea was grouping similar users, based on their entries. Having such a group of users, the app could e.g. provide specific recommendations, based on the group characteristics. Users in such a group could also be brought together in an anonymous chat (if they consent) and share their experiences.

To achieve this, we measured the similarity between the main symptom entries (Mood, Pain, Fatigue and Stiffness) of the users. In order to recognize similar patterns even if they are shifted in time or slightly distorted, we measured the similarity using Dynamic Time Warping (DTW, [5]). We focused on one of the symptoms at a time and computed for all users with at least 10 entries the pairwise similarities between their values using DTW. Next, we grouped the users based on their pairwise distances. We tried different clustering algorithms using Scikit-Learn [6], finding that Spectral Clustering provided the most promising algorithm.

However, on the available app data, it was not possible to find useful clusters. Hardly any user provides daily entries, but rather one entry every few days. Furthermore, the values are discrete values between 1 and 5, which resulted in entry curves where no sensible pattern could be found. With the available values, it is not possible to recognize users that get steadily better or worse over some time. To achieve this, a scale where more precise entries are possible would be required.

3 User-individual Correlations

We figured that the users of the app might not be interested in the development of their values, but also in the relationship between these values. As we showed in Subsection 2.2, significant correlations between the symptoms are present when considering all users at once.

To our surprise, no correlations between symptoms and activities could be found. However, during our consortium discussions, also including patient research partner, we agreed that relationships between activity patterns and symptoms should exist. Not finding any with the current approach could be due to several reasons:

- As discussed in Subsection 2.1, the users had problems entering reasonable values to the activity functions in the app, and as can be seen in Figure 3, the number of entries for activity values is much smaller.
- Users with positive and negative relationships could even each other out when being considered all at once.
- Also when it comes to one user, they don't necessarily have a *linear* relationship between their activities and symptoms, but rather some level of activity where they feel best/worst.

We decided to have a closer look at user-individual relationships between the values, and to not only take into account linear correlations. Additionally, the relationships between a user's individual input values is probably far more interesting to them than the correlations of all users. Therefore, we investigated on a user-individual basis, between which input values we could find the strongest significant relationships.

3.1 New Activity Values

First, we wanted to overcome the problem with entering reasonable activity values into the app. To achieve this, a step counter was added to the application. Of course, this does not cover the whole variety of physical activity (a step counter does not distinguish between walking and jogging, for example), but these values are added to the app automatically and provide a good approximation of the user's level of physical activity. Furthermore, the smiley values were enhanced by activity categories, enabling a user to provide input on a scale of 1 to 5, how physically active they were that day.

3.2 Model

We focus on the relationships between symptoms and activities per user, and consider three different kinds of relationships that could occur between the values:

- Linear relationships, e.g. "The more you walk, the better is your mood."
- Cut-Off values, e.g. "Your mood increases signifi-cantly when you walk around 6,000 steps per day."
- Extreme values, e.g. "Your mood is best when you walk around 6,000 steps per day."

These relationships are computed twice for each symptom-activity-pair, between same-day data as well as between activity data on one day and symptom data the next day. Thus, a possible output could also be "The more you walked *the day before*, the better is your mood." Additionally, every relationship can also be negative, e.g. "The *less* you walk, the better is your mood."

To achieve this, we firstly retrieved a user's recent data from their last 30 entry days. If they provided values for the considered symptom-activity-combination on at least on 10 different days (i.e. if we have at least 10 entry pairs), we fitted the user-data with three different models: A linear regression model (LR), a decision tree (DT), and a piece-wise linear function (PWLF).

Linear Regression Model. We fitted the data with a linear regression curve of the form

$$y_i = a \cdot x_i + b + r_i$$

with y_i being the symptom values, x_i the activity values and r_i the residuals. a is the slope of the function, which is later used to determine if there is a positive or negative relationship between the two values.

Decision Tree. We also fitted the data with a decision tree with one split node and constant values at the leaves.

Piece-wise linear function. If the user provided at least 15 value pairs in the given time frame, we also fitted the data with a continuous piece-wise linear function with one split, using the python library PWLF [8]. In order for this model to be valid in our context, the slopes of the two linear functions must have different signs, i.e. the break point must be a minimum or a maximum value. Additionally, the break point was only allowed within the inner 60% of the data range, and both linear functions must be supported by at least 5 data points. Otherwise, the PWLF would always fit the data better than the other two models without providing additional information.

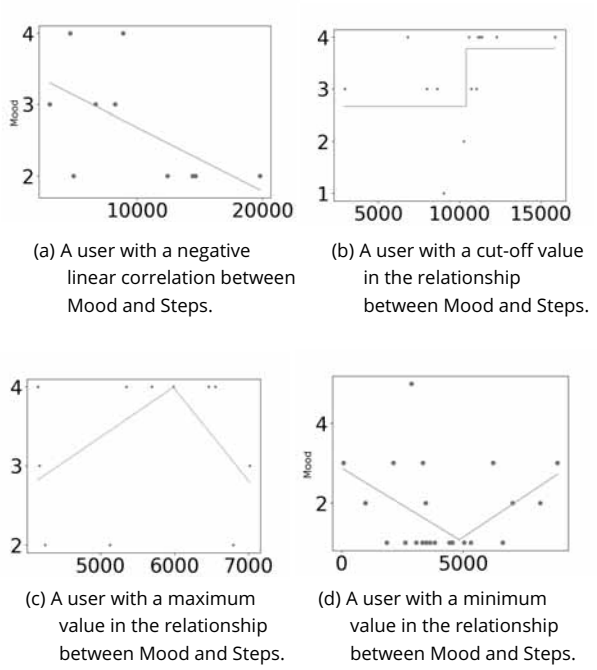

(a) A user with a negative linear correlation between Mood and Steps.

(b) A user with a cut-off value in the relationship between Mood and Steps.

(c) A user with a maximum value in the relationship between Mood and Steps.

(d) A user with a minimum value in the relationship between Mood and Steps.

Figure 6: Example plots of four users, depicting their individual relationships between number of steps and mood. The rather simple models still provide an interpretable relationship between the values.

Figure 6 shows some sample plots of the actual values of four different users, together with the model that fits their data. Note that for Subfigures 6c and 6d, only a very weak linear relationship would have been found. From each of these models, the R^2-Score is computed as a measure of fitting, and the model with the highest R^2 is kept. Thus, for every symptom-activity-combination, we compute one relationship. Finally, from all the symptom-activity-combinations, we choose the one with the highest R^2-Score and display it as an insight to the user.

3.3 Deployment

This feature was added into the RheumaBuddy app. It was deployed via a Docker Container [9] which runs on the server of the app provider DAMAN. Thus, the described relationships are computed in real-time and are communicated live to the users. A sample output from the app can be seen in Figure 7.

However, the number of entries required to obtain a significant relationship is quite high, and only few users entered enough values to obtain such a recommendation.

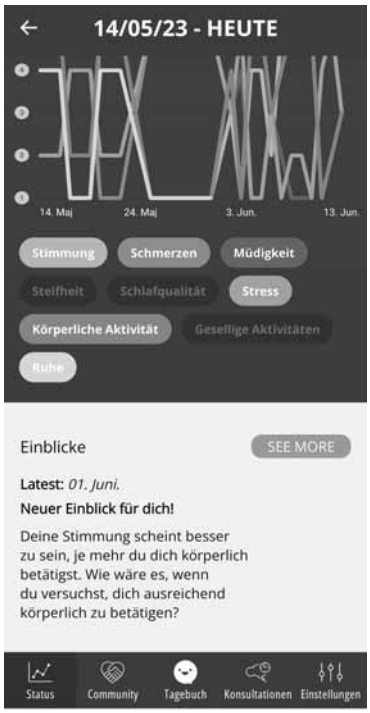

Figure 7: An actual recommendation (in German language) as provided from the **RheumaBuddy** app, stating that this user's mood seems to be better the more physically active they are.

4 Validation Process

The new app features are validated concerning face validity from the app developers. They check whether the app feedback makes sense and fits to the provided user input. Furthermore, they make sure that the insight is prompted to the users, and to how many. A selection of patients from their company review board tests the new features and provides thorough feedback on the functionality and the insights.

However, validation is at this point not complete and refinements would potentially be tackled in several iteration rounds. For putting **RheumaBuddy4.0** on the track for CE marketing, certain aspects of a final software product would need to be submitted.

The validation process can be optimized by integrating results from the observational study at the Medical University of Vienna ("Successful Implementation of an RA management app - the IRAMA study" with ethical approval number: EK-Nr: 1846/2022) which is in process. The major aims of the IRAMA study concern the assessment of the RheumaBuddy mobile app quality, using a standardized questionnaire to evaluate patients' experiences, preferences and needs for the use of the **RheumaBuddy** App in semi-structured telephone interviews, and finally to gain more detailed insight on patients' experiences, needs and preferences in semi-structured focus group sessions.

The data of this study is directly linked with a clinical registry and the app information the users are collecting. Thus, the foundation for a thorough validation via an observational study is already in place.

5 Discussion and Outlook

Overall, it can be stated that the project is progressing successfully. An interesting, helpful feature for the app users has been implemented, and we gained a lot of insights by means of the data analysis and the discussions in the consortium. We expect further interesting insights when the observational study is finalized.

One of the main challenges of the project was the lack of user input into the app. While the functions work well and can give useful insights to the users, hardly any users obtain such recommendations, because they stop entering values into the app too early. Some ways of Gamification to increase the motivation of the app users could be considered, e.g. counting how many days in a row they entered something into the app, and motivating not to break this "streak" - this has been shown to be helpful in many mobile apps [10].

The combination of passively tracked data with traditional or short PROMs as used in RheumaBuddy is potentially more promising to be supportive regarding improvement of the quality of life of people with RA when combined with the treating rheumatology team. As RA can affect people of any age, the background, i.e. experience with technology or eHealth literacy, is very heterogeneous, which makes it challenging to develop digitally assisted technologies that support every patient on an equal basis. Technology has been utterly fast paced over the past years, sharing breaking record news multiple times per year, but medical systems and people work and live on a slower pace. Thus, we would need to harmonise the slopes of development with the needs and opportunities that appear for implementation of novel technologies. This will bring benefit to people living with chronic conditions like RA as well as health care providers and system payers [4].

Acknowledgement

The project RB4.0 (FFG project number 880456) was funded by the Austrian Research Promotion Agency (FFG), the national funding agency for industrial research and development in Austria, as part of the call for proposals *Eurostars-2 CoD 13* (www.ffg.at/en).

Publication Remark

This contribution is the revised version of the conference version published in ***ASIM SST 2024*** *Munich Tagungsband Langbeiträge,* ARGESIM Report 47, e-ISBN978-3-903347-65-6,Vol. DOI 10.11128/arep.47, Article DOI: 10.11128/arep.47.a4725, p 43-50.

References

[1] Symmons D, Turner G, Webb R, Asten P, Barrett E, Lunt M, Scott D, Silman A. *The prevalence of rheumatoid arthritis in the United Kingdom: new estimates for a new century.* Rheumatology (Oxford). 2002 Jul; 41(7):793-800.

[2] Finckh A, Gilbert B, Hodkinson B, Bae S-C, Thomas R, Deane KD, Alpizar-Rodriguez D, Lauper K. *Global epidemiology of rheumatoid arthritis.* Nature Reviews Rheumatology. 2022 2022/09/06 doi:10.1038/s41584-022-00827-y.

[3] Winthrop KL, Mease P, Kerschbaumer A, Voll RE, Breedveld FC, Smolen JS, Gottenberg J-E, Baraliakos X, Kiener HP, Aletaha D, Isaacs JD, Buch MH, Crow MK, Kay J, Crofford L, Vollenhoven RFv, Ospelt C, Siebert S, Kloppenburg M, McInnes IB, Huizinga TW, Gravallese EM. *Unmet need in rheumatology: reports from the Advances in Targeted Therapies meeting, 2023.* Annals of the Rheumatic Diseases. 2023:ard-2023-224916 doi:10.1136/ard-2023-224916.

[4] De Cock D, Myasoedova E, Aletaha D, Studenic P. *Big data analyses and individual health profiling in the arena of rheumatic and musculoskeletal diseases (RMDs).* Ther Adv Musculoskelet Dis. 2022; 14:1759720X221105978 doi:10.1177/1759720X221105978

[5] Springer Berlin Heidelberg. Dynamic Time Warping. In: *Dynamic Time Warping*. 2007. p 69–84.

[6] *Scikit-learn: Machine Learning in Python*, Pedregosa et al., JMLR 12, pp. 2825-2830, 2011.

[7] Bird S., Klein E., Loper E. (2009). *Natural language processing with Python: analyzing text with the natural language toolkit.* " O'Reilly Media, Inc."

[8] Jekel Charles, Venter Gerhard. (2019). *pwlf: A Python Library for Fitting 1D Continuous Piecewise Linear Functions.* 10.13140/RG.2.2.28530.56007.

[9] Cito Jürgen, Ferme Vincenzo, Gall Harald. (2016). *Using Docker Containers to Improve Reproducibility in Software and Web Engineering Research.* 609-612. 10.1007/978-3-319-38791-8_58.

[10] Galetta, Giuseppe. (2013). *The Gamification: Applications and Developments for Creativity and Education.* 10.13140/RG.2.2.24817.68965.

Terrain Identification using Reaction-based Sensor Data in Simulation-driven Terrain-aware Military Logistics

Mihaela Lechner*, Oliver Rose

Chair of Modeling and Simulation, University of the Bundeswehr Munich,
Werner-Heisenberg-Weg 39, 85579 Neubiberg, Germany; *mihaela.lechner@unibw.de

SNE 36(2), 2026, 107-114, DOI: 10.11128/sne.36.tn.10777
Selected ASIM SST 2024 Postconf. Publ.: 2025-06-10
Received Revised: 2025-12-15; Accepted: 2025-12-20
SNE - Simulation Notes Europe, ARGESIM Publisher Vienna
ISSN Print 2305-9974, Online 2306-0271, www.sne-journal.org

Abstract. Military planning operations require navigating constantly changing environments. To support decision-makers, innovative concepts are essential for automatically generating effective solutions tailored to specific logistics operations. These tools aim to accelerate planning procedures, minimize risks, and reduce operating costs. This paper introduces a simulation-based optimization framework designed to enhance the mobility of military vehicles through terrain-aware navigation. It specifically examines a key component of the framework: terrain identification. This challenge is addressed using unsupervised methods, ensuring applicability even in unfamiliar operational settings. The experimental findings demonstrate promising results in identifying terrain characteristics, particularly in discerning surface waviness, slant, and curvature.

Introduction

The mobility of supplies, equipment, and personnel is crucial to the success of land-based military missions. Unlike civilian logistics, which often prioritize the shortest and fastest routes, military operations must consider factors such as environmental uncertainty [17], route vulnerability [16], and terrain passability [14] when determining the most suitable logistics routes.

Furthermore, military operations often extend across geographically diverse regions, where terrain conditions have a direct impact on their specific effectiveness [14].

Therefore, planners must carefully assess terrain characteristics such as landform features, soil conditions, and slope degree when preparing military logistics plans.

The terrain encountered by military land vehicles often falls outside typical mapped areas, leaving planners with limited information regarding its topology. In such scenarios, battlefield commanders rely on terrain analysts to interpret the geographic features of an area and assess their impact on the military mission [18].

Over time, this process has evolved from a predominantly manual endeavor to one increasingly reliant on computer-based systems [15]. One aspect of terrain analysis that can be addressed through computational means is terrain identification. This field of research involves estimating ground characteristics (e.g., cohesion, curvature, inclination) or categorizing terrain types (e.g., gravel, asphalt, sand) by collecting diverse sensor data under various road conditions and analyzing vehicle responses to the terrain.

Numerous researchers have made significant contributions to terrain identification methodologies. Among these, supervised learning techniques such as Support Vector Machines [1, 10], Decision Trees [12], Neural Networks [9, 13], and Gaussian Process Regression [11] have emerged as popular choices. Although these approaches have proven effective, they often require prior human intervention or additional hardware, such as laser line striping sensors, for data labeling. Conversely, unsupervised approaches do not require labeled data and can be directly applied in scenarios where the external environment is unknown.

In addition to the configuration of the learning algorithm, the accuracy of a terrain identification strategy depends on the data it receives. Various sensors can be mounted on the vehicle to collect this data.

Cameras [4, 5], lidars [7, 8], and accelerometers [1, 2, 3] stand out as prominent choices in recent research. Each sensor type has its limitations [6]. For instance, vision-based sensors such as cameras and lidars are sensitive to weather conditions that reduce visibility, such as fog or rain, whereas reaction-based sensors such as accelerometers are sensitive to speed and load variations. Despite this disadvantage, reaction-based techniques demonstrate strong cost-effectiveness and robustness across diverse terrain types [19].

This study focuses on solving the terrain identification problem, aiming to differentiate distinct terrain characteristics such as roughness, waviness, slant, and curvature. The approach involves conducting multiple test drives at military test sites to collect reaction-based data, including acceleration, roll, pitch, and angular rate, captured by an accelerometer and a gyroscope. Initially, the signal data undergo windowing, followed by the segmentation of each route into predetermined lengths.

Subsequently, the unsupervised learning algorithm Multivariate K-Means is used to differentiate between terrain characteristics. We employ the Dynamic Time Warping (DTW) algorithm to calculate the pairwise proximity between road segments.

Moreover, this research introduces a simulation-driven logistics framework that integrates terrain identification, scheduling, and vehicle routing processes to assist planners in developing terrain-aware logistics strategies.

The plans generated by this framework are designed to optimize the utilization of available assets by considering surface characteristics when determining efficient transportation routes. Within the broader logistics context, this approach offers the potential to improve operational efficiency and achieve substantial cost savings.

In addition to immediate reductions in fuel and personnel expenses, it can also contribute to lowering long-term vehicle maintenance costs. This is achieved by implementing intelligent routing strategies that minimize vehicle wear and tear, thereby extending vehicle lifespan and reducing the frequency of repairs and replacements.

1 Conceptual Approach of a Simulation-based Terrain-aware Logistics Framework

Developing military logistics strategies presents a significant challenge in optimizing asset scheduling and route selection for the efficient transportation of personnel, equipment, and supplies to designated destinations. This challenge is further increased by the absence of basic infrastructure in certain locations and the diverse terrain conditions encountered during transit. Additionally, different vehicles are tailored for navigating specific types of terrain. Some are designed for rough, steep terrain with obstacles, while others perform better on smooth, paved roads.

To ensure effective and efficient transportation operations, it is essential to consider the mobility capabilities of vehicles across various surfaces, along with critical logistics factors such as route length, transport duration, and delivery time requirements.

To address these challenges, we introduce the simulation-based logistics framework depicted in Figure 1. The primary objective of this framework is to assist planners in developing efficient military transportation systems by focusing on sustainable resource management and enhancing vehicle mobility across favorable terrain conditions.

The framework begins by prioritizing the identification of terrain characteristics along the routes. These details, along with information on road networks, vehicle availability, and load requirements for transportation between origin and destination points, serve as inputs.

Subsequently, the framework proceeds to optimize fleet utilization. The scheduling component determines which loads should be transported by each vehicle and in what sequence, aiming to minimize costs while satisfying constraints such as vehicle capacities.

Following scheduling, the routing process uses the scheduled assets to establish logistics routes. This process extends beyond selecting the shortest and fastest paths by incorporating terrain conditions. As certain terrains disproportionately affect vehicle performance and wear, selected routes must align with the mobility characteristics of the vehicles.

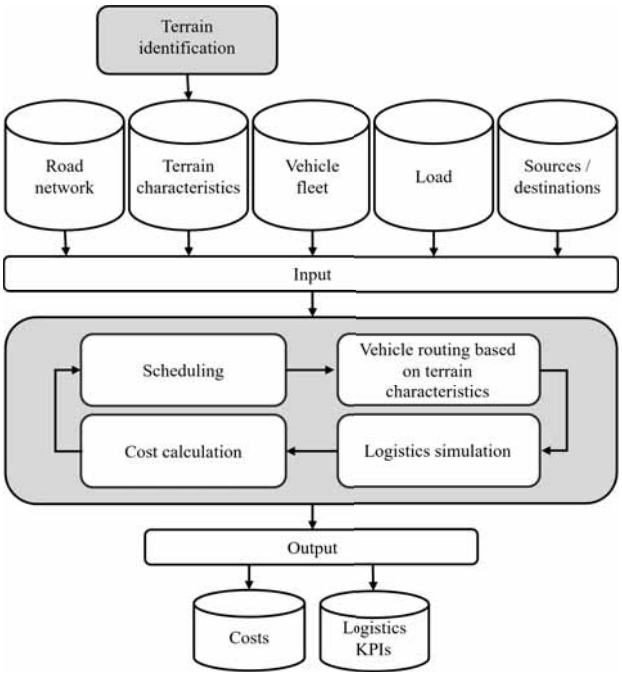

Figure 1: Conceptual model of the proposed simulation-driven terrain-aware logistics framework.

During the simulation phase, logistics plans are executed, and the behavior of simulation agents is monitored. Each transportation task is evaluated using a cost function designed to minimize both duration and cost, while accounting for travel feasibility across different surfaces.

Given the critical role of terrain characteristics in terrain-aware logistics, terrain identification is explored throughout the remainder of this paper.

2 Terrain Identification

This section explores terrain identification, a key component of the logistics framework detailed in Section 1. This process is essential for enabling the computation of terrain-aware logistics routes, as it provides critical information about the interaction between vehicles and the underlying surface conditions.

2.1 Problem Description

We address the challenge of terrain identification using reaction-based sensor measurements collected from vehicles operating in diverse environments.

The primary objective is to differentiate between specific terrain characteristics such as roughness (Figure 2a), waviness (Figure 2b), slant (Figure 2c), and curvature (Figure 2d), even in scenarios where prior knowledge of the terrain is limited or unavailable.

This is achieved through analyzing unique signal patterns captured by standard sensors like accelerometers and gyroscopes, which record the dynamic interaction between the vehicle and the terrain.
To accomplish this task, we introduce the technique detailed in Section 2.2.

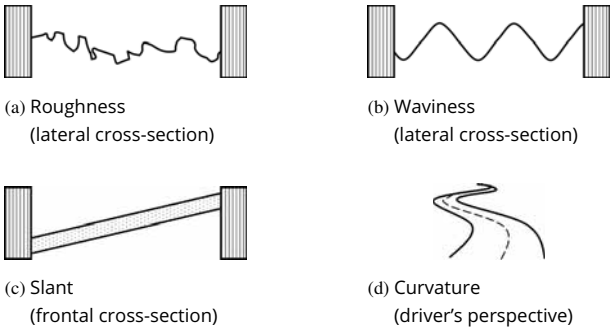

(a) Roughness (lateral cross-section)

(b) Waviness (lateral cross-section)

(c) Slant (frontal cross-section)

(d) Curvature (driver's perspective)

Figure 2: Terrain characteristics under investigation.

2.2 Solution Approach

We propose the methodology illustrated in Figure 3 for terrain identification. This approach relies on data acquired from reaction-based sensors during vehicle operation on various road surfaces.

In the preprocessing phase, the input data are subjected to windowing and segmentation to generate frames for feature extraction. Subsequently, the unsupervised learning technique Multivariate K-Means is applied to identify distinct terrain characteristics.

In the upcoming paragraphs, each component of the terrain identification approach will be elaborated.

Data Acquisition. Over the course of 24 test runs at a military test site, data were collected from multiple ground surfaces exhibiting varying degrees of roughness, waviness, slant, and curvature.

For this purpose, a military vehicle traveled approximately 500 km, equipped with an accelerometer, a tri-axial gyroscope, and a Global Positioning System (GPS). Each sensor recorded data at a sampling rate of 500 Hz.

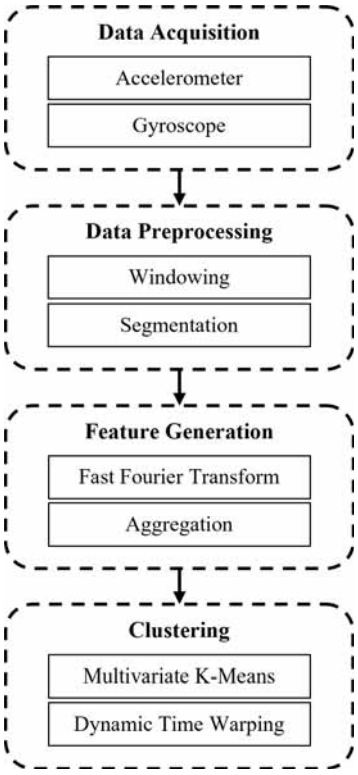

Figure 3: Proposed terrain identification methodology.

To mitigate the speed dependency of reaction-based terrain identification, the vehicle was driven at varying speeds ranging from 5 to 45 km/h.

Data Preprocessing. The preprocessing phase involves two key steps: windowing and segmentation.

Windowing is a technique used to transform sequential data, such as the dataset under consideration, into a format suitable for traditional machine learning algorithms [22].

Additionally, it helps reduce computational complexity. This process involves dividing the sensor data into non-overlapping frames, each consisting of 500 samples, corresponding to one second of data given a sampling frequency of 500 Hz.

Clustering entire routes poses challenges in detecting local similarities. Conversely, clustering individual observations fails to produce cohesive patterns and instead results in fragmented clusters across multiple terrain categories.

To address this issue, we partition each test drive into segments of 40 m, approximately five times the length of the vehicle. Each segment is treated as an individual observation.

Feature Generation. The sensor data in the time domain, including tri-axial acceleration, tri-axial rotation rate, roll, and pitch, are converted into the frequency domain using the Fast Fourier Transform (FFT) algorithm.

Features are extracted by considering observations from both the original time-domain representation and its frequency-domain transformation within the previously generated windows. Each window is aggregated into a single output value by computing statistical measures such as the mean, standard deviation, minimum, maximum, and interquartile range. In total, this process yields 80 features.

Clustering. We approach the task of terrain identification by examining similar patterns within segments of routes traversed by vehicles. Since each segment contains multiple observations, the problem inherently becomes multivariate. To handle this complexity, we utilize Multivariate K-Means clustering.

While deep learning–based clustering techniques could also be applied, they tend to be complex, challenging to interpret, and computationally expensive. However, the K-Means method also has its limitations, particularly its sensitivity to the choice of the number of clusters k.

To address this issue, we employ the Silhouette Coefficient, introduced in [23], to determine an optimal number of 9 clusters.

In the clustering process, we use the DTW proximity measure, a technique proposed in [20]. This method offers advantages over conventional Euclidean distance by effectively recognizing similarities between sequences, even when they differ in length or exhibit slight temporal shifts.

For enhanced visualization and evaluation of the clustering results, we adopt the Multivariate T-distributed Stochastic Neighbor Embedding (m-TSNE) technique introduced by [21].

This approach enables the projection of high-dimensional multivariate data onto a lower-dimensional space while preserving similarity relationships between data sequences. Consequently, sequences that are similar in high-dimensional space remain close in the lower-dimensional space.

3 Experimental Results

The solution described above was implemented and evaluated in Python 3.11.5 on a standard PC running Windows 11, equipped with an 11th-generation Intel Core i7-11370H CPU at 3.30 GHz and 16 GB of RAM. Training the model on a preprocessed dataset of 200 MB requires approximately 15 minutes.

The computational complexity of training arises from the large number of pairwise similarities that must be computed, specifically $\binom{N}{2}$, where N denotes the number of route segments.

The 24 trips are partitioned into approximately 12,000 segments, each assigned to one of 9 clusters using the Multivariate K-Means algorithm with 80 features. To enhance visualization of the high-dimensional space, the data are reduced to two dimensions using the m-TSNE method, as shown in Figure 4. Each point in the plot corresponds to a route segment, revealing discernible separation patterns among groups.

While certain groups, particularly those at the periphery, exhibit clear separation from others, observations in the central regions lack well-defined boundaries. Nevertheless, the clustering method captures the underlying structure, with only a few instances dispersed across multiple groups in the two-dimensional space.

Figures 5a–5d illustrate the key features essential for cluster formation. Each displayed feature is aggregated through windowing using the mean function, as detailed in Section 2.2, and is derived from frequency-domain transformations. Analyzing these plots enables the characterization of clusters based on the distinct terrain traits outlined in Figure 2. High signal magnitudes indicate the presence of specific terrain characteristics, while lower magnitudes suggest their absence.

The accelerometer supports the measurement of the vehicle's vertical displacement relative to the ground (z-axis acceleration), facilitating the evaluation of terrain roughness. Notably, cluster $C5$ stands out as representing rough terrain, as shown in Figure 5a.

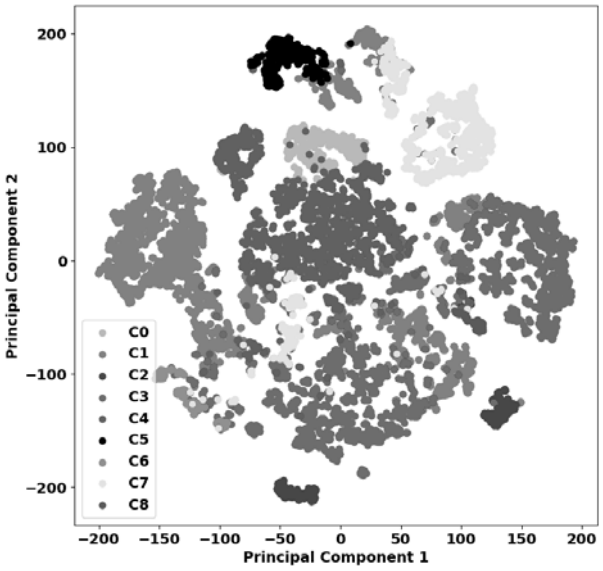

Figure 4: Representation of the two-dimensional m-TSNE components depicting route segments clustered based on the Multivariate K-Means method.

Waviness, in contrast, involves larger, repetitive undulations compared to roughness, resulting in a rocking motion of the vehicle rather than purely vertical acceleration. These movements are captured through pitch measurements from the gyroscope. As depicted in Figure 5b, clusters $C6$ and $C8$ exhibit wavy terrain characteristics. Surface slant, indicative of tilts to the right or left, is discernible via the roll signal. Slanted terrain is observable in clusters $C2$ and $C8$ from Figure 5c. Furthermore, the gyroscope captures the rotational motion of the vehicle, reflecting road curvature, as evident in clusters $C0$ and $C4$ in Figure 5d.

The remaining clusters do not exhibit distinctive terrain characteristics based on the examined features, suggesting that the corresponding road segments are relatively smooth and straight.
An overview of the characteristics exhibited by each cluster is provided in Table 1.

Since the test drives were conducted on a specialized test course, certain segments of the underlying surfaces have known labels. For instance, cluster $C2$ represents the inclined test track, featuring an incline ranging from 20% to 30%. Cluster $C5$ corresponds to the washboard test track, while the sine-wave road is identifiable within cluster $C6$. Cluster $C7$ encompasses cobblestone and gravel surfaces.

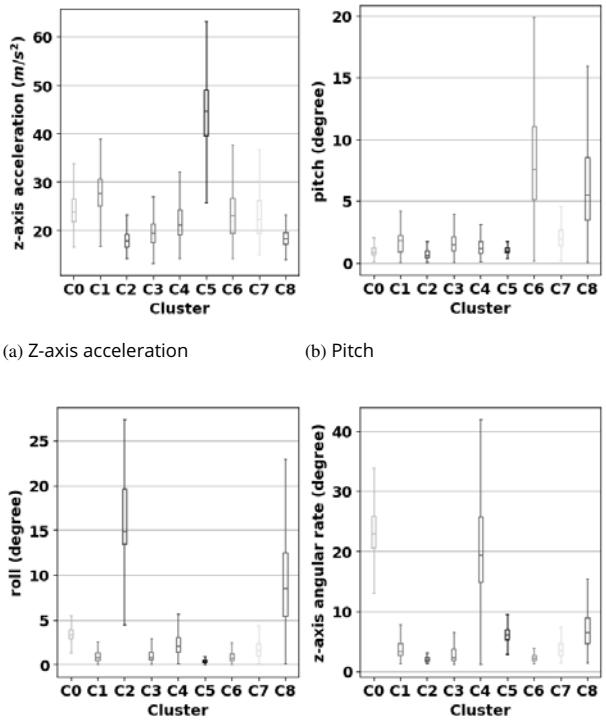

(a) Z-axis acceleration (b) Pitch

(c) Roll (d) Z-axis angular rotation

Figure 5: Selection of features employed in the clustering procedure, presented individually for each cluster. These features were derived from raw signals transformed into the frequency domain and aggregated using the mean function during the windowing process.

	Roughness	Waviness	Slant	Curvature
C0	-	-	-	✓
C1	-	-	-	-
C2	-	-	✓	-
C3	-	-	-	-
C4	-	-	-	✓
C5	✓	-	-	-
C6	-	✓	-	-
C7	-	-	-	-
C8	-	✓	✓	-

Table 1: Summary of the terrain characteristics observed within the clusters.

Lastly, cluster $C8$ represents the distortion road, characterized by alternating waves on each side.

Table 2 presents a comparison between the clustering results and the known ground-truth labels.

An examination of the model's performance across clusters reveals that it performs better for certain road types. Specifically, slanted ($C2$) and distorted ($C8$) roads are identified with high precision, recall, and F1-score. However, the model performs less effectively in identifying washboard ($C5$) and sine-wave ($C6$) tracks.

Cluster	Precision	Recall	F1-score
C2	0.99	0.95	0.97
C5	0.92	0.35	0.51
C6	0.86	0.49	0.62
C7	0.93	0.82	0.87
C8	0.93	0.93	0.93

Table 2: Summary of the model performance.

4 Conclusion and Outlook

In military operations, terrain-aware logistics are crucial, particularly when navigating challenging landscapes with limited infrastructure to transport supplies, equipment, and personnel.

In such contexts, logistics planning must consider not only factors such as travel distance, duration, and delivery schedules but also the unique characteristics of the terrain traversed.

In response to this need, this research introduces a simulation-driven terrain-aware framework designed to support decision-makers in improving the mobility of military vehicles by enabling more efficient navigation across favorable terrain conditions. The primary focus of this paper is the terrain identification process, which employs unsupervised methods to distinguish between terrain characteristics even in the absence of prior knowledge of surface conditions.

The experimental findings d emonstrate promising results in discerning roughness, waviness, slant, and curvature from reaction-based signals. Each terrain characteristic is represented by a dominant signal, for instance, high magnitudes of the z-axis acceleration signal indicate rough terrain. Additionally, terrains exhibiting multiple characteristics can be identified by considering multiple signals. For example, higher magnitudes in the pitch and roll signals suggest a wavy and slanted road.

Despite its effectiveness, this approach requires careful consideration in certain areas. As noted in previous research [6], reaction-based terrain identification is sensitive to vehicle speed and load, causing terrain signatures to vary under different operating conditions. For accurate identification, the algorithm must be trained on a diverse dataset encompassing a wide range of speeds and loads.

Moreover, while unsupervised learning is valuable in the absence of prior terrain knowledge, it requires human interpretation of the results. Defining thresholds for specific signals that indicate particular terrain features is essential for precise categorization. Furthermore, the current approach focuses on identifying terrain features but does not quantify their intensity. Future work should incorporate a scoring system to evaluate terrain surfaces based on their characteristics. Identifying specific surface types, such as concrete, grass, or soil, would further enhance the optimization of logistics route planning.

While this paper emphasizes terrain identification, it is essential to implement the subsequent steps of the framework to fully realize its potential in terrain-aware logistics. This includes integrating fleet scheduling, terrain-informed route planning, and simulation-based evaluation to refine and optimize military logistics operations.

Acknowledgement

We express our gratitude to the Bundeswehr Office for Defence Planning, particularly Ferdinand Rinscheid, for their invaluable assistance, generous support, and willingness to share their knowledge and expertise.

Publication Remark

This contribution is the revised version of the conference version published in

ASIM SST 2024, Munich, September 2024
Tagungsband Langbeiträge,
ARGESIM Report 47,
e-ISBN978-3-903347-65-6,
Vol. DOI 10.11128/arep.47,
Article DOI: 10.11128/arep.47.a4721, p 73-79.

References

[1] Weiss C, Fröhlich H, Zell A. Vibration-based terrain classification using support vector machines.
In: *2006 IEEE/RSJ International Conference on Intelligent Robots and Systems*; 2006; Beijing, China: IEEE. pp. 4429–4434.
doi: 10.1109/IROS.2006.282076

[2] Souza JR, Marchant R, Ott L, Wolf DF, Ramos F. Bayesian optimisation for active perception and smooth navigation.
In: *2014 IEEE International Conference on Robotics and Automation (ICRA)*; 2014; Hong Kong, China: IEEE. pp. 4081–4087.
doi: 10.1109/ICRA.2014.6907452

[3] Wang M, Ye L, Sun X. Adaptive online terrain classification method for mobile robot based on vibration signals.
International Journal of Advanced Robotic Systems. 2021; 18(6):172988142110620.
doi: 10.1177/17298814211062035

[4] Chetan J, Madhava Krishna K, Jawahar CV. An adaptive outdoor terrain classification methodology using monocular camera.
In: *2010 IEEE/RSJ International Conference on Intelligent Robots and Systems*; 2010; Taipei, Taiwan: IEEE. pp. 766–771.
doi: 10.1109/IROS.2010.5651067

[5] Gao B, Zhao X, Zhao H. An active and contrastive learning framework for fine-grained off-road semantic segmentation.
IEEE Transactions on Intelligent Transportation Systems. 2023; 24(1):564–579.
doi: 10.1109/TITS.2022.3218403

[6] Coyle E, Collins EG, Roberts RG. Speed independent terrain classification using singular value decomposition interpolation.
In: *2011 IEEE International Conference on Robotics and Automation*; 2011;
Shanghai, China: IEEE. pp. 4014–4019.
doi: 10.1109/ICRA.2011.5979766

[7] Andersen JC, Blas M, Ravn O, Andersen NA, Blanke M. Traversable terrain classification for outdoor autonomous robots using single 2D laser scans.
Integrated Computer-Aided Engineering. 2006; 13(3):223–232.
doi: 10.3233/ICA-2006-13303

[8] McIver CA, Metcalf JP, Olsen RC. Spectral LiDAR analysis for terrain classification.
In: *Laser Radar Technology and Applications XXII*; 2017; Anaheim, CA, USA: SPIE. pp. 101910J.
doi: 10.1117/12.2276658

[9] Csík D, Odrý Á, Sárosi J, Sarcevic P. Inertial sensor-based outdoor terrain classification for wheeled mobile robots.
In: *2021 IEEE 19th International Symposium on Intelligent Systems and Informatics (SISY)*; 2021; Subotica, Serbia: IEEE. pp. 159–164.
doi: 10.1109/SISY52375.2021.9582504

[10] Oliveira FG, Santos ERS, Neto AA, Campos MFM, Macharet DG. Speed-invariant terrain roughness classification and control based on inertial sensors.
In: *2017 IEEE Latin American Robotics Symposium (LARS) and 2017 Brazilian Symposium on Robotics (SBR)*; 2017; Curitiba, Brazil: IEEE. pp. 1–6.
doi: 10.1109/SBR-LARS-R.2017.8215332

[11] Inotsume H, Kubota T. Terrain traversability prediction for off-road vehicles based on multi-source transfer learning.
Robomech Journal. 2022; 9(1):6–31.
doi: 10.1186/s40648-021-00215-3

[12] Beilfuss T, Kortmann KP, Wielitzka M, Hansen C, Ortmaier T. Real-time classification of road type and condition in passenger vehicles.
IFAC-PapersOnLine. 2020; 53(2):14254–14260.
doi: 10.1016/j.ifacol.2020.12.1161

[13] Sunusi II, Zhou J, Sun C, Makange N. Online terrain parameter estimation for traction control in intelligent electric tractors.
International Journal of Electrical Engineering. 2023; 29(4):97–107.
doi: 10.6329/CIEE.202208_29(4).0001

[14] Dawid W, Pokonieczny K. Methodology of using terrain passability maps for planning the movement of troops and navigation of unmanned ground vehicles.
Sensors. 2021; 21(14):4682.
doi: 10.3390/s21144682

[15] Graff LH. *State-of-the-Art Terrain Analysis Capabilities for Today's Army*. 1996.

[16] Muckensturm J, Longhorn D. Assessing the vulnerability of military theater distribution routes.
Journal of Defense Analytics and Logistics. 2019;3(1):60–82.

[17] Zhao T, Huang J, Shi J, Chen C. Route planning for military ground vehicles in road networks under uncertain battlefield environment.
Journal of Advanced Transportation. 2018; 2018(2):1–10.
doi: 10.1155/2018/2865149

[18] Headquarters Department of The Army. *ATP 2-01.3 Intelligence Preparation of the Battlefield / Battlespace*.
Createspace Independent Publishing Platform; 2017.

[19] Nampoothiri H, Vinayakumar B, Sunny Y, An R. Recent developments in terrain identification, classification, parameter estimation for the navigation of autonomous robots.
SN Applied Sciences. 2021; 3(4):480.
doi: 10.1007/s42452-021-04453-3

[20] Berndt DJ, Clifford J. Using dynamic time warping to find patterns in time series.
In: *Proceedings of the 3rd International Conference on Knowledge Discovery and Data Mining*; 1994; Seattle, WA, USA: AAAI Press. pp. 359–370.
doi: 10.5555/3000850.3000887

[21] Nguyen M, Purushotham S, To H, Shahabi C. *m-TSNE: A Framework for Visualizing High-Dimensional Multivariate Time Series*. 2017.

[22] Dietterich T. Machine learning for sequential data: A review.
In: *Structural, Syntactic, and Statistical Pattern Recognition*;
2002; Ontario, Canada: Springer. pp. 15–30.
doi: 10.1007/3-540-70659-3_2

[23] Kaufman L, Rousseeuw P. *Finding Groups in Data: An Introduction to Cluster Analysis*.
New York: John Wiley; 1990.
doi: 10.2307/2532178

EUROSIM Contact Information

EUROSIM –

the **Federation of European Simulation Societies** was set up in 1989. The purpose of **EUROSIM** is to provide a European forum for simulation societies and groups to promote modelling and simulation in industry, research, and development – by publications and conferences.

EUROSIM members are national simulation societies and regional or international societies and groups dealing with modelling and simulation.

Full Members are ASIM, CEA-SMSG, CSSS, DBSS, KA-SIM, LIOPHANT, LSS, PTSK, NSSM, SIMS, SLOSIM. Observer Members are ALBSIM and ROMSIM. Former Members (societies in reorganisation) are: CROSSIM, FRANCOSIM, HSS, ISCS, UKSIM.

EUROSIM is governed by a Board consisting of one representative of each member society, of president, of past president, and of **SNE** representative.

Each year a major **EUROSIM** event takes place, as the **EUROSIM CONGRESS** organised by a member society, **SIMS EUROSIM Conference**, **MATHMOD Vienna Conference (ASIM**), and others.

The *12th EUROSIM Congress 2026* will be organized by **LIOPHANT** in Genova, September 2026.

Furthermore, **EUROSIM Societies** organize local conferences, and **EUROSIM** co-operates with the organizers of **I3M Conference** and **WinterSim Conference Series.**

Contact Information

www.eurosim.info

President:
Francesco Longo (LIOPHANT)
francesco.longo@unical.it

SNE – Simulation Notes Europe is **EUROSIM's** membership journal with peer-reviewed scientific contributions about all areas of modelling and simulation, including new trends as big data, cyber-physical systems, etc. The EUROSIM societies distribute **e-SNE** in premium version to their members as official membership journal.

SNE has also become a post-conference publication journal for the EUROSIM societies, publishing revised, improved or extended versions of the conference publications.

The basic version of **e-SNE** is available with open access (Creative Commons license CC BY 4.0), the premium version is available for members of the **EUROSIM** socities, for authors and for ARGESIM staff members. Publishers are **ASIM, ARGESIM** and **EUROSIM.**

www.sne-journal.org

SNE-Editor:
Felix Breitenecker (ASIM)
eic@sne-journal.org

EUROSIM Member Societies

ASIM - German Simulation Society
Arbeitsgemeinschaft Simulation

ASIM is the association for simulation in the German speaking area, servicing mainly Germany, Switzerland and Austria.

President
Oliver Rose, *oliver.rose@unibw.de*

Contact Information

www.asim-gi.org

info@asim-gi.org

ASIM – Office Germany, Univ. Bundeswehr Munich, Inst. für Technische Informatik, Tobias Uhlig, Werner-Heisenberg Weg 39, 85577 Neubiberg, Germany

ASIM – Office Austria, dwh Simulation Services, F. Breitenecker, N. Popper, Neustiftgasse 57-59, 1070, Wien, Austria

CEA-SMSG – Spanish Modelling and Simulation Group

CEA is the Spanish Society on Automation and Control. The association is divided into national thematic groups, one of which is centered on Modeling, Simulation and Optimization (**CEA-SMSG**).

Representative
Emilio Jiménez *emilio.jimenez@unirioja.es*

Contact Information

www.ceautomatica.es/modelado-simulacion-y-optimizacion

simulacion@ceautomatica.es

CSSS – Czech and Slovak Simulation Society

CSSS is the Simulation Society with members from the two countries: Czech Republic and Slovakia.

President
Michal Štepanovský
michal.stepanovsky@fit.cvut.cz

Contact Information

cssim.cz
michal.stepanovsky@fit.cvut.cz

CSSS – Český a Slovenský spolek pro simulaci systémů, Novotného lávka 200/5,
11000 Praha 1, Česká republika

DBSS – Dutch Benelux Simulation Society

DBSS was founded in July 1986 in order to create an organisation of simulation professionals within the Dutch language area.

President
M. Mujica Mota, *m.mujica.mota@hva.nl*

Contact Information

www.DutchBSS.org
a.w.heemink@its.tudelft.nl

DBSS / A. W. Heemink, Delft University of Technology,
ITS twi, Mekelweg 4, 2628 CD Delft, The Netherlands

KA-SIM Kosovo Simulation Society

The Kosova Association for Modeling and Simulation (**KA-SIM**) is closely connected to the University for Business and Technology (UBT) in Kosovo.

President
Edmond Hajrizi, *ehajrizi@ubt-uni.net*

Contact Information

www.ubt-uni.net

ehajrizi@ubt-uni.net

Dr. Edmond Hajrizi, Univ. for Business and Technology (UBT), Lagjja Kalabria p.n., 10000 Prishtina, Kosovo

LIOPHANT Simulation

is a non-profit association born in order to be a trait-d'union among simulation developers and users.

LIOPHANT is devoted to promote and diffuse the simulation techniques and methodologies; the Association promotes exchange of students, sabbatical years, organization of International Conferences, courses and internships focused on M&S applications.

President
Marina Massei, *massei@itim.unige.it*

Contact Information

www.liophant.org
info@liophant.org

LIOPHANT Simulation, c/o Marina Massei,
DIPTEM University of Genoa, Savona Campus,
via Cadorna 2, 17100 Savona, Italy.

LSS – Latvian Simulation Society

LSS has been founded in 1990 as the first professional simulation organisation in the field of Modelling and simulation in the post-Soviet area.

President
Artis Teilans, *Artis.Teilans@rta.lv*

Contact Information

www.itl.rtu.lv/imb/
Artis.Teilans@rta.lv, Egils.Ginters@rtu.lv

LSS, Dept. of Modelling and Simulation, Riga Technical University, Kalku street 1, Riga, LV-1658, Latvia

NSSM – National Society for Simulation Modelling (Russia)

NSSM (Национальное Общество Имитационного Моделирования – НОИМ) was officially registered in Russia in 2011.

President
R. M. Yusupov, *yusupov@iias.spb.su*

Contact Information

www.simulation.su
yusupov@iias.spb.su

NSSM / R. M. Yusupov, St. Petersburg Institute of Informatics and Automation RAS,
199178, St. Petersburg, Russia

PTSK – Polish Society for Computer Simulation

PTSK is a scientific, non-profit association of members from universities, research institutes and industry in Poland with common interests in variety of methods of computer simulations and its applications.

President
Tadeusz Nowicki,
Tadeusz.Nowicki@wat.edu.pl

Contact Information

www.ptsk.pl
leon@ibib.waw.pl

PSCS, ul. Gen. Witolda Urbanowicza 2, pok. 222,
00-908 Warszawa 49, Poland

SIMS – Scandinavian Simulation Society

SIMS is the Scandinavian Simulation Society with members from the five Nordic countries Denmark, Finland, Norway, Sweden and Iceland.

President
Tiina Komulainen,
tiina.komulainen@oslomet.no

Contact Information

www.scansims.org

vadime@wolfram.com

Vadim Engelson, Wolfram MathCore AB,Teknikringen 1E, 58330, Linköping, Sweden

SLOSIM – Slovenian Society for Simulation and Modelling

The Slovenian Society for Simulation and Modelling was established in 1994. It promotes modelling and simulation approaches to problem solving in industrial and in academic environments by establishing communication and cooperation among corresponding teams.

President
Goran Andonovski,
goran.andonovski@fe.uni-lj.si

Contact Information

www.slosim.si
slosim@fe.uni-lj.si, vito.logar@fe.uni-lj.si

SLOSIM, Fakulteta za elektrotehniko, Tržaška 25,
1000, Ljubljana, Slovenija

Observer Member Societies

ROMSIM – Romanian Modelling and Simulation Society

Contact Information

florin_h2004@yahoo.com
ROMSIM / Florin Hartescu, National Institute for Research in Informatics, Averescu Av. 8 – 10,
011455 Bucharest, Romania

ALBSIM – Albanian Simulation Society

Contact Information

kozeta.sevrani@unitir.edu.al

Albanian Simulation Goup, attn. Kozeta Sevrani, University of Tirana, Faculty of Economy ,
rr. Elbasanit, Tirana 355, Albania

Publication-Active Member Societies

Publication-Active Societies have a valid full *ARGESIM Publication Society Membership* and provide for their members privileged access to **e-SNE** in premium version:

ASIM	**CEA-SMSG**	**CSSS**
DBSS	**KA-SIM**	**LIOPHANT**
SIMS	**SLOSIM**	

Member Societies in Reorganisation

- **CROSSIM** – Croatian Society for Simulation Modelling
- **FRANCOSIM** – Société Francophone de Simulation (Belgium, France)
- **HSS** – Hungarian Simulation Society
- **UKSIM** – United Kingdom Simulation Society
- **ISCS** – Italian Simulation Society

Association Simulation News

ARGESIM is a non-profit association generally aiming for dissemination of information on system simulation – from research via development to applications of system simulation. **ARGESIM** is following its aims and scope by the following activities and projects:

- Publication of the scientific journal **SNE** – *Simulation Notes Europe* (membership journal of **EUROSIM**, the *Federation of European Simulation Societies*) – *www.sne-journal.org*
- Organisation and Publication of the **ARGESIM Benchmarks** for *Modelling Approaches and Simulation Implementations*
- Publication of the series **ARGESIM Reports** for monographs in system simulation, and proceedings of simulation conferences and workshops
- Publication of the special series **FBS Simulation** – Advances in Simulation / Fortschrittsberichte Simulation - monographs in co-operation with **ASIM**, the German simulation society
- Support of the Conference Series *MATHMOD Vienna*, *EUROSIM Conference*, *ASIM Symposium Simulation Technique* and others (co-operation with **EUROSIM**, **ASIM**, and **TU Wien**)
- Administration of **ASIM** (German Simulation Society) and administrative support for **EUROSIM)**

EUROSIM societies are *ARGESIM Publication Society Members*, they get for their members access to the premium version of **SNE**, they can publish in the **ARGESIM** series **ARGESIM Reports** (proceedings) or **FBS Simulation** (monographs). *ARGESIM Personal Members* are people working on **SNE**, on websites for **SNE**, **EUROSIM** and **ARGESIM**, on related conference activities, etc. - all voluntarily (e.g. editors, layout specialists, web managers etc; at present mainly people from **TU Wien** *Group Mathematics in Simulation and Education* and from **ASIM**) – they have voting right for the *ARGESIM Board*).
And *ARGESIM Review Members* are the scientist from *SNE Review Board* and related review boards.
ARGESIM is a registered non-profit Austrian association (ZVR 213056164) and a registered scientific publisher: **ARGESIM Publisher Vienna**, root ISBN 978-3-901608-(978-3-903347) -xx-y, root DOI 10.11128/z…zz.zz.

Contact

→ **ARGESIM** / Mathematics in Simulation and Education, Inst. of Analysis and Scientific Computing, TU Wien, Wiedner Hauptstrasse 8-10, 1040 Vienna, Austria
Attn. Prof. Dr. F. Breitenecker, Prof. Dr. A. Körner
→ **www.argesim.org** *office@argesim.org*

SNE – Simulation Notes Europe

The scientific journal **SNE – Simulation Notes Europe** provides an international, high-quality forum for presentation of new ideas and approaches in simulation – from modelling to experiment analysis, from implementation to verification, from validation to identification, from numerics to visualisation – in context of the simulation process. **SNE** puts special emphasis on the overall view in simulation, and on comparative investigations.
Furthermore, **SNE** welcomes contributions on education in/for/with simulation.

SNE is also the forum for the **ARGESIM Benchmarks** on *Modelling Approaches and Simulation Implementations* publishing benchmarks definitions, solutions, reports and studies – including model sources via web.

SNE, primarily an electronic journal, follows an open access strategy, *with* free download in a basic version (OA version: B/W, low resolution graphics). This basic version is is licensed under CC BY 4.0 by ARGESIM Vienna -ASIM/ GI – EUROSIM.

SNE is the official membership journal of **EUROSIM**, the *Federation of European* Simulation *Societies*. Members of (most) **EUROSIM Societies** are entitled to download the premium version of e-**SNE** (PM: colour, high-resolution graphics), and to access additional sources of benchmark publications, and related conference publications, etc. (group login for the 'publication-active' societies; please contact your society). Furthermore, **SNE** offers **EUROSIM Societies** a publication forum for post-conference publication of the society's international conferences, and the possibility to compile thematic or event-based **SNE Special Issues**.

Call for SNE Contributions

Simulationists are invited to submit contributions of any type – *Technical Note*, *Short Note*, *Project Note*, *Software Note*, *Educational Note*, *Benchmark Note*, etc. via **SNE**'s website **www.sne-journal.org**

Contact

SNE Editorial Office /ARGESIM
Felix Breitenecker EiC (Organisation, Authors)
Irmgard Husinsky (Web, Electronic Publishing)

ARGESIM / Mathematics in Simulation and Education, Inst. of Analysis and Scientific Computing, TU Wien
Wiedner Hauptstrasse 8-10, 1040 Vienna, Austria

→ **www.sne-journal.org** *office@sne-journal.org, eic@sne-journal.org*

ASIM Books – ASIM Book Series – ASIM Buchreihen

Monographs

Simulation-based Optimization: Industrial Practice in Production and Logistics
Lothar März, Markus Rabe, Oliver Rose (Eds.); to appear; ASIM Mitteilung 191

Energy-related Material Flow Simulation in Production and Logistics.
S. Wenzel, M. Rabe, S. Strassburger, C. von Viebahn (Eds.); Springer Cham 2023, print ISBN 978-3-031-34217-2, eISBN 978-3-031-34218-9, DOI 10.1007/978-3-031-34218-9, ASIM Mitteilung 182

Kostensimulation - Grundlagen, Forschungsansätze, Anwendungsbeispiele
T. Claus, F. Herrmann, E. Teich; Springer Gabler, Wiesbaden, 2019; Print ISBN 978-3-658-25167-3; Online ISBN 978-3-658-25168-0; DOI 10.1007/978-3-658-25168-0; ASIM Mitteilung 169

Proceedings*

Simulation in Produktion und Logistik 2025 - Tagungsband 21. ASIM-Fachtagung Simulation in Produktion und Logistik,
Dresden, 24. bis 26. September 2025, S. Rank, M. Kühn, T. Schmidt (Hrsg.)
ASIM Mitteilung 194, e-ISBN 978-3-86780-809-5, DOI 10.25368/2025.233, Technische Uni Dresden / Qucosa Publ., 2025

Tagungsband ASIM Workshop 2025 - GMMS/STS - ASIM Fachgruppenworkshop 2025, DLR Oberpfaffenhofen
W. Commerell, U. Durak, D. Zimmer (Hrgs.), ARGESIM Report 48; ASIM Mitteilung AM 193
ISBN ebook 978-3-903347-66-3, DOI 10.11128/arep.48, ARGESIM Verlag Wien, 2025

Tagungsband Kurzbeiträge ASIM SST 2024 -27. ASIM Symposium Simulationstechnik, Univ. Bundeswehr München,
München/Neubiberg, Sept. 2024, O. Rose, T. Uhlig (Hrgs.), ARGESIM Report 46; ASIM Mitteilung AM 189
ISBN ebook 978-3-903347-64-9, DOI 10.11128/arep.46, ARGESIM Verlag Wien, 2024

Tagungsband Langbeiträge ASIM SST 2024 -27. ASIM Symposium Simulationstechnik, Univ. Bundeswehr München
München/Neubiberg, Sept. 2024,O. Rose, T. Uhlig (Hrgs.), ARGESIM Report 47; ASIM Mitteilung AM 190
ISBN ebook 978-3-903347-65-6, DOI 10.11128/arep.47, ARGESIM Verlag Wien, 2024

Simulation in Production and Logistics 2023 – Tagungsband 20. ASIM Fachtagung Simulation in Produktion und Logistik
TU Ilmenau, September 2023; S. Bergmann, N. Feldkamp, R. Souren, S. Straßburger (Hrsg.);
ASIM Mitteilung 187; ISBN ebook 978-3-86360-276-5, DOI: 10.22032/dbt.57476, Universitätsverlag Ilmenau, 2023

Proceedings Langbeiträge ASIM Workshop 2023 - STS/GMMS/EDU - ASIM Fachgruppenworkshop 2023
Univ. Magdeburg, März 2023; C. Krull; W. Commerell, U. Durak, A. Körner, T. Pawletta (Hrsg.)
ARGESIM Report 21; ASIM Mitteilung 185; ISBN ebook 978-3-903347-61-8, DOI 10.11128/arep.21, ARGESIM Verlag, Wien, 2023

Kurzbeiträge & Abstract-Beiträge ASIM Workshop 2023 STS/GMMS/EDU - ASIM Fachgruppenworkshop 2023
Univ. Magdeburg, März 2023; C. Krull; W. Commerell, U. Durak, A. Körner, T. Pawletta (Hrsg.)
ARGESIM Report 22; ASIM Mitteilung 186; ISBN ebook 978-3-903347-62-5, DOI 10.11128/arep.22, ARGESIM Verlag, Wien, 2023

Proceedings Langbeiträge ASIM SST 2022 -26. ASIM Symposium Simulationstechnik, TU Wien, Juli 2022
F. Breitenecker, C. Deatcu, U. Durak, A. Körner, T. Pawletta (Hrsg.), ARGESIM Report 20; ASIM Mitteilung AM 180
ISBN ebook 978-3-901608-97-1, DOI 10.11128/arep.20, ARGESIM Verlag Wien, 2022

Book Series Fortschrittsberichte Simulation – Advances in Simulation *

Beschleunigung von Diskret-Ereignisorientierten Simulationsstudien unter Verwendung des DEVS-Formalismus auf HPC-Systemen. D. Jammer, FBS 42, e-ISBN 978-3-903347-43-4, DOI 10.11128/fbs.42, ARGESIM/ASIM Publ. Vienna, 2026.

An Architecture for Model Behavior Generation for Multiple Simulators. H. Folkerts, FBS 42
e-ISBN 978-3-903347-42-7, DOI 10.11128/fbs.32, ARGESIM Publ. Vienna, 2024

Das Verhalten von Transuranelementen in Erdböden - Theorie, Beprobung und radiochemische Analysen. K. Breitenecker, FBS 41; ISBN ebook 978-3-903347-41-0, DOI 10.11128/fbs.41, 2024; ISBN print 978-3-901608-99-5, 2010/2024; ARGESIM Publ. Vienna

Aufgabenorientierte Multi-Robotersteuerungen auf Basis des SBC-Frameworks und DEVS. B. Freymann, FBS 40
ISBN ebook2020_978-3-903347-40-3, DOI 10.11128/fbs.40, ARGESIM Publ. Vienna, 2022

Cooperative and Multirate Simulation: Analysis, Classification and New Hierarchical Approaches. I. Hafner, FBS 39
ISBN ebook978-3-903347-39-7, DOI 10.11128/fbs.39, ARGESIM Publ. Vienna,2022

Die Bedeutung der Risikoanalyse für den Rechtsschutz bei automatisierten Verwaltungsstrafverfahren. T. Preiß, FBS 38
ISBN ebook 978-3-903347-38-0, DOI 10.11128/fbs.38, ARGESIM Publ. Vienna,2020

Methods for Hybrid Modeling and Simulation-Based Optimization in Energy-Aware Production Planning. B. Heinzl, FBS 37
ISBN ebook 978-3-903347-37-3, DOI 10.11128/fbs.37, ARGESIM Publ. Vienna,2020;

Konforme Abbildungen zur Simulation von Modellen mit verteilten Parametern. Martin Holzinger, FBS 36
ISBN ebook 978-3-903347-36-6, DOI 10.11128/fbs.36, ARGESIM Publ. Vienna, 2020

Fractional Diffusion by Random Walks on Hierarchical and Fractal Topological Structures. G. Schneckenreither, FBS 35
ISBN ebook 978-3-903347-35-9, DOI 10.11128/fbs.35, ARGESIM Publ. Vienna, 2024

A Framework Including Artificial Neural Networks in Modelling Hybrid Dynamical Systems. Stefanie Winkler, FBS 34
ISBN ebook 978-3-903347-34-2, DOI 10.11128/fbs.34, ARGESIM Publ. Vienna, 2020

Modelling Synthesis of Lattice Gas Cellular Automata and Random Walk and Application to Gluing of Bulk Material. C. Rößler, FBS 33
ISBN ebook 978-3-903347-33-5, DOI 10.11128/fbs.33, ARGESIM Publ. Vienna, 2021

Combined Models of Pulse Wave and ECG Analysis for Risk Prediction in End-stage Renal Desease Patients. S. Hagmair, FBS 32
ISBN ebook 978-3-903347-32-8, DOI 10.11128/fbs.32, ARGESIM Publ. Vienna, 2024

Mathematical Models for Pulse Wave Analysis Considering Ventriculo-arterial Coupling in Systolic Heart Failure. S. Parragh, FBS 31
ISBN ebook 978-3-903347-31-1, DOI 10.11128/fbs.31, ARGESIM Publ. Vienna, 2024

Variantenmanagement in der Modellbildung und Simulation unter Verwendung des SES/MB Frameworks. A. Schmidt, FBS 30; ISBN ebook 978-3-903347-30-4, DOI 10.11128/fbs.30, ARGESIM Verlag, Wien 2019

12th EUROSIM Congress

Federation of European Simulation Societies' Conference

September 21-23, 2026

Genova, Italy

in collaboration with I3M 2026

Keynote Talks:

Tillal Eldabi, University of Bradford, UK - When AI Meets Simulation: Towards Complementary Intelligence Biographical Sketch

Andreas Körner, TU Wien, Austria
Modelling and Simulation in Computational Biology and Medicine

Plenary Panel

On the convergence of Modelling & Simulation with Artificial Intelligence

Special Track dedicated to contributions from the **ASIM** community:

ASIM - Developments in Simulation Technique

www.msc-les.org/eurosim2026/

www.sne-journal.org
www.argesim.org